# DEVELOPMENT OF A TSUNAMI FORECAST MODEL FOR OCEAN CITY, MARYLAND (DRAFT)

Yong Wei

August, 2010

Abstract

As part of NOAA's tsunami forecast system, this study addresses the development, validation, and stability tests of the tsunami forecast model for Ocean City, Maryland. Based on the Method of Splitting Tsunami (MOST), the tsunami forecast model is constructed at a spatial resolution of approximately 36 m in the finest grid to accomplish a 4-hour simulation of wave inundation onto dry land within 20 minutes of CPU time. A reference inundation model is developed in parallel, using grid size up to eight meters to provide a reference for the forecast model. The present study conducted the sensitivity tests to optimize the grid extension and resolution of the forecast model. Due to lack of historical tsunami data, the Ocean City forecast model was carefully evaluated using the 1755 Lisbon earthquake, the source of which is still in debate within tsunami science community. The model validations show excellent agreement between the forecast model and reference model, suggesting that the forecast model is qualified to provide quantitative estimation of the inundation, runup and computed maximum values for potential threats posed by future tsunamis. The stability of the forecast model is further evaluated with eight synthetic scenarios generated in the Puerto Rico Trench, Hispaniola Trench, Cayman Trough, Los Muertos Trough and South Sandwich Island at magnitudes ranging from $M_w$ 7.5 to $M_w$ 9.3.

## 1. Background and Objectives

The National Oceanic and Atmospheric Administration (NOAA) Center for Tsunami, Research (NCTR) at the NOAA Pacific Marine Environmental Laboratory (PMEL) has developed a tsunami forecasting capability for operational use by NOAA's two Tsunami Warning Centers located in Hawaii and Alaska (Titov *et al.*, 2005). The system is designed to efficiently provide basin-wide warning of approaching tsunami waves accurately and quickly. The system, termed Short-term Inundation Forecast of Tsunamis (SIFT), combines real-time tsunami event data with numerical models to produce estimates of tsunami wave arrival times and amplitudes at a coastal community of interest. The SIFT system integrates several key components: deep-ocean observations of tsunamis in real time, a basin-wide pre-computed propagation database of water level and flow velocities based on potential seismic unit sources, an inversion algorithm to refine the tsunami source based on deep-ocean observations during an event, and high-resolution tsunami forecast models.

Maryland's Atlantic coast features the barrier island beaches of Fenwick and Assateague Islands (**Figure 1a** and **Figure 1b**). Of the 40 miles of beaches in Maryland, only about 10 miles are maintained by the state. Ocean City, Maryland's only coastal resort, occupies the entire 8 miles of Fenwick Island within Maryland. Although it was founded from a single beach-front cottage in 1869, Ocean City established itself as one of the world's greatest fishing ports when a powerful storm in 1933 helped to form the Ocean City Inlet, offering easy access to the fishing grounds of the Atlantic Ocean. Extending from the inlet northward, the strip of barrier island that constitutes Ocean City now supports hotels, motels, apartment houses and condominiums. Rapid expansion of Ocean City took place during the post-war boom. In 1952, with the completion of the Chesapeake Bay Bridge, Ocean City became easily accessible to people in the Baltimore-Washington corridor. In 1964, with the completion of the Chesapeaker Bay Bridge tunnel, another new pathway to the south was opened. Ocean City became one of the largest vacation areas of the east. By the 1970s, big business flourished and created a spectacular sight of high-rise apartments. Today, Ocean City still remains as one of the most popular recreation barrier islands in the Atlantic coasts. Ocean City has a total area of 94.3 square kilometers. According to Census 2010, Ocean City has only 7,102 permanent residents (http://2010.census.gov/2010census/index.php). Most of the population in Ocean City comes from the tourists - the summer weekend population in Ocean City is estimated to be 320,000 to 345,000. Thus, the vulnerability of Ocean City to the potential coastal hazards poses challenging, yet long-standing, tasks for the coastal communities on how to protect their lives and properties.

Due to low land elevation, all properties in Ocean City, MD are in a flood hazard area and subject to flooding from the ocean, coastal bays and heavy rainfall. Minor flooding is not uncommon, and major flooding happens occasionally. On 26 April, 2010, Ocean City was designated as a National Weather Service Storm-Ready Community that is better prepared to save lives from the onslaught of severe weather through advanced planning, education and awareness (Ocean City Department of Emergency Services, 2010). In Ocean City, rapid shoreward erosion of the barrier islands jeopardizes both property and economy. Massive development of Fenwick Island has both increased the urgency for and complicated the process of beach restoration. Like many Atlantic coast communities, Ocean City has been under beach nourishment and dune management as the primary maintenance strategy since 1988. Currently utilized sand resources are located north of Ocean City Inlet, within the three-mile limit of state jurisdiction. These sands are committed to the reconstruction and periodic nourishment of Ocean City beaches (http://www.mgs.md.gov/coastal/osr/ocsand2.html). Titus et al. (1987) evaluated the potential impacts of sea level rise on the beach at Ocean City. They concluded that the sea level rise could double the rate of erosion at Ocean Cit in the next forty years. If no additional erosion control measures are taken, the shore will erode 85-153 feet by 2025, assuming current sea level trends. The projected rise in sea level would increase the quantity of sand necessary to maintain the current shoreline from 5-10 million cubic yards for the next 40 years at current trends to 11 – 15 million cubic yards for an accelerated sea level rise regime.

Since it is one of the largest barrier islands in the U.S. Atlantic coast that has been transformed into high-density year-round urban complexes, Ocean City has been evaluated and studied for various coastal hazards as mentioned above. However, the potential tsunami impact on the coast of Ocean City is significantly understudied, probably due to uncommon tsunami activities in the Atlantic and la ack of historical tsunami data. The only reported tsunami height at the Ocean City tide gauge was the 0.3

m due to a large submarine slump triggered by a magnitude 7.2 earthquake in Grand Banks, Canada on 18 November 1929 (http://earthquakescanada.nrcan.gc.ca/). ten Brink et al. (2007) evaluated all tsunami sources with the potential to impact the U.S. Atlantic and Gulf Coasts. Their report indicated that earthquake sources located west of Gibraltar and in the Puerto Rico Trench are capable of generating trans-oceanic tsunamis. A large tsunamigenic earthquake taking place in the Puerto Rico trench may be destructive to many parts of the U.S. East Coast, although the ability of this plate boundary to generate earthquakes is being investigated. ten Brink et al. (2008) also speculated that landslides along the U.S. Atlantic margin have the potential to cause tsunamis locally. For instance, the Currituck Slide occurred less than 200 km southeast of Ocean City and is one of the major mass movements that have taken place on the Atlantic continental margin over the last 100,000 years (Prior et al., 1986) and could have caused a damaging tsunami to the East Coast of United States. The landslide modeling results of Geist et al. (2009) showed that the failure of Currituck landslide could trigger tsunami waves of up to 3 m in amplitude on the shelf offshore of Ocean City. Titov et al. (2009) employed high-resolution tsunami inundation forecast models to assess the potential tsunami hazards for coastal communities in U.S. Atlantic coasts due to distant earthquake- and landslide-generated tsunamis in the Atlantic. The development of the Ocean City tsunami forecast model in the present study is a valuable supplement to this assessment, and more importantly adds another essential contribution to the existing NOAA's tsunami forecasting system in the Atlantic.

## 2. Forecast Methodology

A high-resolution inundation model was used as the basis for development of a tsunami forecast model to operationally provide an estimate of wave arrival time, wave height, and inundation at Ocean City, Maryland following tsunami generation. All tsunami forecast models are run in real time while a tsunami is propagating across the open ocean. The Ocean City model was designed and tested to perform under stringent time constraints given that time is generally the single limiting factor in saving lives and property. The goal of this work is to maximize the length of time that the community of Ocean City has to react to a tsunami threat by providing accurate information quickly to emergency managers and other officials responsible for the community and infrastructure.

The general tsunami forecast model, based on the Method of Splitting Tsunami (MOST), is used in the tsunami inundation and forecasting system to provide real-time tsunami forecasts at selected coastal communities. The model runs in minutes while employing high-resolution grids constructed by the National Geophysical Data Center. The Method of Splitting Tsunami (MOST) is a suite of numerical simulation codes capable of simulating three processes of tsunami evolution: earthquake, transoceanic propagation, and inundation of dry land. The MOST model has been extensively tested against a number of laboratory experiments and benchmarks (Synolakis *et al.*, 2008) and was successfully used for simulations of many historical tsunami events. The main objective of a forecast model is to provide an accurate, yet rapid, estimate of wave arrival time, wave height, and inundation in the minutes following a tsunami event. Titov and

González (1997) describe the technical aspects of forecast model development, stability, testing, and robustness, and Tang *et al*. (2009) provide detailed forecast methodology

A basin-wide database of pre-computed water elevations and flow velocities for unit sources covering worldwide subduction zones has been generated to expedite forecasts (Gica *et al.*, 2008). As the tsunami wave propagates across the ocean and successively reaches tsunameter observation sites, recorded sea level is ingested into the tsunami forecast application in near real-time and incorporated into an inversion algorithm to produce an improved estimate of the tsunami source. A linear combination of the pre-computed database is then performed based on this tsunami source, now reflecting the transfer of energy to the fluid body, to produce synthetic boundary conditions of water elevation and flow velocities to initiate the forecast model computation.

Accurate forecasting of the tsunami impact on a coastal community largely relies on the accuracies of bathymetry and topography and the numerical computation. The high spatial and temporal grid resolution necessary for modeling accuracy poses a challenge in the run-time requirement for real-time forecasts. Each forecast model consists of three telescoped grids with increasing spatial resolution in the finest grid, and temporal resolution for simulation of wave inundation onto dry land. The forecast model utilizes the most recent bathymetry and topography available to reproduce the correct wave dynamics during the inundation computation. Forecast models, including the Ocean City model, are constructed for at-risk populous coastal communities in the Pacific and Atlantic Oceans. Previous and present development of forecast models in the Pacific (Titov *et al*., 2005; Titov, 2009; Tang *et al*., 2008; Wei *et al*., 2008) have validated the accuracy and efficiency of each forecast model currently implemented in the real-time tsunami forecast system. Models are tested when the opportunity arises and are used for scientific research. Tang *et al*., 2009 provide forecast methodology details.

## 3. Model development

The general methodology for modeling at-risk coastal communities is to develop a set of three nested grids, referred to as A, B, and C-grids, each of which becomes successively finer in resolution as they telescope into the population and economic center of the community of interest. The offshore area is covered by the largest and lowest resolution A-grid while the near-shore details are resolved within the finest scale C-grid to the point that tide gauge observations recorded during historical tsunamis are resolved within expected accuracy limits. The procedure is to begin development with large spatial extent merged bathymetric topographic grids at high resolution, and then optimize these grids by sub sampling to coarsen the resolution and shrink the overall grid dimensions to achieve a 4 to 10 hr simulation of modeled tsunami waves within the required time period of 10 min of wall-clock time. The basis for these grids is a high-resolution digital elevation model constructed by the National Geophysical Data Center and NCTR using all available bathymetric, topographic, and shoreline data to reproduce the wave dynamics during the inundation computation for an at-risk community. For each community, data are compiled from a variety of sources to produce a digital elevation model referenced to Mean High Water in the vertical and to the World Geodetic System 1984 in the horizontal (http://ngdc.noaa.gov/mgg/inundation/tsunami/inundation.html). From these digital elevation models, a set of three high-resolution, ‘reference’ elevation grids are constructed for development of a high-resolution reference model from which an 'optimized' model is constructed to run in an operationally specified period of time. The operationally developed model is referred to as the 'optimized tsunami forecast' model or 'forecast model' for brevity.

## 3.1 Forecast area

### 3.1.1 Ocean City as a barrier island

Barrier islands are dynamic landforms, subject to storm-surge flooding and sand transport processes. These coastal features are particularly vulnerable areas for human habitation, since they extend seaward of the mainland and are composed entirely of loose sediment (Leatherman, 1982). Like all ocean beaches, the beach at Ocean City exhibits a seasonal pattern. Winter storms erode the beach, while the calm waves of spring and summer rebuild it. In the long term, however, the shoreline has shown a slow but steady erosion trend. In the last 50 years, the beach has eroded over 30 meters (Titus et al., 1985). Studies by Leatherman (1985) and Everts (1985) have offered different explanation for the causes of this erosion, arguing the erosion is caused by either the long-term sea level rise or the substantial quantities of sand transported along the shore and old Fenwick Island. Leatherman (1985) identified another possible cause of the erosion due to the opening of Ocean City inlet, which was formed during a hurricane in 1933.

### 3.1.2 Ocean City Inlet and jetties

The Ocean City Inlet separated the Assateague Island into two sections at the southern end of Ocean City. Subsequent construction of two stone jetties to maintain the inlet for navigation interrupted the longshore transport of sand to the south. Since then, the jetties have trapped sand, building the Ocean City shores seaward by 250 meters by the mid-1970s (Dean and Perlin, 1977). In the contrast, the south of the inlet experienced sand starvation on the northern part of Assateague Island, which has migrated almost 700 meters landward and transformed the barrier into a low-relief, overwash-dominated barrier (Leatherman, 1979; 1984). Since 1988, the U.S. Army Corps of Enginers and National Park Service have been mechanically transferring sand from the inlet and the ebb and flood tide deltas, where the sand is trapped, to the shallow nearshore regions along the north end of Assateague Island, making the island barrier more robust. As this nourishment project continues, new sources of offshore sand are needed for future nourishment projects. However, the area of critical erosion caused by jetties continues to move southerly along the shoreline.

While trapping sands, the jetties also change the bathymetric features at the entrance of the Ocean City Inlet. A multibeam survey study by Buttolph et al. (2006) showed that the rehabilitation of the south jetty in 2002 has strengthened the ebb jet, causing the seaward ridge of the ebb shoal to migrate radially outward. Differences in measured bathymetry between the 2004 and 2005 surveys indicate that the shoal expansion may still be ongoing.

The width of Ocean City Inlet is about 340 m at its widest. Two jetties were constructed in 1934 and 1935, following the opening formed by the 1933 hurricane. The jetty on the north side is about 335 m long with a crest elevation of 2.05 m above Mean High Water (MHW) and a crown width of 3.7 m. The total length of the dog-leg-shape jetty on the south side is about 730 m with a crest elevation of 1.15 m above MHW and a crown width of 2.7 m. Several repairs and rehabilitations were conducted on both jetties due to slope failures.

### 3.1.3 Ocean City tide gauge

The Ocean City tide gauge is located on a pier in a small boat basin (38.3282°N, 75.0917°W according to NOAA tides and currents), 350 m north of the inlet, on the west side of the Ocean City barrier island (**Figure 2**). Located at a water depth of 3.1 m (Mean High Water), the gauge is sheltered by a thin wall of piles that separate the boat basin from the inlet. This National Ocean Service (NOS) station was established on 5 June 1978, and upgraded to its present installation on 17 November 1997. The local mean tide range is about 0.65 m, and the diurnal range is 0.76 m.

## 3.2 Historical events and data

National Geophysical Data Center (NGDC)'s tsunami runup database (http://www.ngdc.noaa.gov/nndc/struts/form?t=101650&s=167&d=166) shows that there have been a number of historical tsunamis affecting the coasts of Virginia, Maryland, Delaware, New Jersey and New York (**Figure 3** and **Table 1**). Only a small tsunami of 0.3-m wave amplitude was reported at Ocean City due to an earthquake-triggered submarine landslide in Grand Banks on the 18 November 1929.

The 1929 Grand Banks tsunami is notable for a number of reasons: this event is Canada's most tragic earthquake ($M_w$ 7.2) with 28 lives lost (Ruffman, 1996); it was one of the very few catastrophic tsunamis, up to 27 m tsunami runup, to occur in the Atlantic; and it was one of the very few transoceanic tsunamis generated by a landslide (Pasad et al., 2009). Natural Resources Canada (2006) reported that "the earthquake triggered a large submarine slump (an estimated volume of 200 cubic kilometers of material was moved on the Laurentian slope), which ruptured 12 transatlantic cables in multiple places, and generated a tsunami. The tsunami was recorded along the eastern seaboard as far south as South Carolina and across the Atlantic Ocean in Portugal." Lockridge et al. (2002) reported that the Ocean City tide gauge recorded a change of approximately 0.3 m. Tide gauge records showed that it was also recorded at Atlantic City, New Jersey, with about the same height as Ocean City at these two locations, and on the tide gauge at Charleston, South Carolina.

Past tsunami waves that have affected the coasts from Virginia to New York had complex triggering mechanisms, including earthquake, landslide or meteorological events (**Table 1**). In some of these cases, shortly after the local earthquakes occurred, unusual tsunami-like waves were reported on coasts located within 200-kilometers distance from the earthquake location. Such earthquakes are the 1817 Philadelphia, 1840 Philadelphia, 1871 New York, 1884 New York, and 1895 New Jersey events. Some of the distant tsunamis that have impacted the Virginia-New York coasts were triggered by earthquakes in the Puerto Rico and the Hispaniola Trenches in the northeast of the Caribbean, such as the 1973 Mona Passage, 4 August 1946 Dominican Republic, and 8 August 1946

Dominican Republic events. Since they were all recorded by the tide gage in Atlantic City, NJ, where is only about 135 km northeast to Ocean City, Ocean City may have also been affected when these tsunami waves passed by. Except for the 1929 Grand Banks, trans-Atlantic tsunamis that may have produced impact on Ocean City is the 1755 Lisbon tsunami due to an $M_w$ 8.5 – 9.0 earthquake (Barkan et al., 2008; Roger et al., 2009; Muir-Wood and Mignan, 2009). Runup reports from the 1755 Lisbon tsunami were documented in the Caribbean, Brazil and Newfoundland (Canada), and no reports were documented along the U.S. East Coast (Barkan et al., 2009). A model simulation of the Lisbon tsunami (see section 4.1 of this report) shows that the computed maximum wave amplitudes are about 30 cm along the Ocean City's shoreline and about 10 cm at the tide gage inside the inlet. The global reach of the catastrophic 26 December 2004 Indian Ocean tsunami was also recorded on the East Coast of United States, with 0.11 m at Atlantic City, NJ and 0.06 m at Cape May, NJ (Titov et al., 2005). Although Ocean City may not have detected distinct waves during the 2004 Indian Ocean tsunami, it is worth noting that large tsunamis can propagate substantial and damaging wave energy to distant coasts, including different oceans, through a combination of source focusing and topographic waveguides, and local resonant effects, which may strongly amplify the arriving waves too (Titov et al., 2005).

Other than confirmed earthquake-generated tsunamis, tsunami-like waves have also beenrecorded at tide gages in U.S. East Coast with unclear generation mechanisms. Some of them have been associated with passing hurricanes or meteorological pressure changes. For instances, tsunami-like waves were observed in Virginia when a category 4 hurricane passed over on 3 September 1821. When "heavy tides" were observed in Atlantic City on 10 June of 1913, they were unable to be linked to either storms or earthquakes (Lockridge et al., 2002). These types of waves were frequently seen on the coast of New Jersey and New York in 1923, 1924, 1931, 1932, 1938, 1944, and 1964. Some of them were attributed to either submarine landslides or abnormal weather events. Whether or not Ocean City has historically been affected by these tsunami-like waves remains unclear. Therefore, an inundation model is needed to equip the Ocean City area with the capability of tsunami forecasting and hazard assessment.

## 3.3 Model setup

### 3.3.1 Grid boundary and resolution

The wide continental shelf on the East Coast of United States complicates the modeling of tsunami waves approaching the shoreline. When a tsunami reaches continental shelf and begins to shoal, it will slow down and increase in height while introducing model diffusion and dispersion. Burwell et al. (2007) studied the diffusion and dispersion characterization of MOST model, and concluded that the nature of the scheme, at all resolvable wave numbers, is diffusive and dispersive for $\beta = (gd)^{1/2}\Delta t/\Delta x \neq 1$, where $\Delta t$ is the temporal step and $\Delta x$ is the space step. Diffusive effects are stronger for poorly resolved waves (large space step compared to wave length). As $\beta$ decreases, diffusive effects are reduced and dispersion continues to increase. Thus, numerical dispersion can be an issue closer to shore, but can be controlled though a careful choice of $\beta$, or in other words, the ratio between $\Delta t$ and $\Delta x$. The tsunami propagation database (Gica et al., 2008) was developed at a grid spacing of 4-arc-minute (about 7.2 km at the equator) and saved at 16-arc-minute (about 28.8 km at the equator) resolution. This resolution may introduce large model diffusion effects if applied directly to continental shelf, where water depth is generally less than 100 m. The telescoped grids adopted in the MOST model are thus critical for wave transformation over the continental shelf, and for the inundation modeling at the coastline. Ideally, manipulation of $\beta$ value may reduce the effects of diffusion and mimic the real-world dispersion through numerical dispersion.

The outmost grid (A grid as referred hereafter) provides a smooth transition from tsunami propagation database to the inundation forecast model. As stated above, this boundary connection must not occur over the continental shelf, and must extend further beyond the continental shelf, where the numerical diffusion can be significantly reduced during the transition. **Figure 4** shows a sensitive study of the wave amplitude difference between a 1-arc-min (~ 1.5 km at latitude 38 degree) and 30-arc-sec (~ 750 m at latitude 38 degree) grid resolutions along different transects for the synthetic tsunami scenario ATSZ 46-55. When the eastern boundary of A grid is placed at 71.5°W (section A-A'), the wave amplitude difference is mostly negligible over time (**Figure 4**) with a root-mean-square of 0.53 cm after 7-hours of model run time between the two resolutions. As the boundary is moved closer to the coastline, the difference increases as more shelf area is taken into account, with most of the differences occurring in the portion over the shelf along the transects. When the eastern boundary is placed at 75°W, the root-mean-square of the difference is 18.2 cm, nearly 35 times the amplification of the differences when the deep-ocean boundary is placed at 71.5°W. To save model computational time, the entire eastern boundary of the intermediate grid (B grid as referred hereafter) is located on the shelf between transects E-E' and F-F', where differences were up to 50 cm. A 30-arc-second (~ 750 m at latitude 38 degree) resolution was implemented for grid A to provide more accurate boundary conditions for grid B. The eastern boundary of grid A is also placed at longitude 71°W, beyond the continental shelf, in order to minimize the numerical diffusion, as discussed above.

### 3.3.2 Digital Elevation Model of Ocean City

Medley et al. (2009) at the National Geophysical Data Center (NGDC) developed a 1/3-arc-sec (~ 8 m at latitude 38 degree) digital elevation model of Ocean City, Maryland. The bathymetry was developed based on the hydrographic survey data from NGDC's NOS Hydrographic Survey Database and US Army Corps of Engineers (USACE) survey. The topographic datasets imcoporated the Coastal Service Center (CSC) Lidar data since 2000. Medley et al. (2009) also evaluated but did not use the Shuttle Radar Topographic Mission (SRTM) Elevation 1-arc-second DEM from USGS. The Ocean City Inlet jetty on Assateague Island was digitized using ArcMap, based on USGS jetty shapefile, and was included in the final coastline. Medley et al. (2009) also stated that many of the inlets and harbors in Ocean City Harbor had not been surveyed, and therefore do not have accurate depths. These have been manually assigned a water depth of 2 m for the inlets and 3 m for the harbor.

The bathymetry and topography used in the development of this forecast model was based on a digital elevation model provided by the National Geophysical Data Center and the author considers it to be an adequate representation of the local topography/bathymetry. As new digital elevation models become available, forecast models will be updated and report updates will be posted at http://nctr.pmel.noaa.gov/forecast_reports/.

As aforementioned, the Ocean City tide gage is located in a small boat basin in the inlet, and is protected by a thin-wall of piles, which cannot be seen in the 1/3-arc-sec grid. **Figure 5a** shows the shoreline at the boat basin, which was clearly missing from the 1/3-arc-sec grid. In the present development, these piles were manually constructed to mimic the real-world sheltering of the tide gage (**Figure 5b**), although they may have been enlarged to fit the grid points.

### 3.3.3 Development of model grids

Development of an optimized tsunami forecast model for Ocean City began with the spatial extent merged bathymetric/topographic grids shown in **Figure 6-10**. A significant portion of the modeled tsunami waves, typically 4 to 10 hr of modeled tsunami time, pass through the model domain without appreciable signal degradation. **Table 2** provides specific details of both reference and tsunami forecast model grids, including extents and complete input parameter information for the model runs is provided in **Appendix 1**.

**Figure 6** shows the coverage of the A grid, which has a spatial resolution of 30 arc seconds (~ 750 m at 38°N). It is used in both the optimized tsunami forecast model and the reference model. This grid is obtained from the Pacific 30-sec database. For the reasons that were laid out in section 3.3.1, the eastern boundary of the A grid is specified at 71°W, where the water depth ranges from 2,000 m to more than 4,000 m. The northeastern corner of the grid almost reaches the toe of the shelf. One can see the abrupt depth change, from 2,000 m to less then 100 m, along the continental slope. The continental shelf extends more than 100 km offshore, typically with water depths of less than 100 m and with 80% of the shelf shallower than 50 m. This grid entirely encompasses two large water bodies, Delaware Bay and Chesapeake Bay, in order to reduce the artificial effects introduced by un-natural model boundaries.

**Figure 7** and **Figure 8** show the bathymetry and topography of B grid for the optimized forecast model and the reference model. The two grids have the same model extent (Table 2) but different grid resolutions, 12 arc second (~ 290 m at latitude 38 degree) for the forecast model and 3 arc second (~ 73 m at latitude 38 degree) for the reference model. Both grids were obtained from the Ocean City 1/3-arc-sec DEM developed by NGDC (Medley et al., 2009). The eastern boundary of the B grid is located about 40 km offshore of Ocean City with a maximum water depth of 40 m. Fenwick Island and the Assateague Island are also fully entirely encompassed, and Ocean City is located at the center of B grid to reduce the numerical errors introduced by the boundary between A and B grids. The high grid resolution clearly shows the sand ripples offshore, caused by the long-term longshore sediment transport, and these may be important bathymetric features affecting tsunami propagation within the continental shelf.

To satisfy the model computing time requirement, the C grid of the optimized forecast model has a smaller coverage than that of the reference model. Although the south boundary of the forecast model includes only the northern part of Assateague Island, where there are no residents, the forecast model covers the entire 13-kilometer barrier island of Ocean City to the north. To adequately describe the Ocean City inlet jetties and the boat basin hosting the tide gage, a 1.5-arc-sec (~ 36 m at latitude 38 degree) spatial resolution was employed in the forecast model, while a 1/3-arc-sec (~ 8 m at latitude 38 degree) space resolution is used in the reference model. Both grids were based on the Ocean City 1/3-arc-sec DEM developed by NGDC (Medley et al., 2009). The eastern boundary of the forecast model is located about 8 km offshore of the Ocean City coastline with a maximum water depth of 20 m (**Figure 9**). Other than the noticeable sand ripples formed by the longshore sediment transport, Figure 8 and 9 shows the DEM clearly describes the ebb shoal at the inlet entrance due to the rehabilitation of the south jetty (Buttolph et al., 2006). The reference model has broader boundaries on the southern, eastern and northern sides than the forecast model (**Figure 10**), which provides accurate model reference to confirm whether the boundary selection of forecast model affects the modeling results.

The boat basin hosting the tide gage has a fairly small dimension of 35 m (east-west) by 70 m (south-north), which can barely represented by one grid node (~ 36 m in east-west dimension and 50 m in south-north dimension) in the forecast model. The thin wall of piles (less then 1-m wide) separating the boat basin from the inlet is therefore ignored at this level of grid resolution. However, this wall is manually added in the reference model, to be of the same length but wider than the real size (**Figure 5**). This way, the reference model can be used to evaluate the forecast model by comparing model results both at the entrance and inside the boat basin; this will be discussed in the next section.

## 4. Results and Discussion

### 4.1 Model validation

Lack of tsunami measurements in the Atlantic is a major issue of model validation for the tsunami forecast models developed for U.S. East Coast and Caribbean. An alternative approach is to employ model-to-model comparison. Unfortunately, other than this study, no known tsunami modeling for Ocean City has been conducted by any tsunami modeling or research group. Another crude validation technique is to test the model with a historical case where tsunami impact is well known at the modeling site or its vicinity, and consider the model is validated if this model gives no “surprising” results. The 1755 Lisbon tsunami is a representative case for such a model validation for Ocean City.

The earthquake source of the 1755 Lisbon tsunami is not fully understood. Previous studies have proposed several source mechanisms that may have potentially produced this basin-wide tsunami. The magnitude of the proposed earthquakes ranges from 8.0 to 9.0 (Barkan et al., 2009; Muir-Wood, 2009; Titov et al., 2009; Roger et al., 2009), while the rupture area varies between 6000 km$^2$ and 480000 km$^2$. Titov et al. (2009) compared five tsunami scenarios for different earthquake sources, and they all indicate that the tsunami impact on U.S. East Coast is minor, and is not reported or documented anywhere in United States. The preferred scenario is that of Barkan et al. (2009), which produced very similar result after comparing the tsunami records at many places in the Atlantic, particularly in the Caribbean (**Figure 11** and **Figure 12**).

This report uses the Barkan et al. (2009) scenario as a model "validation" case study for the Ocean City models. **Figure 13** shows the computed time series at the tide gage location of Ocean City. One can see that the maximum wave amplitude is about 10 cm, and the maximum wave height is about 25 cm. A tsunami of this amplitude or height, along with a 15 to 20 minutes wave period, cannot produce a significant coastal impact on the Ocean City and should be considered as a "no surprise" result. The computed maximum wave amplitude and maximum current speed in **Figure 14** indicates two offshore areas where the highest wave amplitudes of 40 cm occur: the northern part of Assateague Island up to the south jetty of the Ocean City Inlet, and the central-north of Ocean City. Both models indicate no tsunami inundation. The computational results show high-speed currents up to 50 cm/sec (about 1 knot) in the Ocean City inlet, which provides the only access point for tsunami waves to enter through the barrier islands. The currents induced by tsunami waves move faster when they pass by the offshore ripples and the ebb shoals at the inlet entrance. As the forecast model was tested for a 24-hour run, one can see that the tsunami energy has largely reduced after it passes the narrow channels and enters the ambient water body behind the barrier islands.

However, as mentioned in 3.1.1, the shoreline of Assateague Island and Fenwick Island has experienced significant changes - the two barrier islands were connected before 1850 (and before 1933 when the inlet was formed, **Figure 15**). It is noted here that to achieve a realistic model validation, the 1755 Lisbon tsunami should have been modeled based on the shoreline before 1850. However, we used the present model setup of Ocean City for this "validation" here since there are no measurements with which a comparison can be made. It may be more meaningful to evaluate the potential tsunami impact with the present model setup when struck by the 1755 Lisbon event or a similar tsunami in the future.

The results obtained from both the optimized forecast model and the reference model, when compared to each other, show a close match in wave amplitude, wave period, arrival time, and current speed. The computed time series at the tide gage (**Figure 13**) obtained from the reference model shows slightly deeper troughs than those from the forecast model, probably due to the different grid resolutions implemented for the small boat basin. **Figure 14** shows that the forecast model represents the reference model very well despite the former computing the tsunami dynamics over a smaller domain and with coarser grid resolution. The error introduced from the boundary of C grid is negligible.

## 4.2 Model stability testing using synthetic scenarios

Model stability testing using synthetic scenarios provides important case studies to test the robustness, durability, and efficiency of the developed models in the following ways:

1. Synthetic scenarios that examine the developed models' dynamics under extreme tsunami conditions. Scenarios are, usually generated by mega earthquakes or landslides, to check model stability under these conditions, and to ensure the efficiency of the forecast model during a catastrophic event.

2. Synthetic scenarios that also examine the developed models with tsunamis of medium size (amplitude and velocities). Scenarios are generated by intermediate-size earthquakes, to check model stability under small wave conditions, and to ensure the efficiency of the forecast model during a moderate event.

3. Synthetic scenarios that examine the developed models with tsunami forcing of negligible size (amplitude and velocities). Such scenarios are generated by insignificant earthquakes in distance, to guarantee the modeling results are not interfered with by the numerical noise.

4. The synthetic scenarios were selected in such a way that there is at least one test from each potential tsunami source zone. These cases are used to examine the reliability of the developed models in response to the directionality of tsunami waves.

**Table 3** summarizes the synthetic scenarios (plotted in **Figure 12**) used in the model testing. Except for the 1755 Lisbon (used as a model validation in section 4.1), other scenarios were artificially constructed from the combination of the unit sources, shown as black boxes. Table 3 gives the details of the unit sources used and their scaling coefficient for a total of eight scenarios, six with magnitude 9.3, one with magnitude 7.5 and one no-wave. Five of the magnitude-9.3 cases were selected in the Puerto Rico Trench and Hispaniola Trench since they are considered the most dangerous tsunamigenic earthquake zones in the Atlantic (ten Brink et al., 2007). The earthquake zones between the Caribbean and South American plates have been relatively inactive, and tsunami waves generated there have minor impact on the U.S. East Coast, based on the tsunami hazard assessment study by Titov et al. (2009, Chapter 2). Therefore, no synthetic scenarios were selected from this area. The magnitude-9.3 scenario from South Sandwich source zone was used as a stability test in response to different tsunami directionalities.

The synthetic scenario ATSZ 48-57, generated by an $M_w$ 9.3 earthquake from Puerto Rico Trench  that is akin to the 2004 Indian Ocean tsunami, would create catastrophic impact to Ocean City. The modeling results in **Figure 16** show that Fenwick Island and Assateague Island would be almost entirely flooded by waves up to 6 meters at the coastline. Occurring between four and five hours after the tsunami waves are generated, the flood waters impact upon the two barrier islands with strong currents at speeds of more than 5 to 6 m/s on land. After rushing into the inlet, the waves further inundate part of the coastline of West Ocean City on west bank of the inlet (**Figure 16 b**). The jetties at the inlet are both overtopped by the incoming waves. Figure 16 shows the waves amplified grow rapidly (indicated by the red and purple color) within the five-km shallow shelf seaward from the shoreline, reaching their maximum at the shoreline. The time series indicates a dominant first wave up to 1.4 m high at the tide gage followed by a series of smaller waves with a maximum trough of 1 m (**Figure 17**). The modeled time series after 12 hours demonstrates a lengthening wave period from 20 minutest to two hours, indicating possible wave resonance in the inlet. The time series computed by forecast model agrees with that of the reference model , except it shows shallower troughs.

The synthetic scenario ATSZ 38-47, despite having the same magnitude as synthetic scenario ATSZ48-57, has minor impact on the coastline of Ocean City with maximum wave amplitudes up to 2 m. The northern tip of the Assateague Island and south to the southern jetty show minor flooding at the shoreline. After passing the jetties, the induced tsunami waves enter the inlet with attenuated wave amplitudes up to 0.8 m but high current speeds up to 3 m/s (**Figure 18 c** and **Figure 18 d**). Except for the inlet entrance near where the ebb shoal is located, the current speed along the shoreline is less than 1 m/s. The wave amplitude near the inlet entrance is generally larger than that everywhere else. The maximum tsunami amplitude is about 0.5 m at the tide gage. Also in contrast to ATSZ 48-57, there is no obvious wave resonance computed in the train of late waves after 12 hours (**Figure 19**).

With similar fault orientation and location, the synthetic scenarios ATSZ 58-67 and ATSZ 82-91 give analogous computational results at Ocean City. Both scenarios show minor inundation on the west side of Assateague Island and south of Ocean City harbor. **Figure 20** and **Figure 22** indicate in both scenarios waves up to 1 m in amplitude and current flows up to 0.2 m/s along the coastline. The narrow opening at the inlet entrance speeds the flow to about 2 m/s, which, in turn, affect the current fields in the south and north channels of the inlet on the west of the barrier islands, including the small boat basin hosting the tide gage. A notable feature of the time series at the tide gage in both scenarios (**Figure 21** and **Figure 23**) is the leading depression N-waves (Tadepalli and Synolakis, 1994), which propagates from the tsunami source. Unlike the Puerto Rico Trench and the Hispaniola Trench, where the North America plate was subducting southwesterly beneath the Caribbean plate, the geological setting at ATSZ 58-67 and ATSZ 82-91 features submarine troughs – the Cayman Trough at ATSZ 58-67 and Los the Muertos Trough at ATSZ 82-91. The Cayman Trough is a complex transform fault zone bounded by strike-slip faults, while the Los Muertos trough is formed by northerly dipping Caribbean Plate and associated seismic zones (in contrast to the south-dipping Puerto Rico – Lesser Antilles subduction zone described in LaForge and McCann (2005)). The northerly dipping of the Los Muertos Trough results in an uplift at its south, but a subsidence at the north, which corresponds to the leading depression when the tsunami waves propagate in the Atlantic. ATSZ 58-67 in the Cayman Trough disturbs the water surface in a similar, but more conservative way by simulating these faults using a subducting mechanism rather than a strike-slip mechanism.

The synthetic scenario of ATSZ 68-77 is a special case that highlights two important characteristics of tsunami waves: wave period and late waves. The computed time series at the Ocean City tide gage shows that the wave period of ATSZ 68-77 scenario, approximately one and half to two hours in length, is considerably longer than most other tsunami waves. The wave amplitude did not reach its maximum until almost 20 hours after the tsunami was generated, while the first wave had arrived about six hours into the event. When comparing the modeling results between the forecast model and the reference model for the first nine hours, one can see excellent match in both the computed wave amplitude and flow speed (**Figure 24** and **Figure 25**), although the latter was only computed up to nine hours after the tsunami was generated. **Figure 26** shows the computed maximum wave amplitude and flow speed after a 24-hour model run, which indicates greater tsunami impact in the coast of Ocean City due to larger late waves that are obviously not present in the nine-hour modeling results. The synthetic scenario of ATSZ 68-77 stresses the need of retaining the tsunami warning or watch for more than 24 hours for the coasts of Ocean City during a real tsunami event.

Excellent agreement was also found between the forecast model and reference model for the synthetic scenario of SSSZ 1-10 (**Figure 27** and **Figure 28**), which represents a Mw 9.3 earthquake-generated tsunami waves from South Sandwich source zone. The model results show wave amplitudes of 50 to 80 cm along the coastline and the flow speeds in the inlet of approximately 1 m/s. The maximum wave amplitude at the tide gauge is only of the order of 25 cm and there is very limited impact to the coastline. Similar to ATSZ 68-77, the largest wave arrives about five hours later than the first wave, probably due to the reflected waves from Africa.

The synthetic scenario of magnitude 7.5, ATSZ b52, produces wave amplitudes up to 5 cm along the shoreline of Ocean City, and 1 cm at the tide gauge. Both the forecast model and reference model show good agreement and stability in terms of maximum wave amplitudes, flow speed (**Figure 29**) and the time series at the tide gage (**Figure 30**).

## 5. Summary and conclusions

Ocean City of Maryland is a city built on a strip of barrier islands in the Atlantic. While providing popular recreation to attract tourists from all over the world, Ocean City is also known for its vulnerability to potential coastal hazards such as beach erosion, sea level change, storm surge and tsunamis, which pose challenging, yet long-standing tasks for the Ocean City community on how to protect lives and property. Previous studies for Ocean City have assessed the hazards posed by, and developed forecast methodologies for beach erosion, sea level change and storm surge. However, tsunami forecast and hazard assessment in Ocean City remains significantly understudied, probably due to the minor impact and infrequent occurrence of tsunamis throughout Ocean City’s history.

The tsunami forecast model developed in this study for the community of Ocean City, Maryland is being implemented into NOAA’s tsunami forecast system. It will provide real-time modeling forecasts of tsunami wave characteristics, runup and inundation along Ocean City’s coastline. Discussion of the details of each of the individual components of the forecast model, including the bathymetry and topography, the basic model setup, and the model parameters are provided in the report. The forecast model employs grids as fine as 36 m and can accomplish a four-hour simulation after tsunami arrival in 20 minutes of computer CPU time. A reference model was developed in parallel using grids as fine as 8 m to provide a basis for evaluating the performance of the forecast model.

Due to a lack of historical tsunami records, the 1755 Lisbon tsunami is used as a model validation case to show the Ocean City models do not produce “surprising” results. Based on the Barkan et al. (2009) source of the 1755 tsunami, the modeling results showed a 40 cm maximum wave amplitude in the nearshore of Ocean City and 10 cm at the tide gage, with no tsunami inundation. The highest current speed was about 50 cm/sec in the Ocean City inlet. It is noted that the modeling in Ocean City of 1755 Lisbon tsunami was based on present bathymetric and topographic features, instead of those present at that time, when Fenwick Island and Assateague Island were connected before the storm opened an inlet between them in 1933. The results from both the forecast model and the reference model showed excellent agreement in wave amplitude, wave period, arrival time, and current speed.

A total of eight synthetic scenarios, including six of catastrophic and one of small-size, were used to examine the stability of the developed forecast model and reference model for Ocean City. The synthetic scenarios were selected in such a way that at least one from each of the Puerto Rico Trench, Hispaniola Trench and South Sandwich source zones were tested. Both the forecast model and reference model give stable, and consistent between the two models. The results for the synthetic scenarios encompass tsunami waves emanating from different source locations and different directionalities. Other than testing the model stability, these synthetic scenarios are also useful in summarizing some of the characteristics common to tsunami waves generated from these source zones.

1. A magnitude of 9.3 earthquake in Puerto Rico Trench, represented by ATSZ 48-57 in this report, may generate a catastrophic tsunami for many communities in the Atlantic coast of United States. The modeling results show such a tsunami inundated most of the barrier islands, upon which Ocean City is built on, with a maximum wave amplitude of 6 m along the coastline and 5 to 6 m/s current speed on land.

2. Tsunamis caused by a magnitude of 9.3 earthquake from other source zones pose less threatening impacts on Ocean City. These source zones include the Lesser-Antilles (scenario ATSZ 38-47), Hispaniola Trench (scenario ATSZ 58-67), Cayman Trough (scenario ATSZ 68-77), Los Muertos Trough (scenario ATSZ 82-91) and South Sandwich source zone (scenario SSSZ 1-10).

3. Tsunamis generated from submarine troughs display a leading depression when propagating in the Atlantic toward U.S. East Coast. The northerly dipping of the Los Muertos Trough (scenario ATSZ 82-91) results in uplift at its south, but subsidence at the north, which corresponds to the leading depression. The faults in Cayman Trough (scenario ATSZ 68-77) were simulated using a subducting mechanism rather than a strike-slip mechanism.

4. For tsunamis generated in the Cayman trough or in South Sandwich source zone, the model simulations show the late waves are higher than the first waves and may pose larger impact to Ocean City's coastline. Along with these waves are longer wave period up to one and half hours. This demonstrates the need of retain the tsunami warnings or watches for more than 24 hours for the coasts of Ocean City during a real tsunami event.

All model validation and stability tests demonstrated that both the forecast and reference models for Ocean City, Maryland, are robust and efficient in their application towards both the short-term real-time forecasting of tsunami and the long-term investigation of the tsunami inundation, although model accuracy still requires validation using future real events. The optimized forecast model developed for Ocean City, Maryland provides a four-hour forecast of first wave arrival, amplitudes, and inundation within 20 minutes based on the testing presented in this report.

6. Acknowledgements

The author wish to thank Edison Gica and Jean Newman for their work with the propagation database, Burak Uslu for providing propagation database tabular unit source information and graphics, and the entire modeling group of NCTR for helpful suggestions and discussion. The author especially acknowledges and thanks Marie C. Eble for providing invaluable technical assistance and for editorial review. Collaborative contribution of the National Weather Service, the National Geophysical Data Center, and the National Data Buoy Center were invaluable.

Funding for this publication and all work leading to development of a tsunami forecast model for Kodiak, Alaska was provided by the National Oceanic and Atmospheric Administration. This publication was partially funded by the Joint Institute for the Study of the Atmosphere and Ocean (JISAO) under NOAA Cooperative Agreement NO. NA17RJ1232, JISAO Contribution No. 1763. This is PMEL Contribution No. 3343.

7. References:

Burwell, D., E. Tolkova, and A. Chawla (2007), Diffusion and dispersion characterization of a numerical tsunami model, *Ocean Modeling*, 19, 10-30.

Barkan, R., U.S. ten Brink, and J. Lin (2009), Far filed tsunami simulations of the 1755 Lisbon earthquake: implications for tsunami hazards to the U.S. East Coast and the Caribbean, *Marine Geology*, 264, 109-122, doi: 10.1016/j/margeo.2008.10.010.

Buttolph, A.M., W.G. Grosskpf, G.P. Bass, and N.C. Kraus (2006), Natural sand bypassing and response of ebb shoal to jetty rehabilitation, Ocean City Inlet, Maryland, USA, *Proceedings 30$^{th}$ Coastal Engineering Conference*, World Scientific Press, 3,344-3,356.

Dean, R.G., and Perlin, M. (1977). Coastal engineering study of Ocean City Inlet, Maryland. *Proc. Coastal Sediments '77*, ASCE, 520-542.

Everts, C. H. (1985).Effect of sea level rise and net sand volume change on shoreline position at Ocean City, Maryland. Chapter 3 in Potential Impacts of Sea level Rise on the Beach at Ocean City, Maryland, *United States Environmental Protection Agency EPA 230-10-85-013*.

Geist, E.L., P.J. Lynett and J.D. Chayton (2009), Hydrodynamic modeling of tsunamis from the Currituck landslide, *Marine Geology*, 264, 41-52.

Gica, E., M. Spillane, V.V. Titov, C. Chamberlin, and J.C. Newman (2008), Development of the forecast propagation database for NOAA's Short-term Inundation Forecast for Tsunamis (SIFT). NOAA Tech. Memo. OAR PMEL-139, 89 pp.

LaForge, R.C. and W.R. McCann (2005). A seismic source model for Puerto Rico, for use in probabilistic ground motion hazard analyses, Active Tectonics and Seismic Hazards of Puerto Rico, the Virgin Islands, and Offshore Areas, edited by P. Mann, The Geological Society of America special Paper 385, 223-248.

Leatherman, S.P. (1979). Migration of Assateague Island, Maryland, by inlet and overwash processes, *Geology*, 7, 104-107.

Leatherman, S.P. (1982). Barrier island handbook. College Park, Md.: University of Maryland, 109pp.

Leatherman, S.P. (1984). Shoreline evolution of North Assateague Island, Maryland. *Shore and Beach*, 52, 3-10.

Leatherman, S. P. (1985). Geomorphic effects of accelerated sea level rise on Ocean City, Maryland. Chapter 2 in Potential Impacts of Sea level Rise on the Beach at Ocean City, Maryland, *United States Environmental Protection Agency EPA 230-10-85-013*, 33-66.

Lockridge, P.A., L.S. Whiteside, J.F. Lander (2002), Tsunamis and tsunami-like waves of the eastern United States, *Science of Tsunami Hazards*, 20(3), 120-157.

Medley, P.R., L.A. Taylor, B.W. Eakins, R.R. Warnken, K.S. Carignan, E. Lim, R.J. Caldwell, and D.Z. Friday (2009), Digital elevation model of Ocean City, Maryland: procedures, data sources and analysis, prepared for the Pacific Marine Environmental Laboratory (PMEL) – NOAA Center for Tsunami Research, Cooperative Institute for Research in Environmental Sciences, Univeristy of Colorado at Boulder, and NOAA National Geophysical Data Center, Boulder, Colorado, 36p.

Muir-Wood, R. and A. Mignan (2009), A phenomenological reconstruction of the Mw9 Novermber 1st 1755 earthquake source, *The 1755 Lisbon Earthquake: Revisited*, *Geotechnical, Geological, and Earthquake Engineering*, 7, Part III, 121-146, doi: 10.1007/978-1-4020-8609-0_8.

Natural Resource Canada (2006), Earthquakes Canada; Canadian Hazard Information Service. Historic Earthquakes Web Pages, http://earthquakescanada.nrcan.gc.ca/

Pasad, R., E. Cunningham, and G. Bagchi (2009), Tsunami hazard assessment at nuclear power plant sites in the United States of America – Final Report, United States Nuclear Regulatory Commission, NUREG/CR-6966 and PNNL-17397, NRC Job Code J3301, Office of New Reactors, p84.

Prior, D.P., Doyle, E.H., and Neurauter, T. (1986), The Currituck Slide, Mid Atlantic continental slope-revisited, *Marine Geology*, V73, p25-4.

Roger, J., S. Allgeyer, H. Hebert, M.A. Baptista, A. Loevenbruck, F. Schindele (2009), The 1755 Lisbon tsunami in guadeloup Archipelago: source sensitivity and investigation of resonance effects, *The Open Oceanography Journal*, 3, 1-13.

Ruffman, A (1996). Tsunami runup mapping as an emergency preparedness planning tool: the 1929 tsunami in St. Lawrance, Newfoundland. *Geomarine Associates Ltd.*, Contract Report for Emergency Preparedness Canada (EPC), Office of the Senior Scientific Advisor, Ottawa, Ontario, V1 – Report, 107 pp.; V2 – Appendices and Enclosures, 281 pp.

Synolakis, C.E., E.N. Bernard, V.V. Titov, U. Kânoğlu, and F.I. González (2008): Validation and verification of tsunami numerical models. *Pure Appl. Geophys.*, *165*(11–12), 2197–2228.

Tadepalli, S. and C.E. Synolakis (1994). The run-up of N-waves on sloping beaches. Proc. R. Soc. A 445, 99-112.

Tang, L., V.V. Titov, Y. Wei, H.O. Mofjeld, M. Spillane, D. Arcas, E.N. Bernard, C. Chamberlin, E. Gica, and J. Newman (2008): Tsunami forecast analysis for the May 2006 Tonga tsunami. *J. Geophys. Res.*, *113*, C12015, doi: 10.1029/2008JC004922.

Tang, L., V. V. Titov, and C. D. Chamberlin (2009), Development, testing, and applications of site-specific tsunami inundation models for real-time forecasting, J. Geophys. Res., 114, C12025, doi:10.1029/2009JC005476.

ten Brink, U., D. Twichell, E. Geist, J. Chaytor, J. Locat, H. Lee, B. Buczkowski, R. Barkan, A. Solow, B. Andrews, T. Parsons, P. Lynett, J. Lin, and M. Sansoucy (2008): Evaluation of tsunami sources with the potential to impact the U.S. Atlantic and Gulf coasts, *USGS Administrative report to the Nuclear Regulatory Commission*, 300pp.

Titov, V.V. (2009): Tsunami forecasting. Chapter 12 in *The Sea, Volume 15: Tsunamis*, Harvard University Press, Cambridge, MA and London, England, 371–400.

Titov, V.V, E. Gica, M. Spillane, Y. Wei, C. Moore, H. Zhou and R. Weiss (2009), Tsunami hazard assessment for the U.S. East Coast based on generation, propagation and inundation modeling, *NCTR Letter Report to the Nuclear Regulatory Commission*, 117pp.

Titov, V., and F.I. González (1997): Implementation and testing of the Method of Splitting Tsunami (MOST) model. NOAA Tech. Memo. ERL PMEL-112 (PB98-122773), NOAA/Pacific Marine Environmental Laboratory, Seattle, WA, 11 pp.

Titov, V.V., F.I. González, E.N. Bernard, M.C. Eble, H.O. Mofjeld, J.C. Newman, and A.J. Venturato (2005): Real-time tsunami forecasting: Challenges and solutions. Nat. Hazards, 35(1), Special Issue, U.S. National Tsunami Hazard Mitigation Program, 41–58.

Titov, V.V., A.B. Rabinovich, H.O. Mofjeld, R.E. Thomson, and F.I. González (2005), The global reach of the 26 December 2004 Sumatra Tsunami. *Science*. doi: 10.1126/science.1114576.

Titus. J. G., K.E. Anderson, D.R. Cahoon, D.B. Gesch, S.K. Grll, B.T. Gutierrez, E. R. Thieler and S.J. Willams (2009), Coastal sensitivity to sea-level rise: a focus on the mid-Atlantic region. *Report by the U.S. Climate Change Science Program and the Subcommittee on Global Change Research: Synthesis and Assessment Product 4.1*, p298.

Titus, J.G., S. P. Leatherman, C.H. Everts, D.L. Kriebel and R.G. Dean (1985), Potential impacts of sea level rise on the beach at Ocean City, Maryland. *United States Encironmental Protection Agency*, 27pp.

Wei, Y., E. Bernard, L. Tang, R. Weiss, V. Titov, C. Moore, M. Spillane, M. Hopkins, and U. Kânoğlu (2008): Real-time experimental forecast of the Peruvian tsunami of August 2007 for U.S. coastlines. *Geophys. Res. Lett.*, *35*, L04609, doi: 10.1029/2007GL032250.

Tables:

Table 1: Historical tsunami events that have affected the central north of the U.S. East Coast, including Ocean City, Maryland.

Table 2: MOST setup parameters for the reference and forecast models for Ocean City, Maryland.

Table 3: Synthetic tsunami events – Atlantic.

Table 1. Historical tsunami events that have affected central north of U.S. East Coast, including Ocean City, Maryland

| Event | Date, Time (UTC), Epicenter | Magnitude | Earthquake source area |
|---|---|---|---|
| 1755 Lisbon | 01 Nov. 10:16:00, 36.0ºN 11.0ºW | 8.5 – 9.0 | Portugal: Lisbon |
| 1817 Philadelphia | 08 Jan, 39.95ºN 75.1ºW | ? | Philadelphia |
| 1821 | 03 Sep | / | Meteorological |
| 1840 Philadelphia | 11 Nov, 39.8ºN 75.2ºW | 5.2 | Philadelphia |
| 1871 New York | 18 Jun, 40.5ºN 73.9ºW | ? | New York |
| 1884 New York | 10 Aug 10:07:00, 40.6ºN 73.75ºW | 5.5 | New York |
| 1895 New Jersey | 1 Sep 11:09:00, 40.667ºN 74.883ºW | 4.3 | New Jersey |
| 1913 | 9 Jun | / | Unknown |
| 1918 Puerto Rico | 11 Oct 14:14:00 18.5ºN 67.5ºW | 7.3 | Atlantic (ATSZ) |
| 1923 | 6 Aug | / | Unknown |
| 1924 | 8 Aug | / | Unknown |
| 1929 Grand Banks | 18 Nov 20:32:00, 44.69ºN 56.0ºW | 7.2 | Canada: Grand Banks |
| 1931 | 19 Aug | / | Meteorological |
| 1932 | 10 Nov | / | Meteorological |
| 1938 | 21 Sep | / | Meteorological |
| 1944 | 14 Sep | / | Meteorological |
| 1946 Dominican Republic | 4 Aug 17:51:6.0, 19.3ºN 68.9ºW | 7.8 | Atlantic (ATSZ) |
| 1946 Dominican Republic | 8 Aug 13:28:0.0, 19.71ºN 69.51ºW | 7.4 | Atlantic (ATSZ) |
| 1964 | 19 May | / | Possibly a submarine landslide |
| 2004 Sumatra | 26 Dec 00:58:53.4, 3.295ºN 5.982ºE | 9.0 - 9.3 | Indian Ocean (IOSZ) |

Table 2: MOST setup parameters for reference and forecast models for Ocean City, Maryland.

| | | Reference Model | | | | Forecast Model | | | |
|---|---|---|---|---|---|---|---|---|---|
| Grid | Region | Coverage Lat. [ºN] Lon. [ºW] | Cell Size [“] | nx x ny | Time Step [sec] | Coverage Lat. [ºX] Lon. [ºX] | Cell Size [“] | nx x ny | Time Step [sec] |
| A | Central north of U.S. East Coast | 36.5 - 39.7<br>77.5 – 71.0 | 30” | 781 × 385 | 3.2 | 36.5 - 39.7<br>77.5 – 71.0 | 30” | 781 × 385 | 3.6 |
| B | East of Maryland and Delaware | 37.75-38.85<br>75.5 – 74.75 | 3” | 901 × 1321 | 2.8 | 37.75-38.85<br>75.5 – 74.75 | 12” | 226 × 331 | 12.6 |
| C | Ocean City | 75.1749878 – 74.9500122 | 1/3” | 2431 × 2809 | 0.4 | 38.30 -38.42<br>75.175 – 75.0 | 1.5” | 421 × 289 | 1.8 |
| Minimum offshore depth [m] | | | | 1.0 | | | | 1.0 | |
| Water depth for dry land [m] | | | | 0.1 | | | | 0.1 | |
| Friction coefficient [$n^2$] | | | | 0.0009 | | | | 0.0009 | |
| CPU time for 4-hr simulation | | | | ~ 37 hours | | | | ~ 20 minutes | |

Computations were performed on a single Intel Xeon processor at 3.6 GHz, Dell PowerEdge 1850.

Table 3. Synthetic tsunami events – Atlantic

| Sce. No | Scenario Name | Source Zone | Tsunami Source | α (m) |
|---|---|---|---|---|
| | | **Mega-tsunami scenario** | | |
| 1 | ATSZ 38-47 | Atlantic | A38-A47, A38-A47 | 25 |
| 2 | ATSZ 48-57 | Atlantic | A48-A57, B48-B57 | 25 |
| 3 | ATSZ 58-67 | Atlantic | A58-A67, B58-B67 | 25 |
| 4 | ATSZ 68-77 | Atlantic | A68-A77, B68-B77 | 25 |
| 5 | ATSZ 82-91 | Atlantic | A82-A91, B82-B91 | 25 |
| 6 | SSSZ 1-10 | South Sandwich | A1-A10, B1-B10 | 25 |
| | | **Mw 7.5 Scenario** | | |
| 7 | ATSZ B52 | Atlantic | B52 | 1 |
| | | **Micro-tsunami Scenario** | | |
| 8 | SSSZ B11 | South Sandwich | B11 | 0.01 |

Figures:

Figure 1. (a) Aerial view of Fenwick Island, upon which Ocean City is built, and Assateague Island; (b) Closer aerial view of Ocean City Inlet.

Figure 2. Location of Ocean City tide gauge. (a) Google aerial view of south end of Ocean City and the Ocean City Inlet; (b) Location of the Ocean City tide gauge - area indicated by the red box in (a); (c) Location of Ocean City tide gauge within the boat basin (photo courtesy of http://tideandcurrents.noaa.gov).

Figure 3. Historical tsunami events that have affected central north of U.S. East Coast, The earthquake location are indicated by ● and The meteorological tsunamis are indicated by 'M'. The black boxes are the tsunami propagation unit sources (Gica et al., 2008).

Figure 4. Computed wave amplitude difference between 1-arcmin and 30 arcsec resolutions along transects in the A grid.

Figure 5. (a) Comparison of the shoreline from the DEM developed by NGDC with an aerial photo by Google. Note how the boat basin is missing from the NGDC DEM. (b) Shoreline comparison after the piles of the boat basin were manually constructed in the 1/3-arc-second grid.

Figure 6. A-grid bathymetry and topography for both the forecast model and the reference model, where the black boxes indicate the coverage of B grid and C grid. The the red circle indicates the location of Ocean City tide gauge.

Figure 7. B-grid bathymetry and topography for the forecast model, where the black box indicate coverage of the C grid in forecast model. The red circle indicates the location of Ocean City gauge.

Figure 8. B-grid bathymetry and topography for the reference model, where the black box indicate coverage of C grid in forecast model. The red circle indicates the location of Ocean City tide gauge.

Figure 9. C-grid bathymetry and topography for the forecast model, where the red circle indicates the location of Ocean City tide gauge.

Figure 10. C-grid bathymetry and topography for the reference model, where the red circle indicates the location of Ocean City tide gauge.

Figure 11. Tsunami energy projection (or computed maximum wave amplitude) of the 1755 Lisbon tsunami in the Atlantic.

Figure 12. Model scenarios used in model validation and model stability testing. Parameters of the model scenarios are listed in Table 3.

Figure 13. Comparison of computed time series between the forecast and reference models at the Ocean City tide gauge for 1755 Lisbon tsunami. The upper panel is a enlarged view of eight to 16 hours in the lower panel.

Figure 14. Computed maximum wave amplitude and maximum current speed in the C grid for the 1755 Lisbon tsunami. (a) Maximum wave amplitude in the C grid for the reference model, where the black box indicates the computational domain of the forecast model; (b) maximum wave amplitude in the C grid for the forecast model; (c) maximum current speed in the C grid for the reference model, where the black box indicates the computational domain of the forecast model; (d) maximum current speed in the C grid for the forecast model.

Figure 15. Aerial photo of northern Assateague Island and Ocean City, Maryland showing former barrier positions. Note that in 1850, a single barrier island, shown in outlined in yellow, occupied this stretch of coast. In 1933, Ocean City inlet was created by a hurricane. By 1942, the barrier south of the inlet had migrated landward (show as a green shaded region). Courtesy: Titus et al. (2009).

Figure 16. Computed maximum wave amplitude and maximum current speed in the C grid for the ATSZ 48-57 scenario. (a) Maximum wave amplitude in the C grid for the reference model, where the black box indicates the computational domain of the forecast model; (b) maximum wave amplitude in C grid computed with the forecast model; (c) maximum current speed in the C grid for the reference model, where the black box indicates the computational domain of the forecast model; (d) maximum current speed in the C grid for the forecast model.

Figure 17. Comparison of computed time series between the forecast and reference models at the Ocean City tide gauge for the ATSZ 48-57 scenario. The upper panel is an enlarged view of two to ten hours in the lower panel.

Figure 18. Computed maximum wave amplitude and maximum current speed in the C grid for the ATSZ 38-47 scenario. (a) Maximum wave amplitude in the C grid for the reference model, where the black box indicates the computational domain of the forecast model; (b) maximum wave amplitude in the C grid for the forecast model; (c) maximum current speed in the C grid for the reference model, where the black box indicates the computational domain of the forecast model; (d) maximum current speed in the C grid for the forecast model.

Figure 19. Comparison of computed time series between the forecast and reference models at the Ocean City tide gauge for the ATSZ 38-47 scenario. The upper panel is an enlarged view of two to ten hours in the lower panel.

Figure 20. Computed maximum wave amplitude and maximum current speed in the C grid for the ATSZ 58-67 scenario. (a) Maximum wave amplitude in the C grid for the reference model, where the black box indicates the computational domain of the forecast model; (b) maximum wave amplitude in the C grid for the forecast model; (c) maximum current speed in the C grid for the reference model, where the black box indicates the

computational domain of the forecast model; (d) maximum current speed in the C grid for the forecast model.

Figure 21. Comparison of computed time series between the forecast and reference models at the Ocean City tide gauge for the ATSZ 58-67 scenario. The upper panel is an enlarged view of two to ten hours in the lower panel.

Figure 22. Computed maximum wave amplitude and maximum current speed in the C grid for the ATSZ 82-91 scenario. (a) Maximum wave amplitude in the C grid for the reference model, where the black box indicates the computational domain of the forecast model; (b) maximum wave amplitude in the C grid for the forecast model; (c) maximum current speed in the C grid for the reference model, where the black box indicates the computational domain of the forecast model; (d) maximum current speed in the C grid for the forecast model.

Figure 23. Comparison of computed time series between the forecast and reference models at the Ocean City tide gauge for the ATSZ 82-91 scenario. The upper panel is an enlarged view of two to ten hours in the lower panel.

Figure 24. Computed maximum wave amplitude and maximum current speed of the first nine hours after tsunami arrival in the C grid for the ATSZ 68-77 scenario. (a) Maximum wave amplitude in the C grid for the reference model, where the black box indicates the computational domain of the forecast model; (b) maximum wave amplitude in the C grid for the forecast model; (c) maximum current speed in the C grid for the reference model, where the black box indicates the computational domain of the forecast model; (d) maximum current speed in the C grid for the forecast model.

Figure 25. Computed maximum wave amplitude and maximum current speed of 24 hours after tsunami arrival in the C grid for the ATSZ 68-77 scenario. (a) Maximum wave amplitude in the C grid for the reference model, where the black box indicates the computational domain of the forecast model; (b) maximum wave amplitude in the C grid for the forecast model; (c) maximum current speed in the C grid for the reference model, where the black box indicates the computational domain of the forecast model; (d) maximum current speed in the C grid for the forecast model.

Figure 26. Comparison of computed time series between forecast and reference models at the Ocean City tide gauge for the ATSZ 68-77 scenario. The upper panel is an enlarged view of three to 11 hours in the lower panel.

Figure 27. Computed maximum wave amplitude and maximum current speed in the C grid for the SSSZ 1-10 scenario. (a) Maximum wave amplitude in the C grid for the reference model, where the black box indicates the computational domain of the forecast model; (b) maximum wave amplitude in the C grid for the forecast model; (c) maximum current speed in the C grid for the reference model, where the black box indicates the computational domain of the forecast model; (d) maximum current speed in the C grid for the forecast model.

Figure 28. Comparison of computed time series between the forecast and reference models at the Ocean City tide gauge for the SSSZ 01-10 scenario. The upper panel is an enlarged view of 16 to 24 hours in the lower panel.

Figure 29. Computed maximum wave amplitude and maximum current speed in the C grid for the ATSZ B52 scenario. (a) Maximum wave amplitude in the C grid for the reference model, where the black box indicates the computational domain of the forecast model; (b) maximum wave amplitude in the C grid for the forecast model; (c) maximum current speed in the C grid for the reference model, where the black box indicates the computational domain of the forecast model; (d) maximum current speed in the C grid for the forecast model.

Figure 30. Comparison of computed time series between the forecast and reference models at the Ocean City tide gauge for the ATSZ B52 scenario. The upper panel is an enlarged view of three to 11 hours in the lower panel.

Figure 1a

Figure 1b

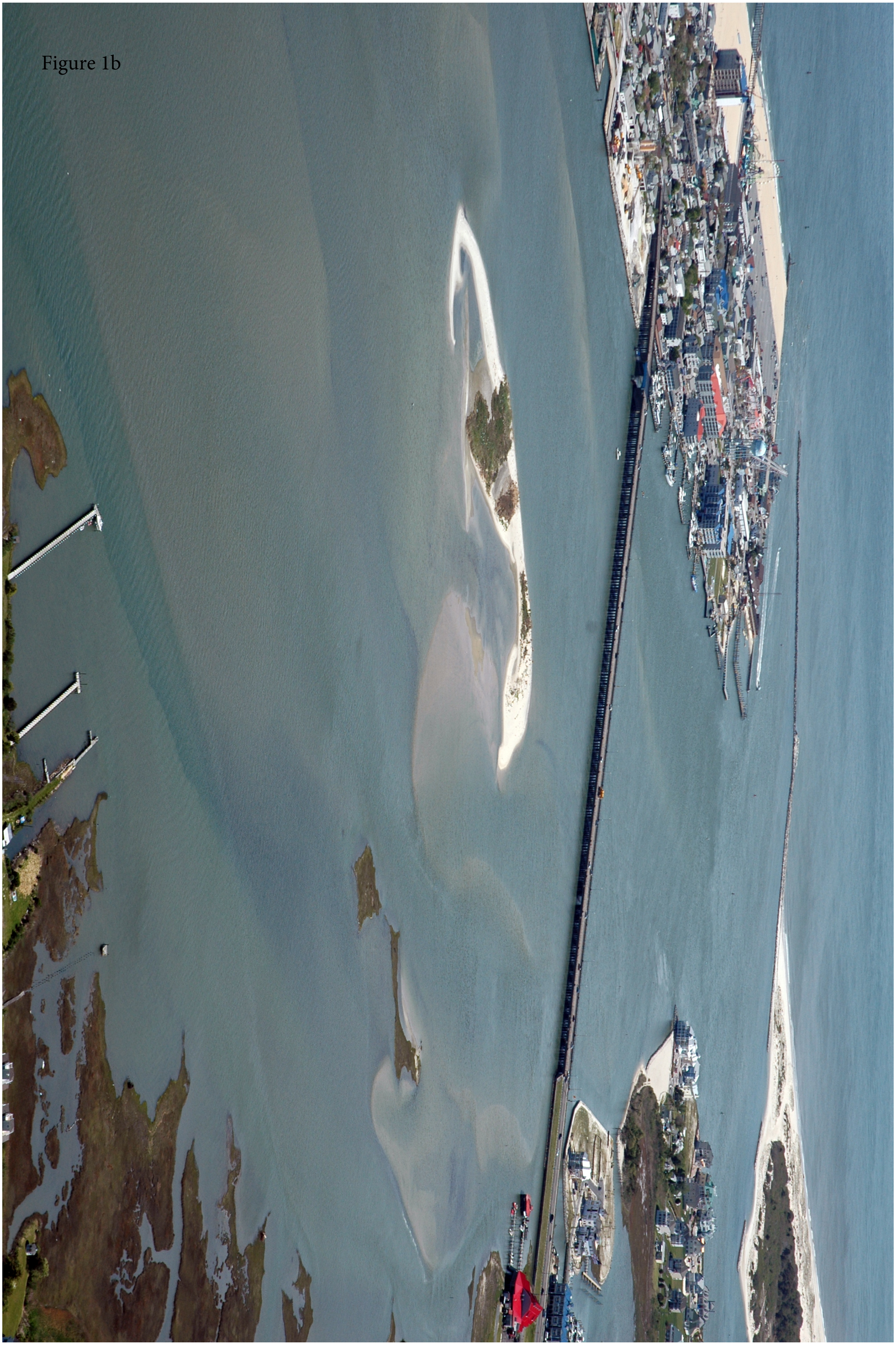

Figure 2

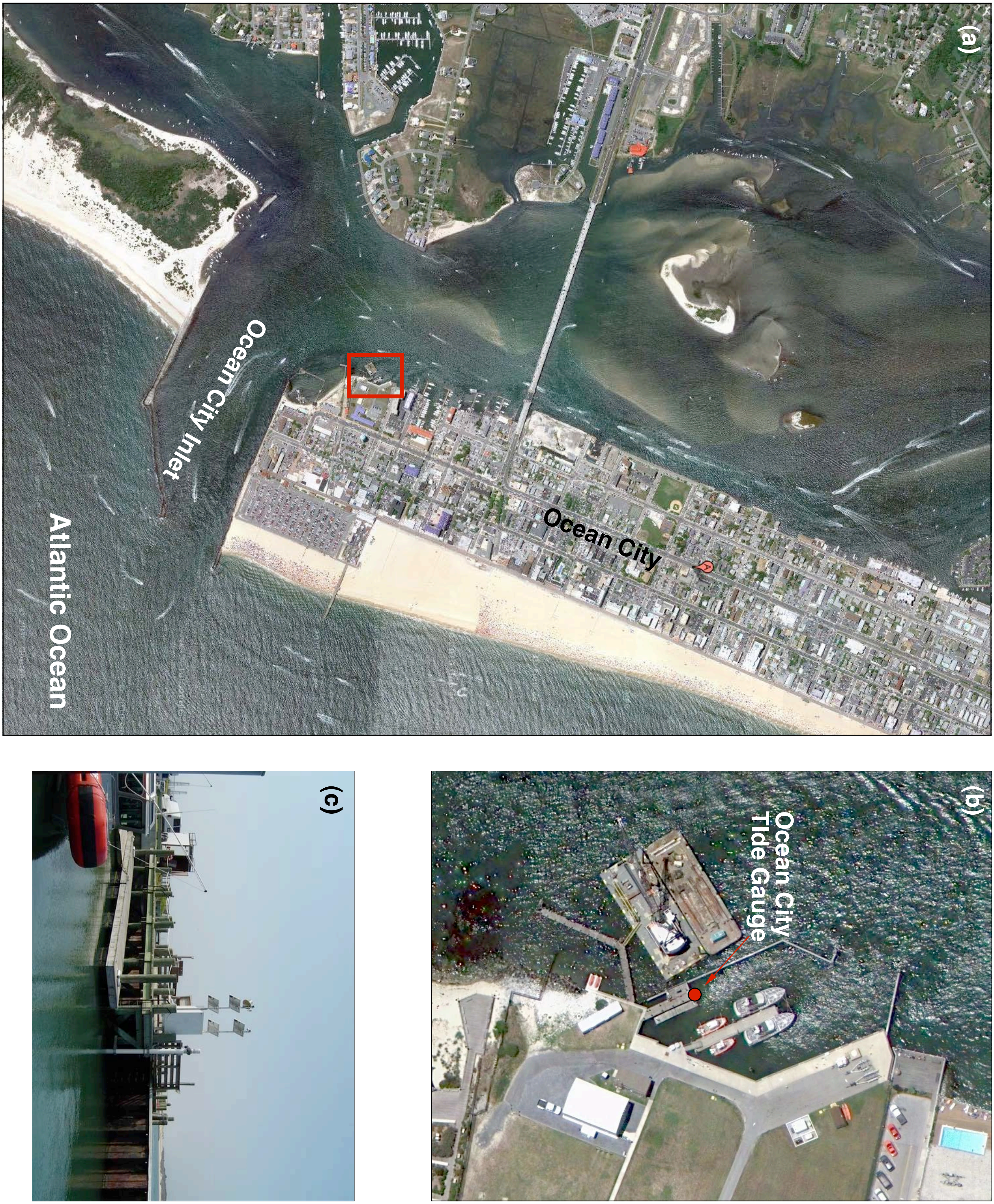
(a)
Ocean City Inlet
Atlantic Ocean
Ocean City
(b)
Ocean City
Tide Gauge
(c)

Figure 3

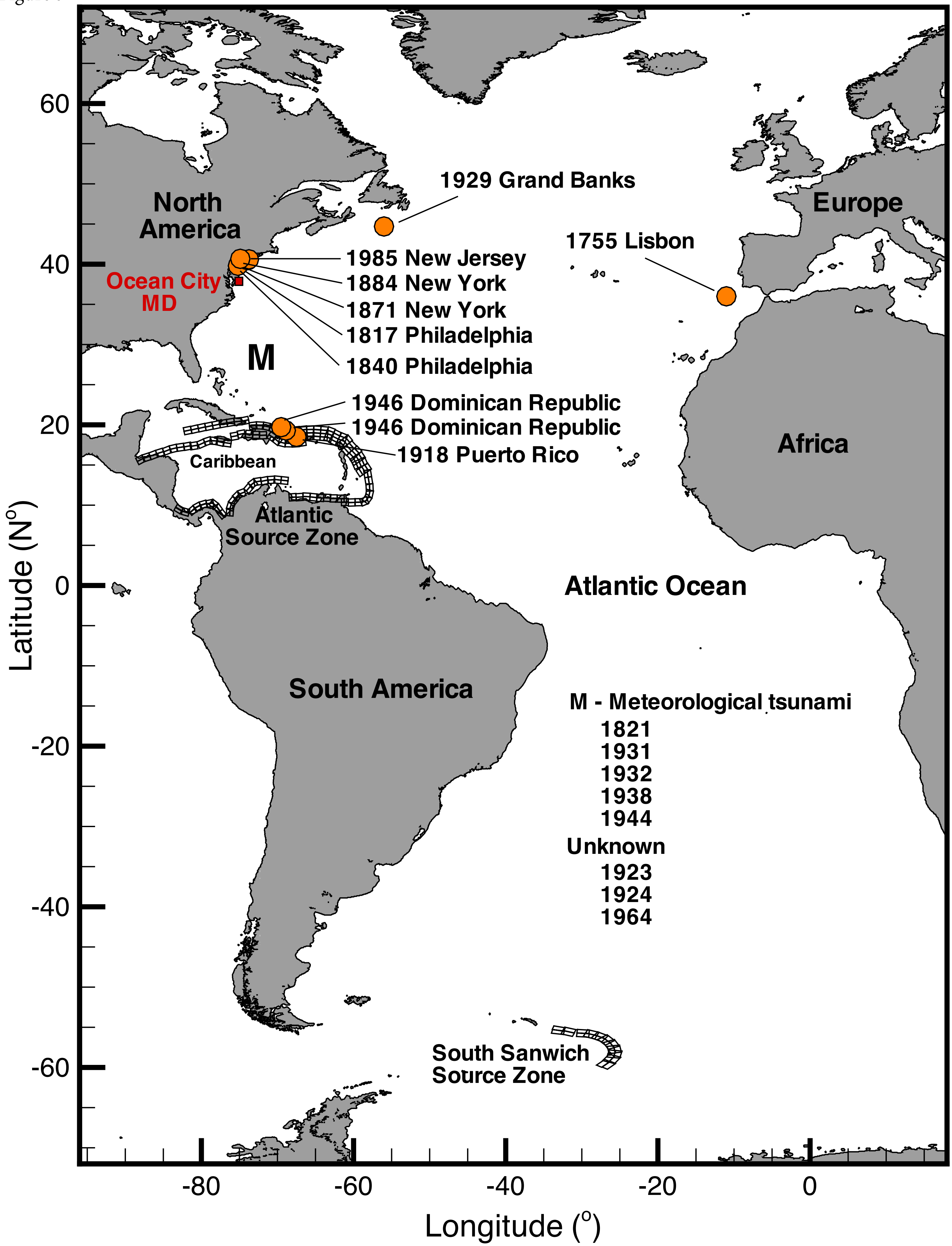

1929 Grand Banks
North America
Europe
1755 Lisbon
1985 New Jersey
Ocean City MD
1884 New York
1871 New York
1817 Philadelphia
M
1840 Philadelphia
1946 Dominican Republic
1946 Dominican Republic
1918 Puerto Rico
Caribbean
Africa
Atlantic Source Zone
Atlantic Ocean
South America
M - Meteorological tsunami
1821
1931
1932
1938
1944
Unknown
1923
1924
1964
South Sanwich Source Zone
60
40
20
0
-20
-40
-60
Latitude (N°)
-80
-60
-40
-20
0
Longitude (°)

Figure 4

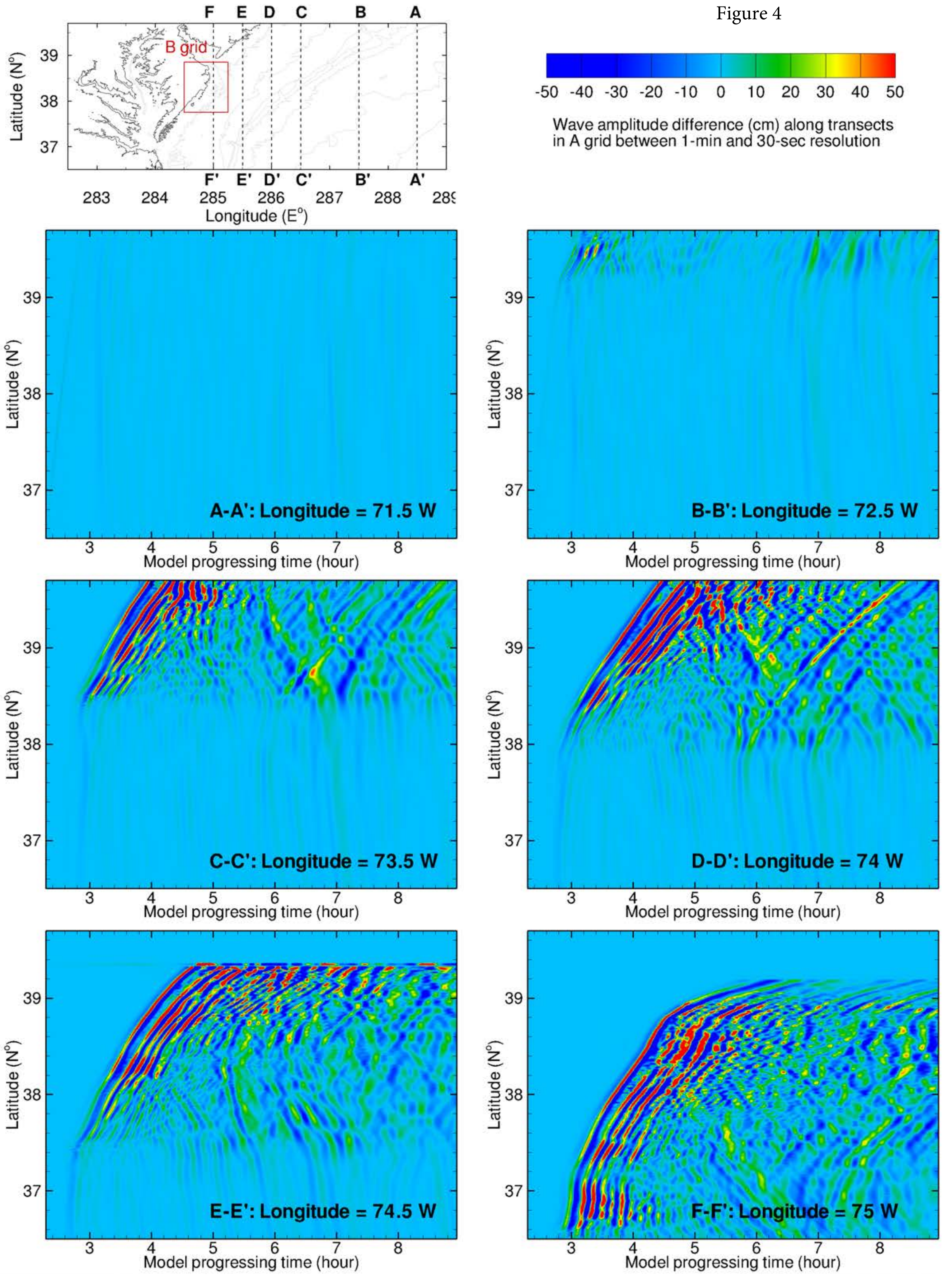

F E D C B A
B grid
Latitude (N°)
39
38
37
F' E' D' C' B' A'
283 284 285 286 287 288 289
Longitude (E°)
-50 -40 -30 -20 -10 0 10 20 30 40 50
Wave amplitude difference (cm) along transects
in A grid between 1-min and 30-sec resolution
A-A': Longitude = 71.5 W
B-B': Longitude = 72.5 W
C-C': Longitude = 73.5 W
D-D': Longitude = 74 W
E-E': Longitude = 74.5 W
F-F': Longitude = 75 W
3 4 5 6 7 8
Model progressing time (hour)

Fugure 5a

Figure 5b

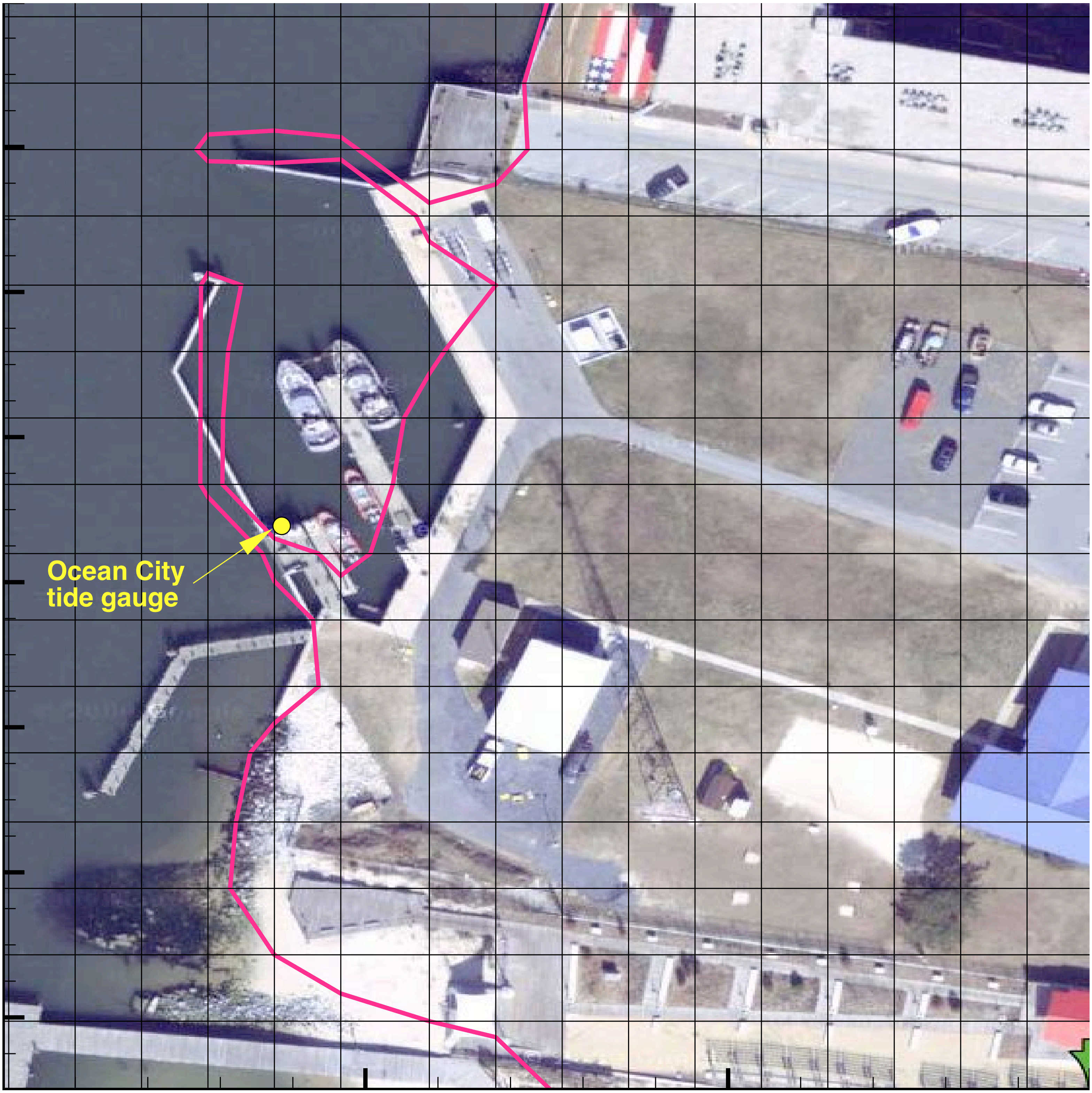

Figure 6

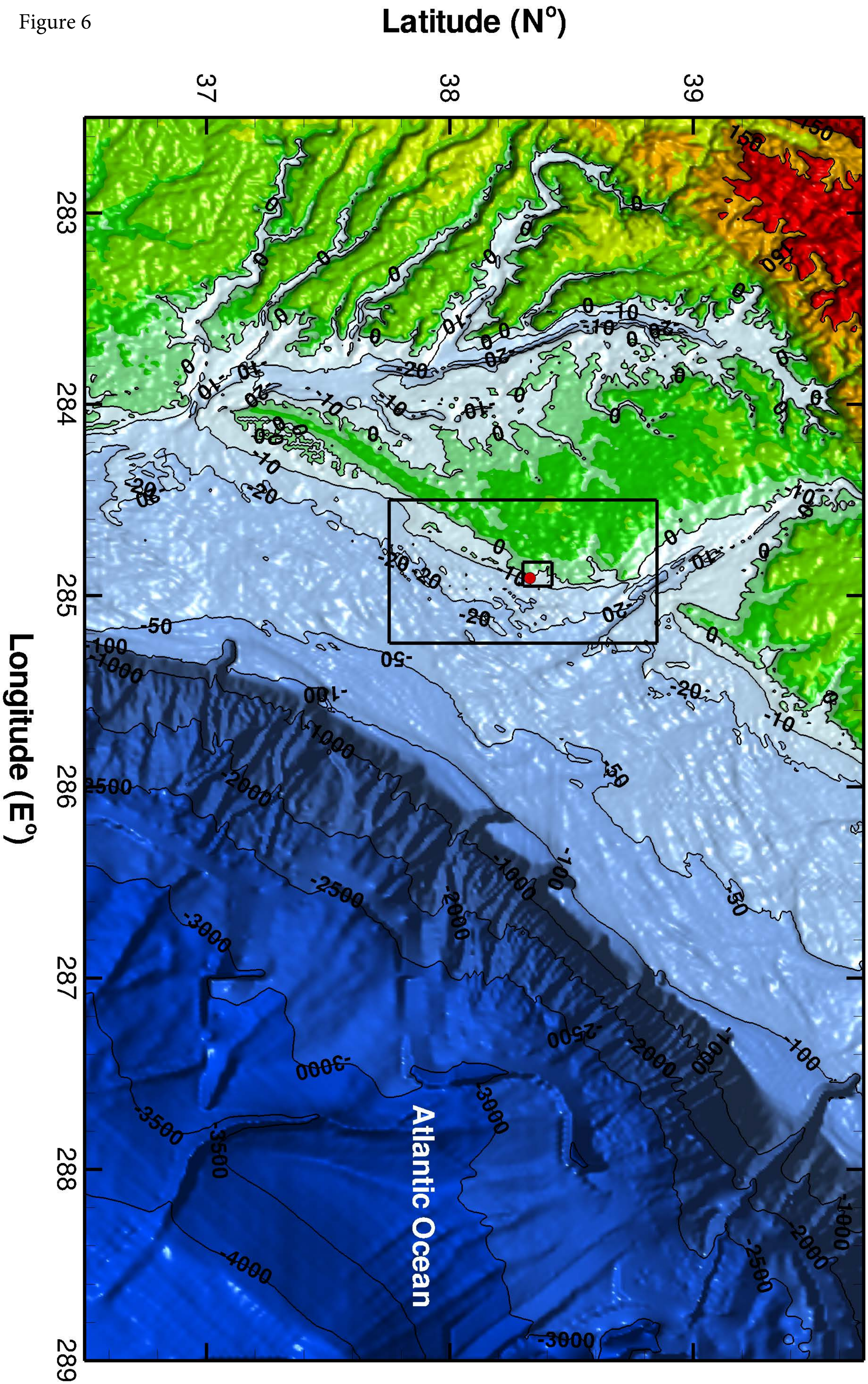

Latitude (N°)
37
38
39
Longitude (E°)
283
284
285
286
287
288
289
Atlantic Ocean

Figure 7

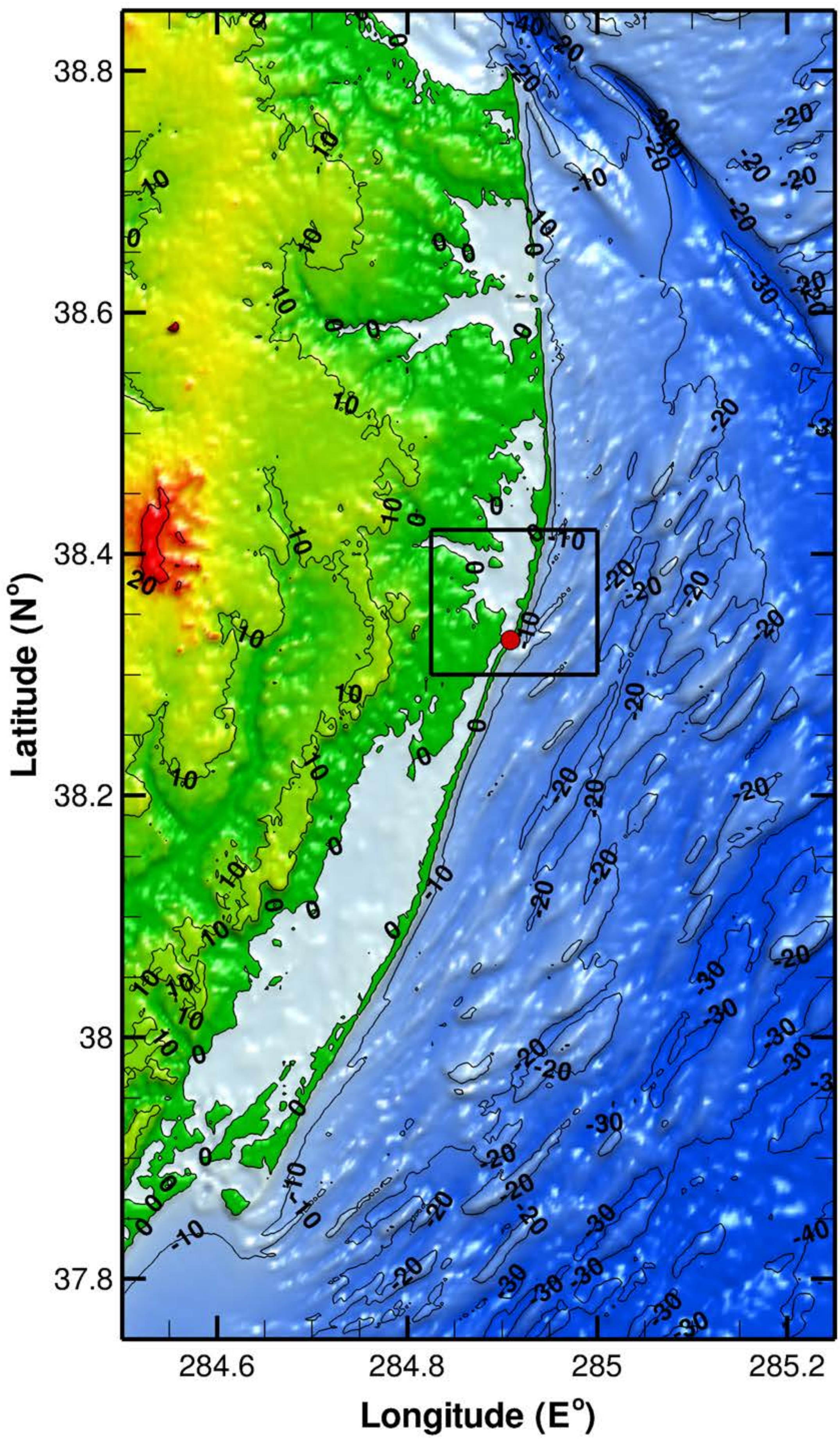

Latitude (N°)
Longitude (E°)
38.8
38.6
38.4
38.2
38
37.8
284.6
284.8
285
285.2

Figure 8

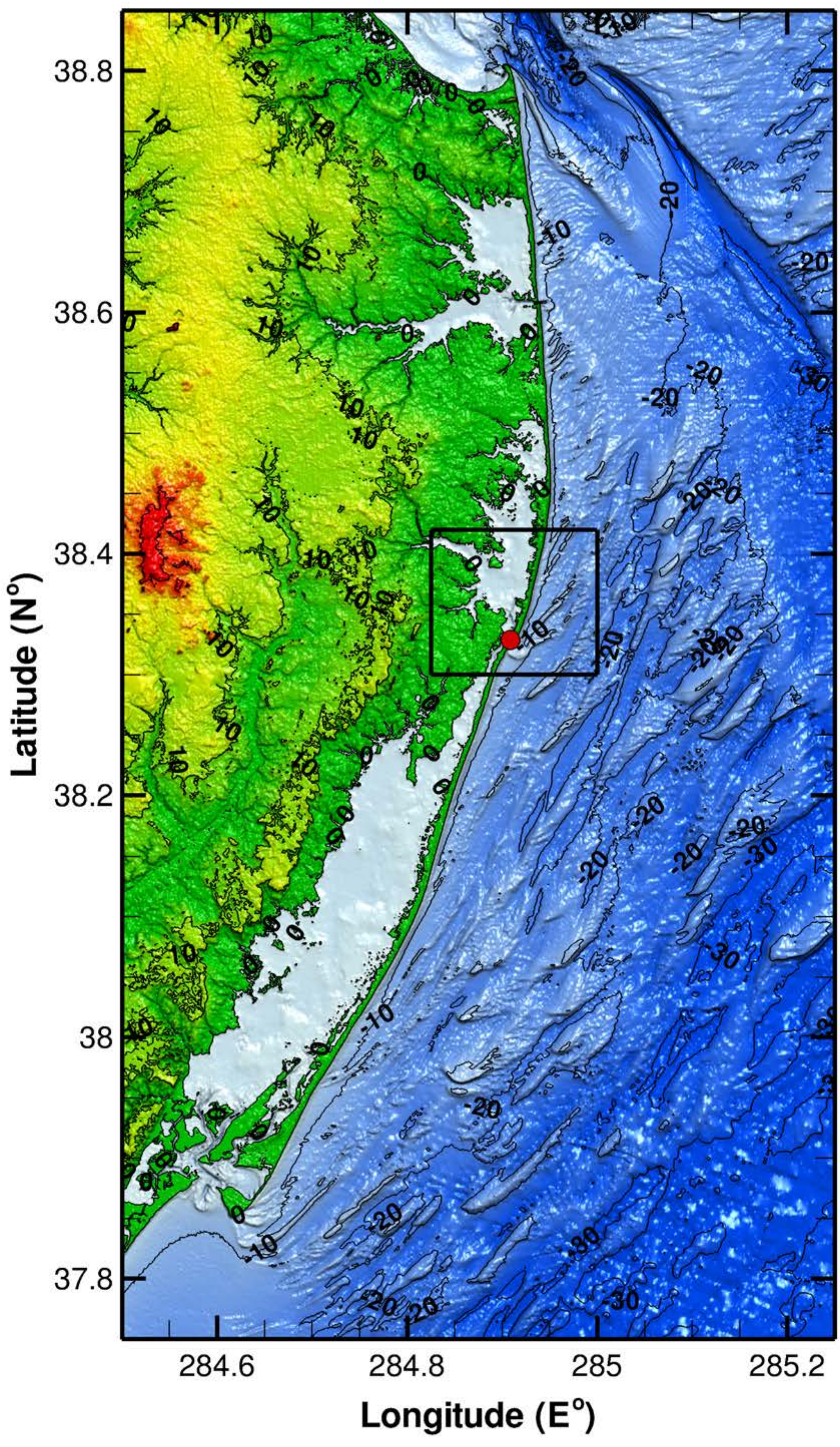

Latitude (N°)
Longitude (E°)
38.8
38.6
38.4
38.2
38
37.8
284.6
284.8
285
285.2

Figure 9

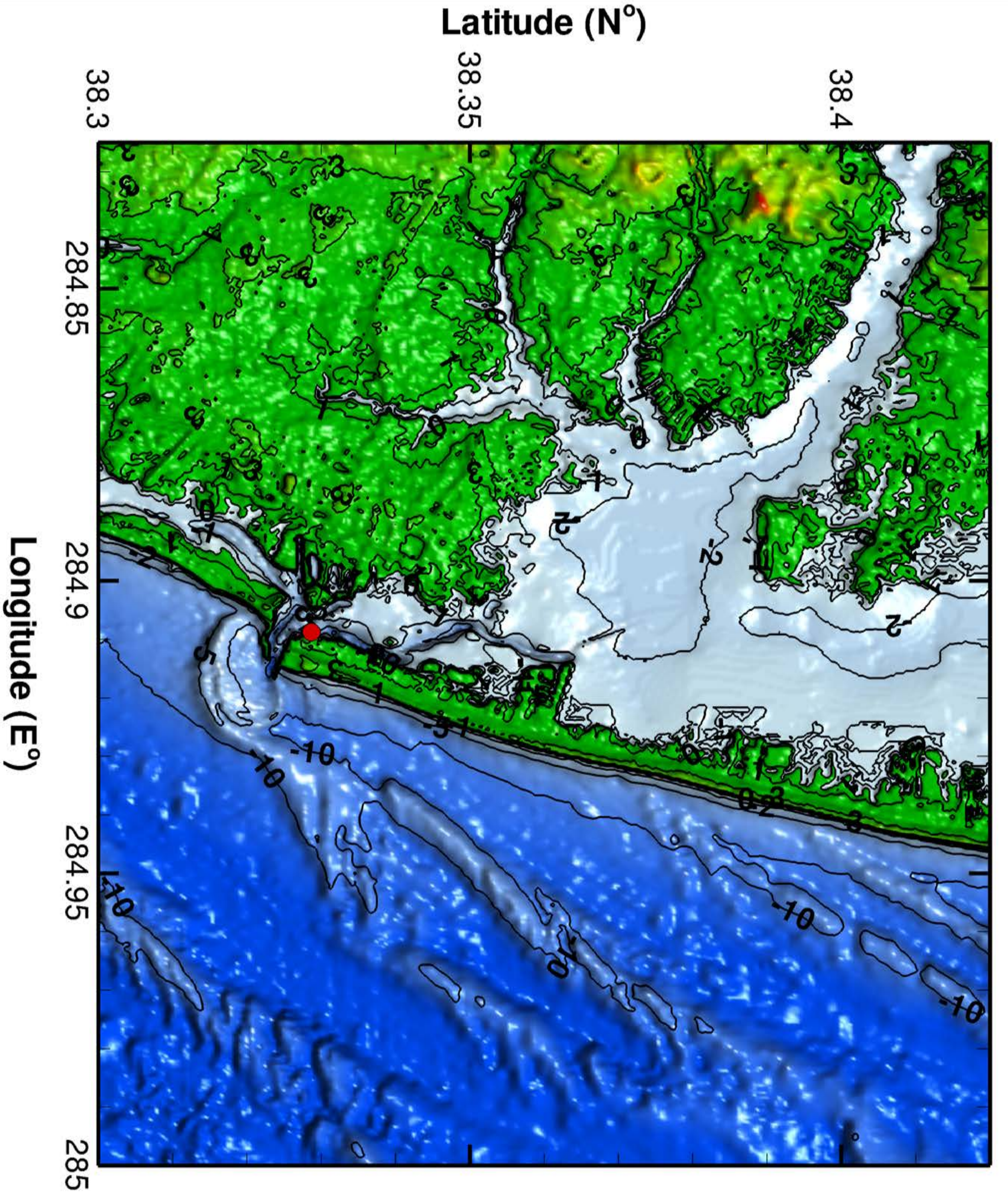

Figure 10

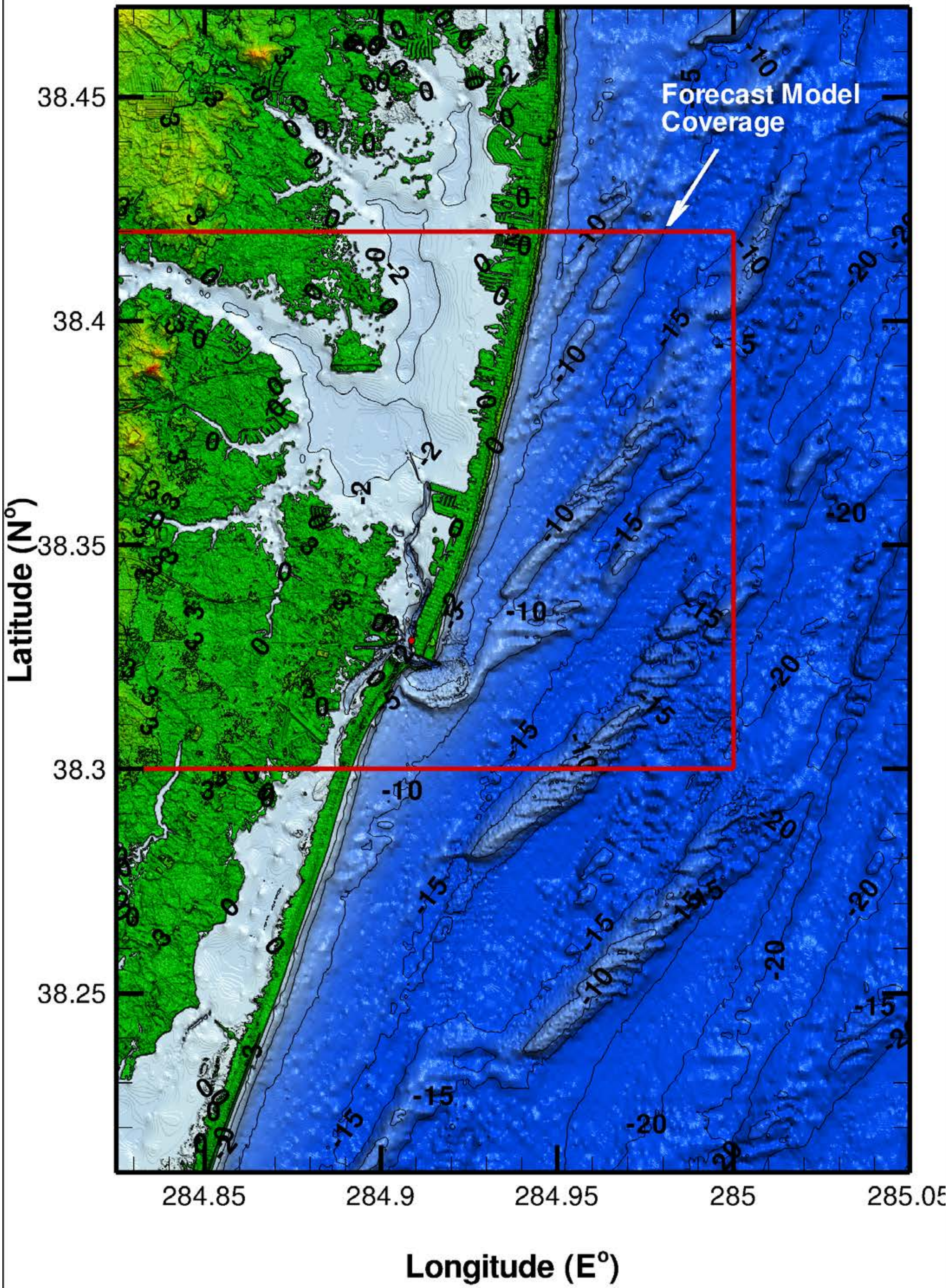
Forecast Model
Coverage
38.45
38.4
38.35
38.3
38.25
Latitude (N°)
284.85
284.9
284.95
285
285.05
Longitude (E°)

Figure 11

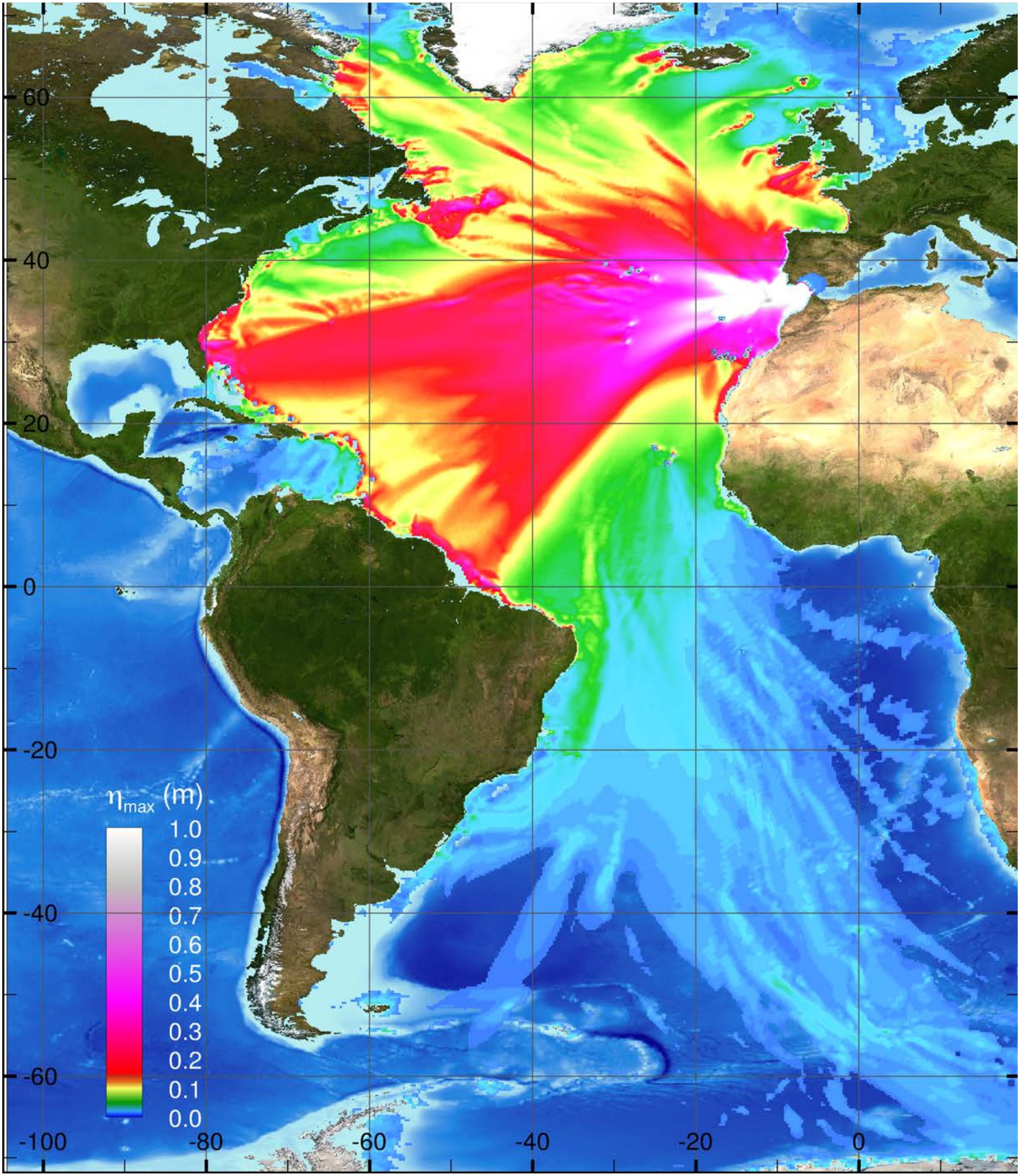

60
40
20
0
-20
-40
-60
-100
-80
-60
-40
-20
0
$\eta_{max}$ (m)
1.0
0.9
0.8
0.7
0.6
0.5
0.4
0.3
0.2
0.1
0.0

Figure 12

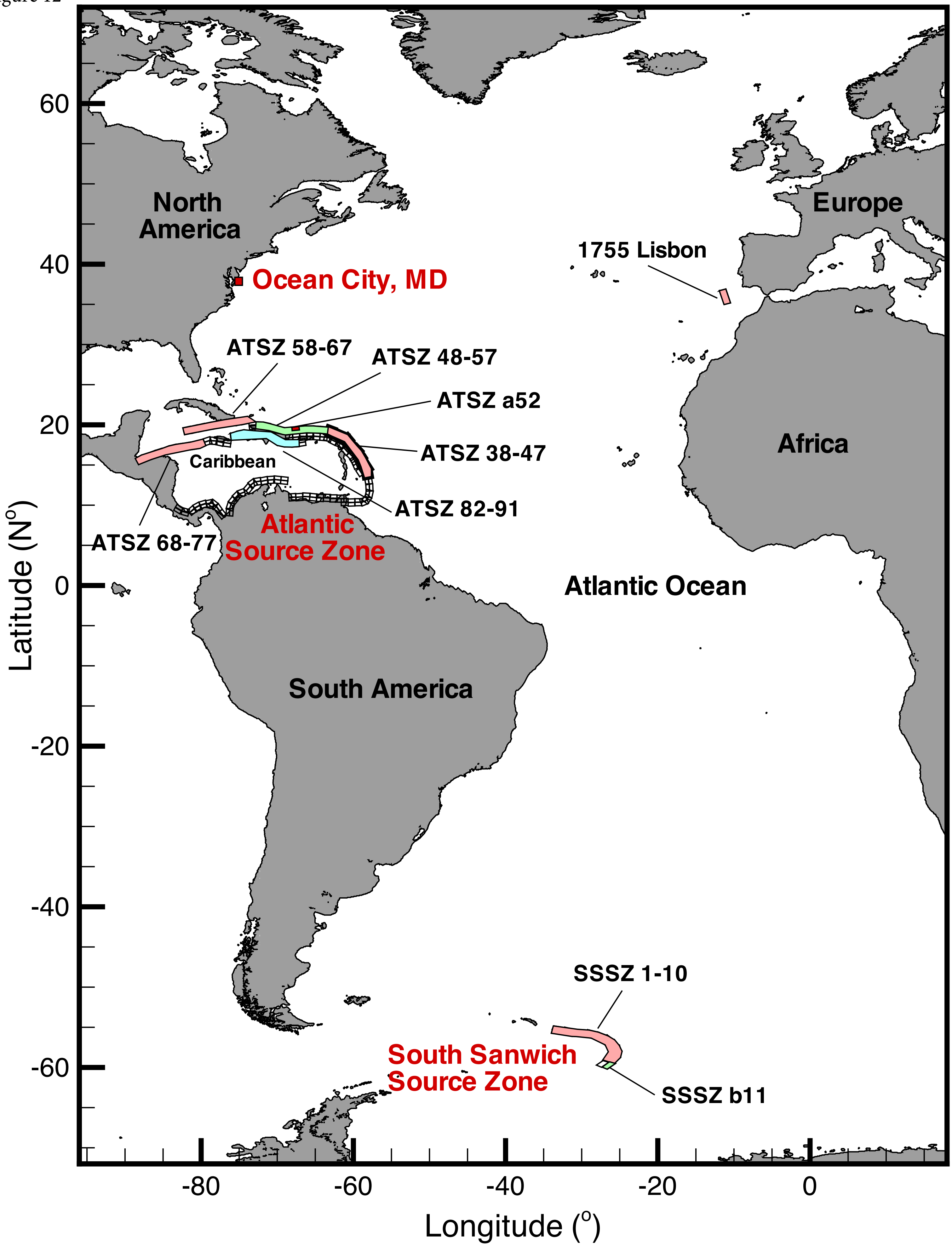
North America
Europe
Africa
South America
Atlantic Ocean
Ocean City, MD
1755 Lisbon
ATSZ 58-67
ATSZ 48-57
ATSZ a52
ATSZ 38-47
ATSZ 82-91
ATSZ 68-77
Caribbean
Atlantic Source Zone
SSSZ 1-10
SSSZ b11
South Sanwich Source Zone
Latitude (N°)
Longitude (°)
60
40
20
0
-20
-40
-60
-80
-60
-40
-20
0

Figure 13

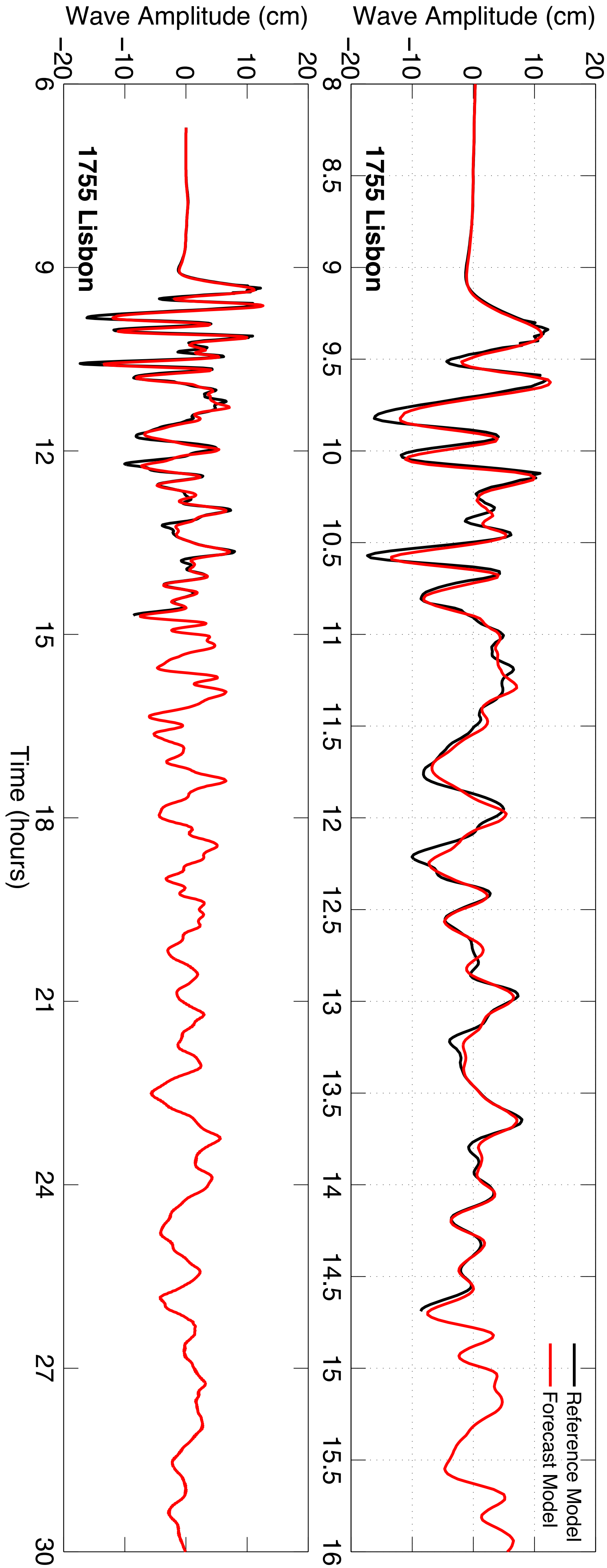
Wave Amplitude (cm)
Wave Amplitude (cm)
1755 Lisbon
1755 Lisbon
Reference Model
Forecast Model
Time (hours)

Figure 14

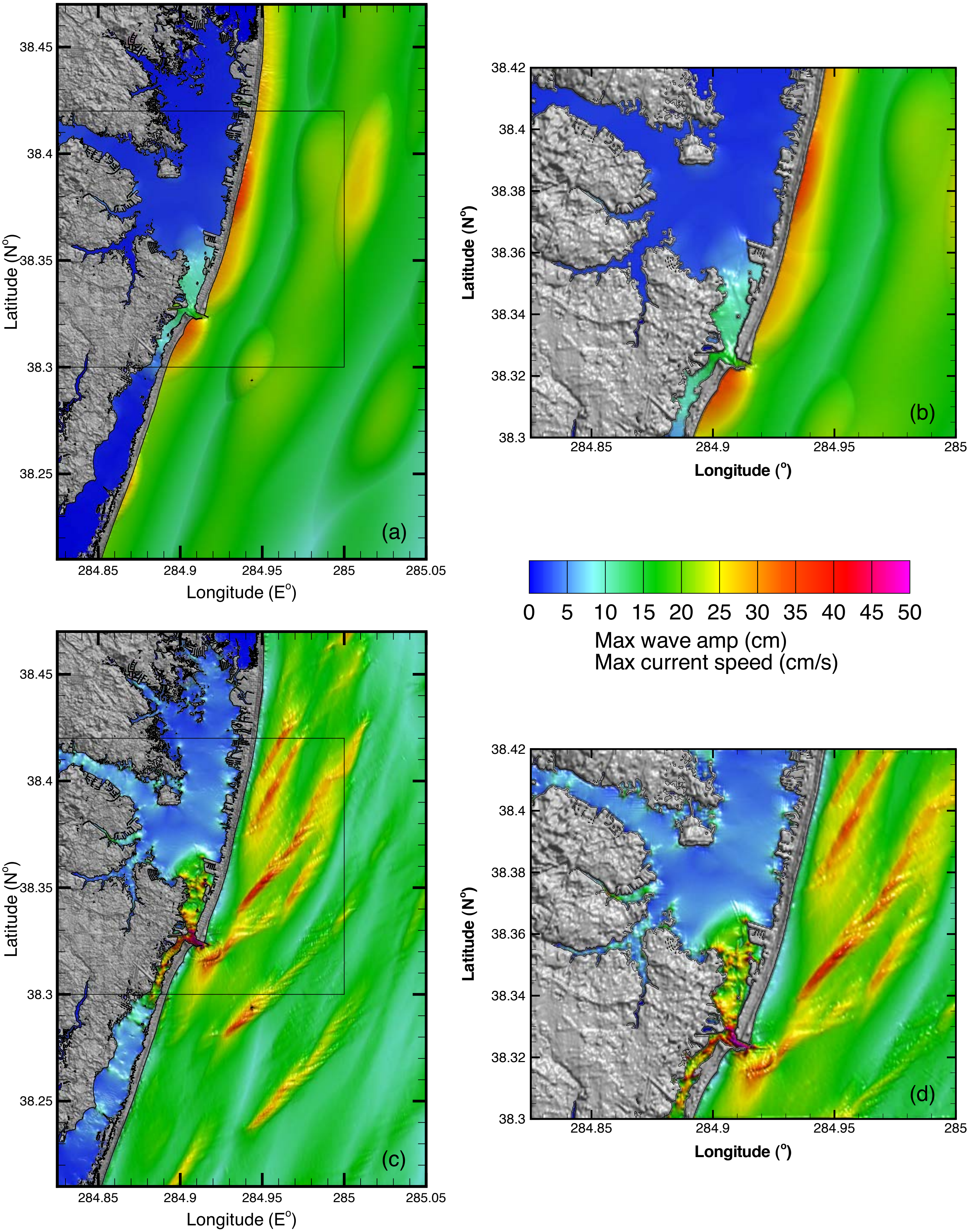
(a)
(b)
(c)
(d)
Latitude (N°)
Longitude (E°)
Longitude (°)
38.45
38.4
38.35
38.3
38.25
38.42
38.38
38.36
38.34
38.32
284.85
284.9
284.95
285
285.05
0
5
10
15
20
25
30
35
40
45
50
Max wave amp (cm)
Max current speed (cm/s)

Figure 15

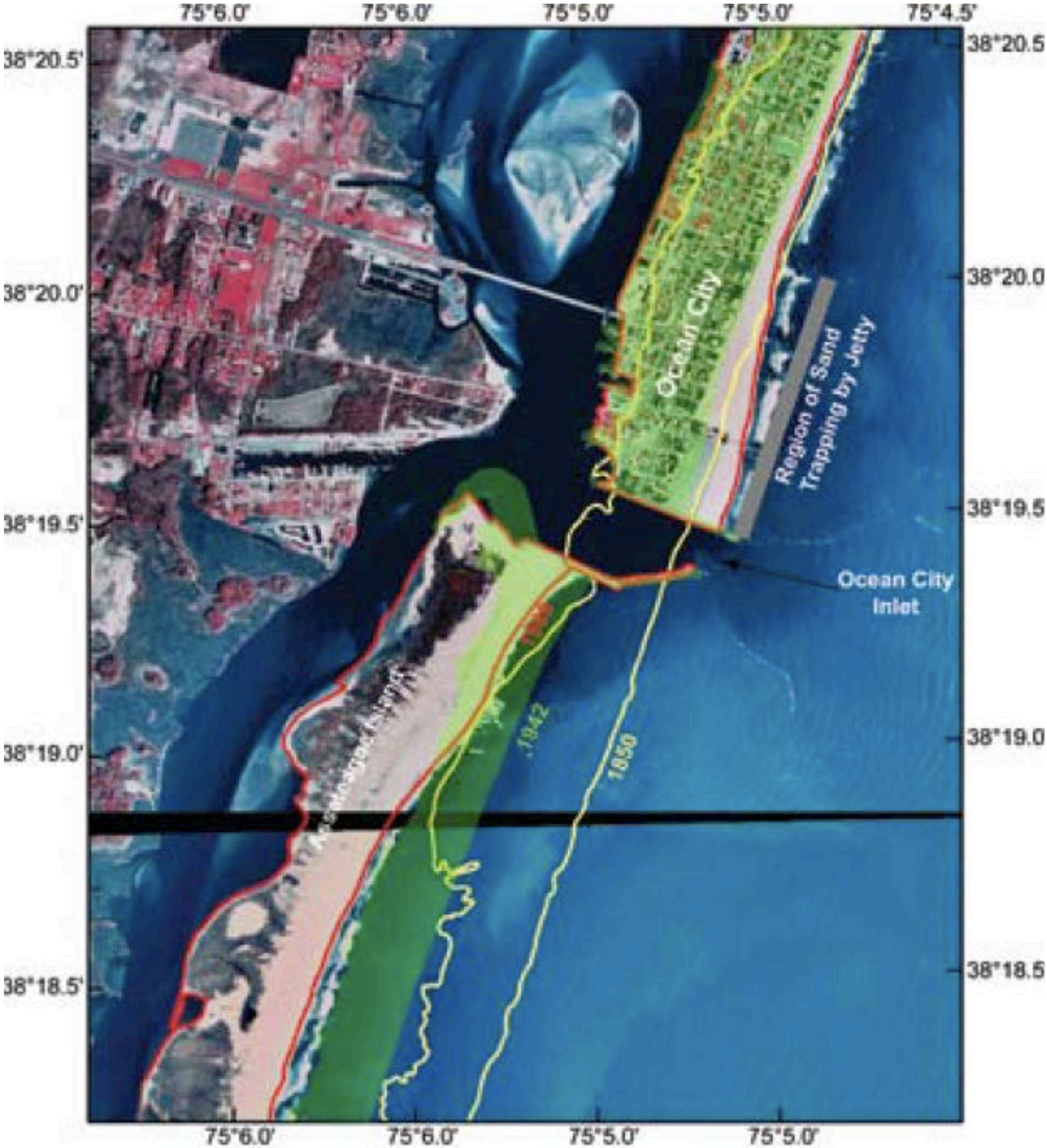
75°6.0'
75°6.0'
75°5.0'
75°5.0'
75°4.5'
38°20.5'
38°20.0'
38°19.5'
38°19.0'
38°18.5'
38°20.5
38°20.0
38°19.5
38°19.0
38°18.5
Ocean City
Region of Sand Trapping by Jetty
Ocean City Inlet
1942
1850
75°6.0'
75°6.0'
75°5.0'
75°5.0'

Figure 16

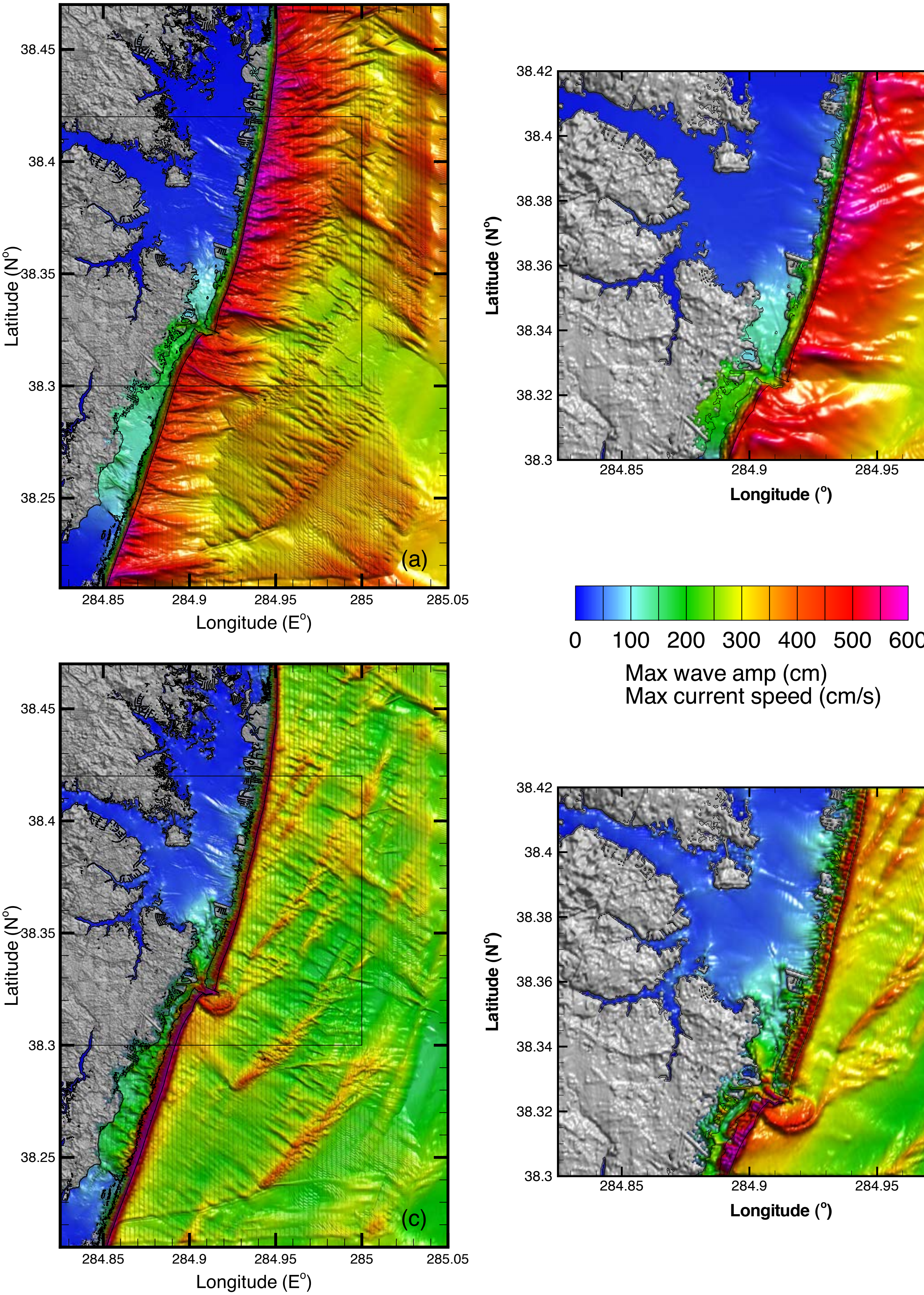

(a)
Latitude (N°)
Longitude (E°)
38.45
38.4
38.35
38.3
38.25
284.85
284.9
284.95
285
285.05
(b)
Latitude (N°)
Longitude (°)
38.42
38.4
38.38
38.36
38.34
38.32
38.3
284.85
284.9
284.95
285
0
100
200
300
400
500
600
Max wave amp (cm)
Max current speed (cm/s)
(c)
(d)

Figure 17

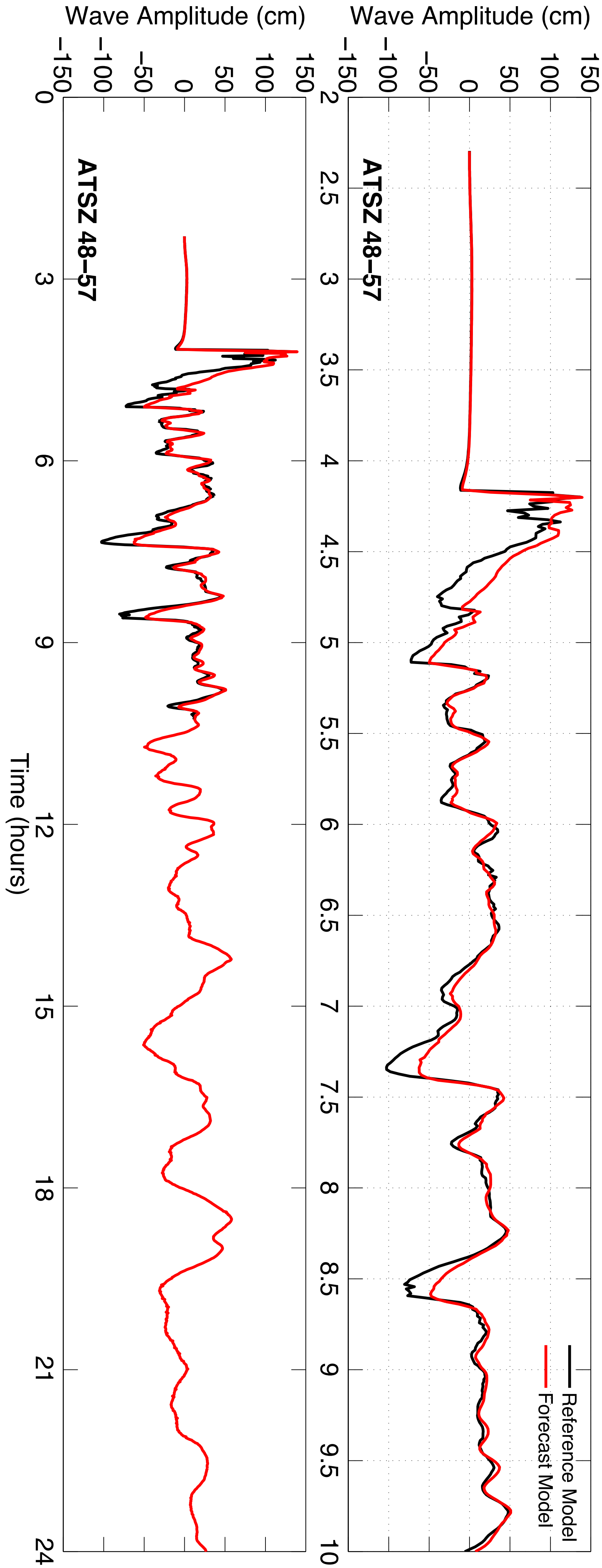

Wave Amplitude (cm)
Wave Amplitude (cm)
ATSZ 48–57
ATSZ 48–57
Reference Model
Forecast Model
Time (hours)

Figure 18

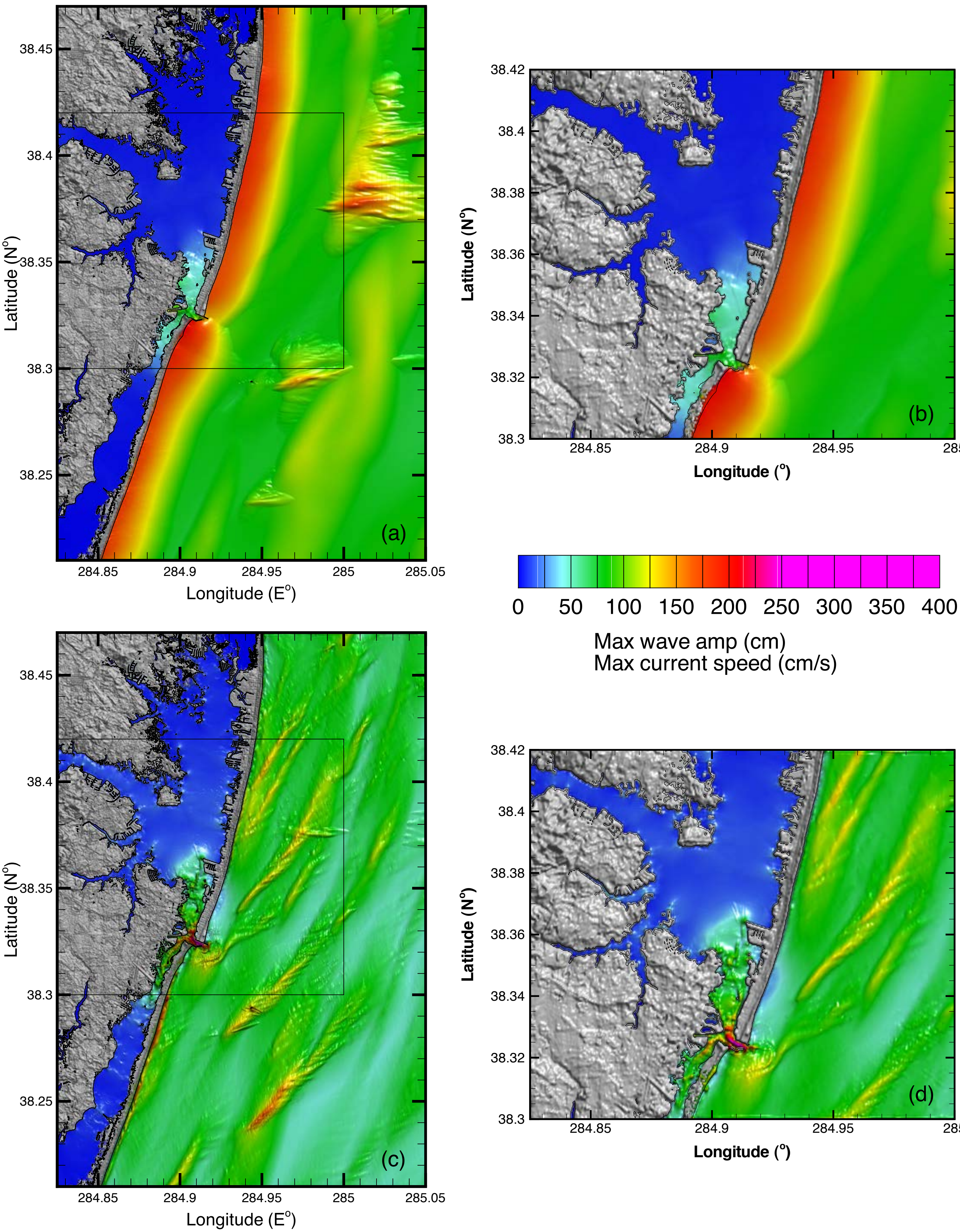

(a)
Latitude (N°)
Longitude (E°)
38.45
38.4
38.35
38.3
38.25
284.85
284.9
284.95
285
285.05
(b)
Latitude (N°)
Longitude (°)
38.42
38.4
38.38
38.36
38.34
38.32
38.3
284.85
284.9
284.95
285
0
50
100
150
200
250
300
350
400
Max wave amp (cm)
Max current speed (cm/s)
(c)
(d)

Figure 19

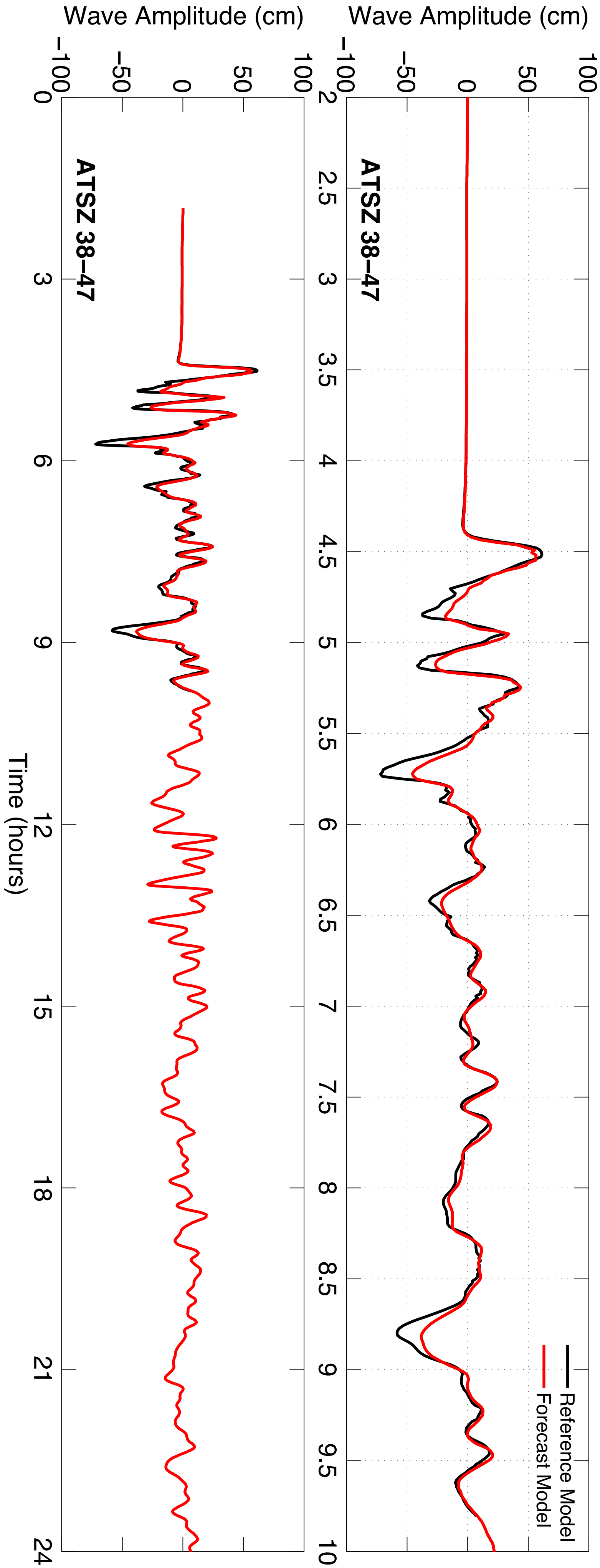

Wave Amplitude (cm)
Wave Amplitude (cm)
ATSZ 38–47
ATSZ 38–47
Reference Model
Forecast Model
Time (hours)

Figure 20

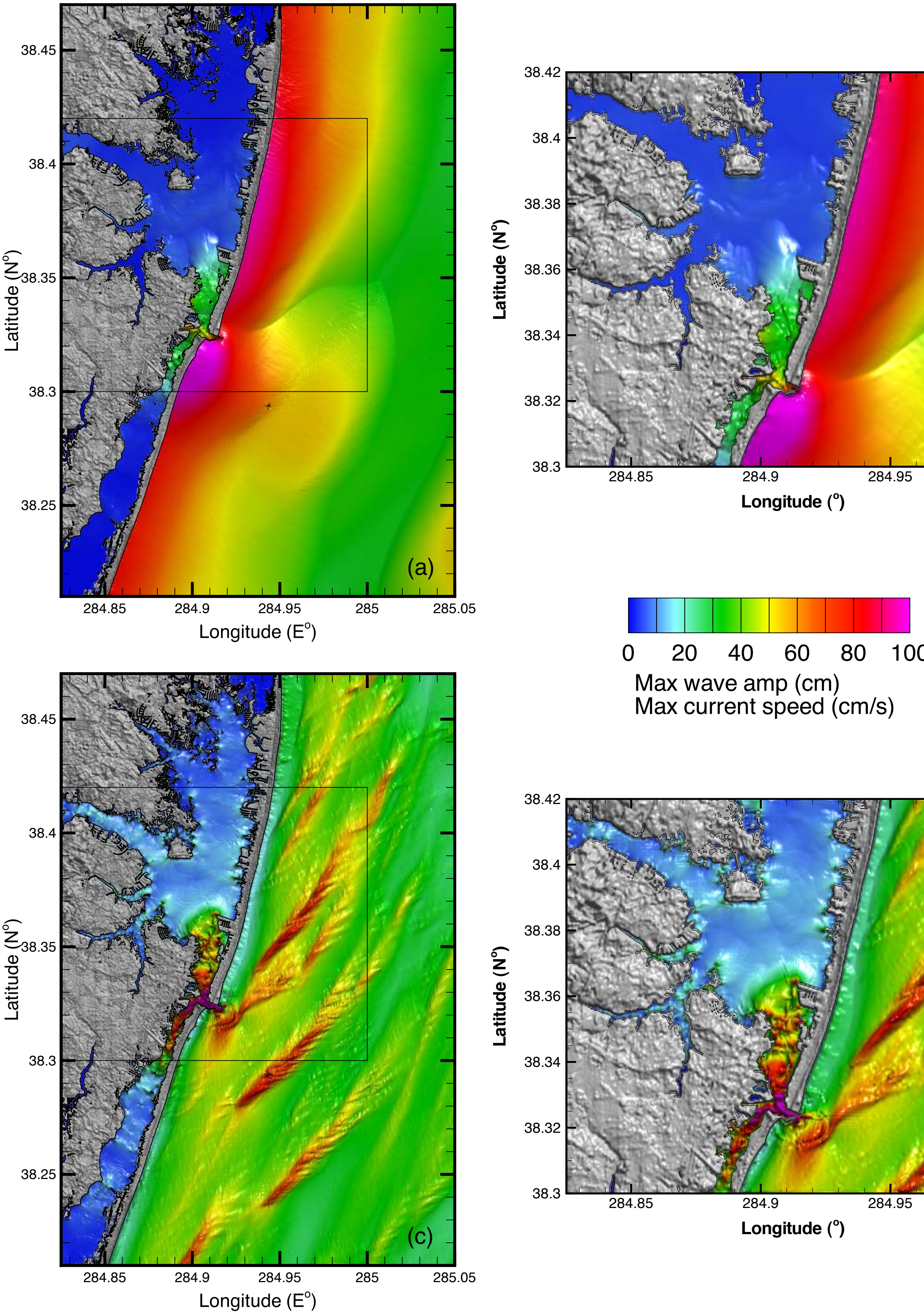

(a)
(b)
(c)
(d)
Latitude (N°)
Longitude (E°)
Longitude (°)
0
20
40
60
80
100
Max wave amp (cm)
Max current speed (cm/s)

Figure 21

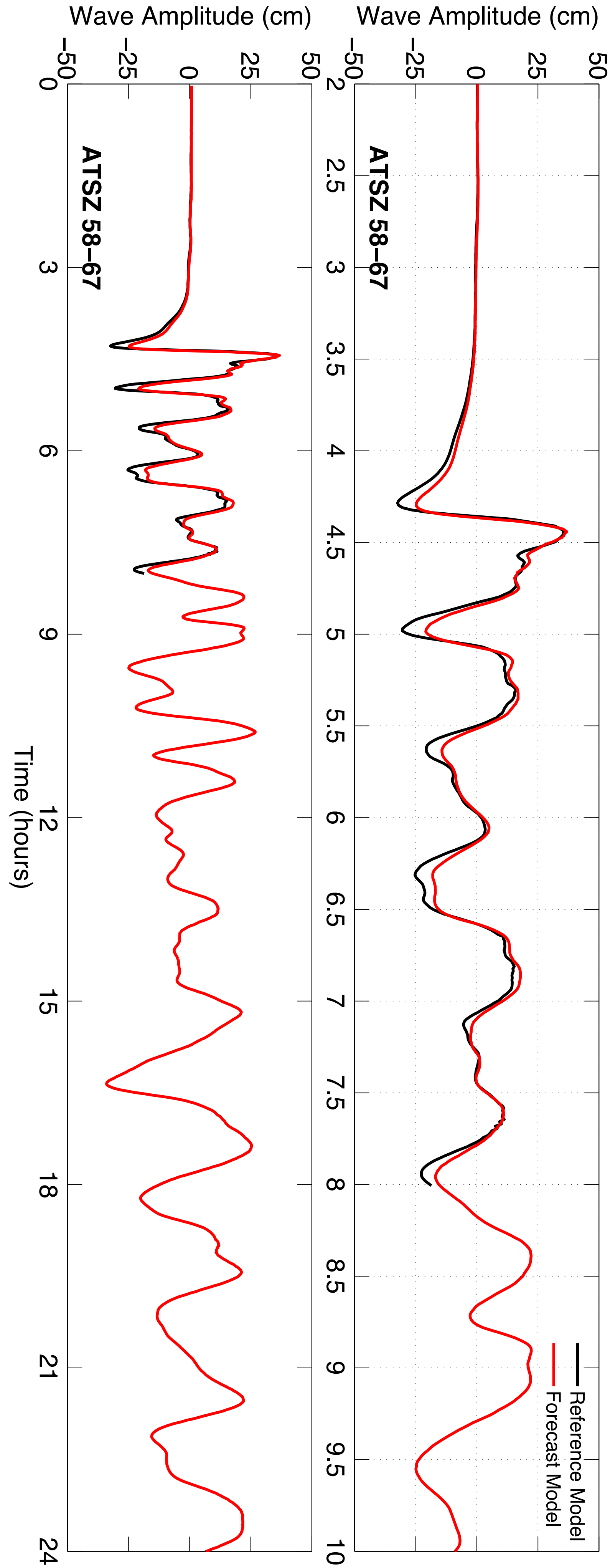

Wave Amplitude (cm)
Wave Amplitude (cm)
ATSZ 58–67
ATSZ 58–67
Reference Model
Forecast Model
Time (hours)

Figure 22

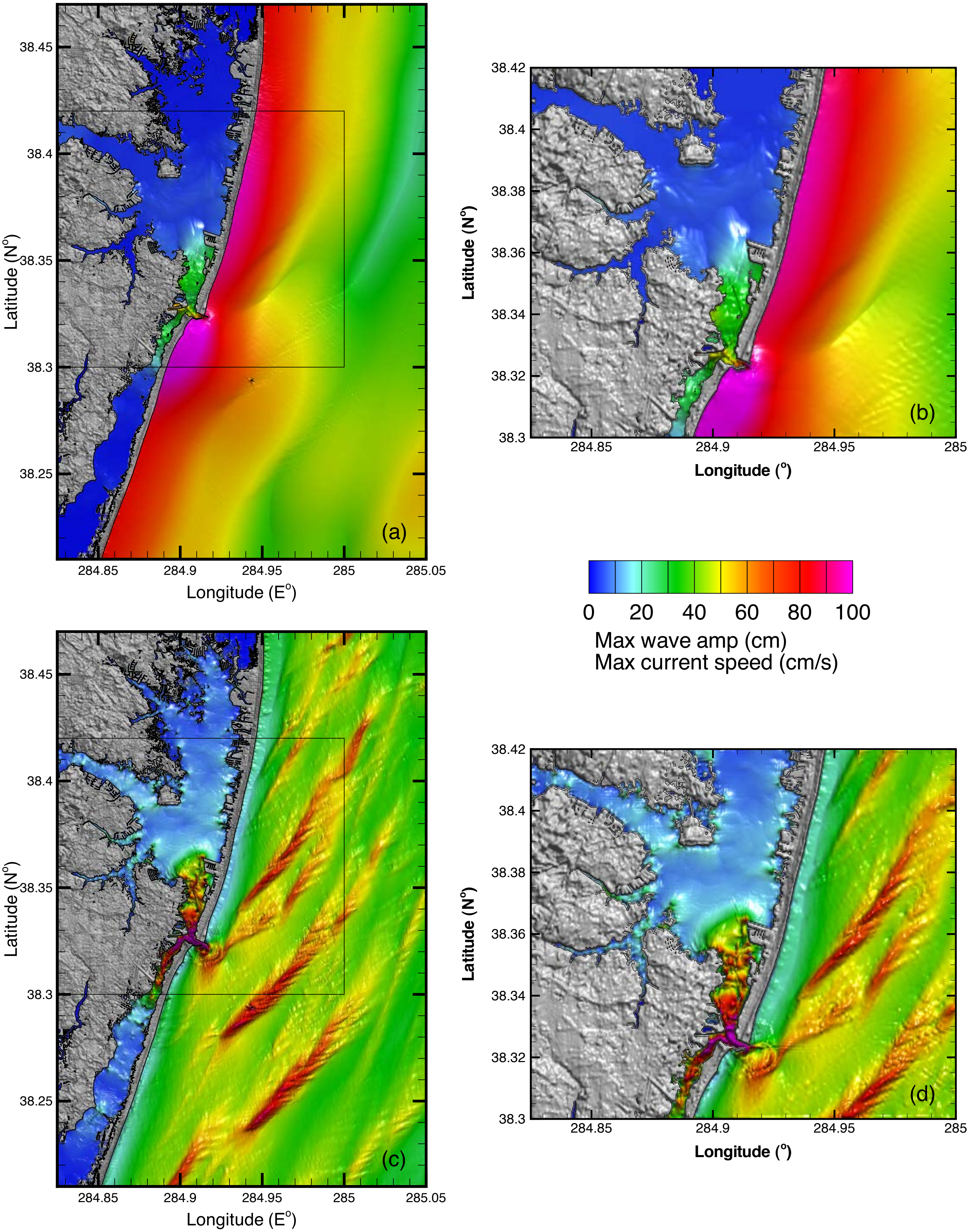

(a)
(b)
(c)
(d)
Latitude (N°)
Longitude (E°)
Longitude (°)
0
20
40
60
80
100
Max wave amp (cm)
Max current speed (cm/s)

Figure 23

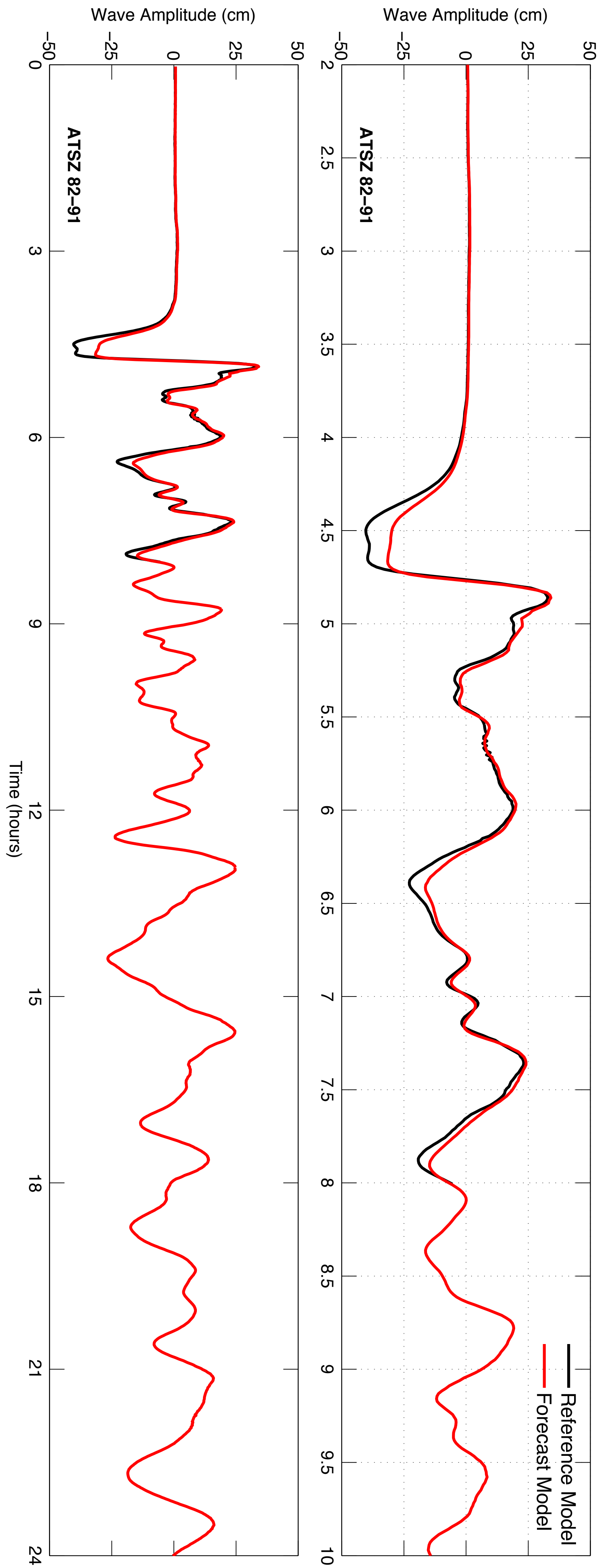

Wave Amplitude (cm)
Wave Amplitude (cm)
ATSZ 82–91
ATSZ 82–91
Reference Model
Forecast Model
Time (hours)

Figure 24

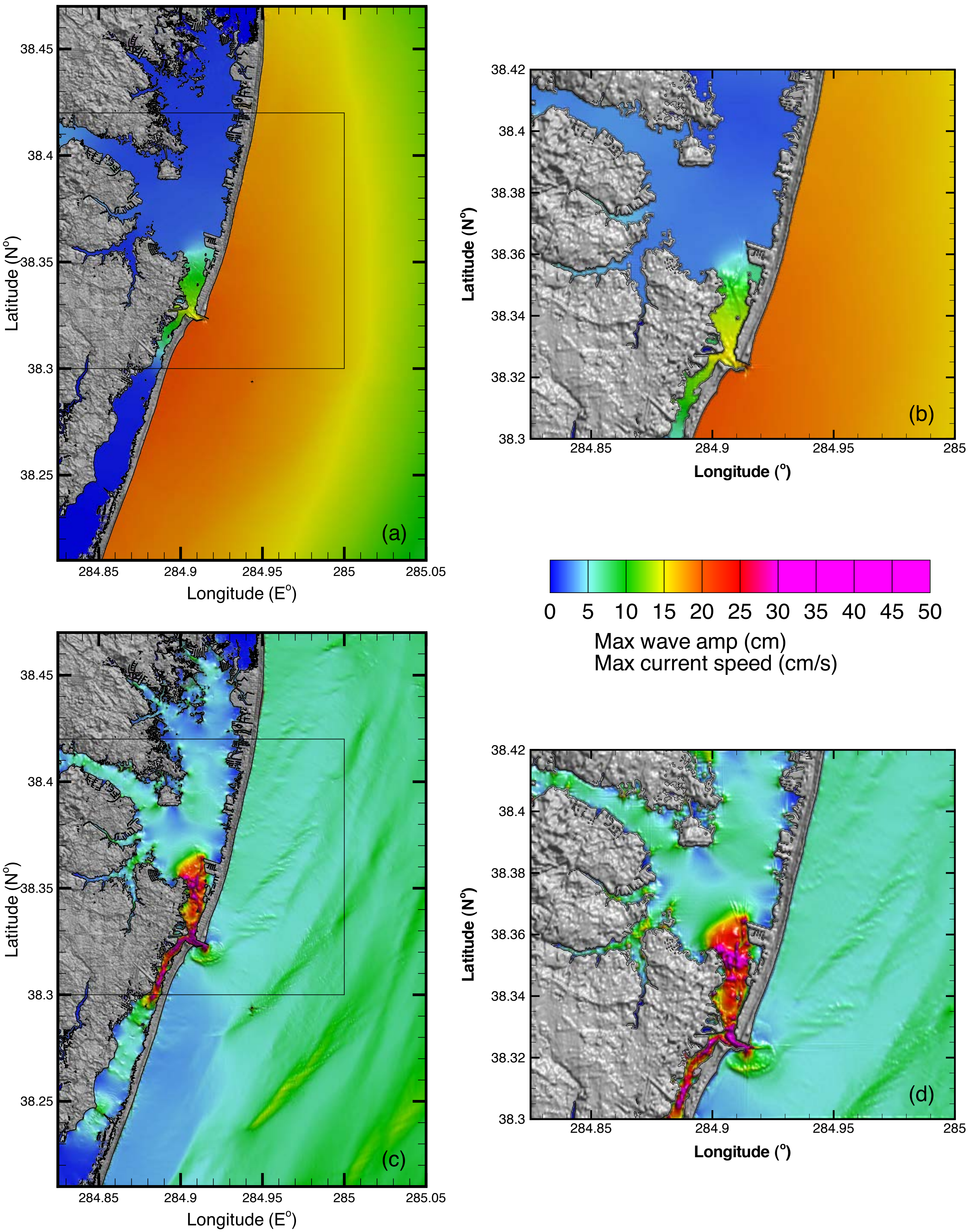

(a)
(b)
(c)
(d)
Latitude (N°)
Longitude (E°)
Longitude (°)
38.45
38.4
38.35
38.3
38.25
38.42
38.38
38.36
38.34
38.32
284.85
284.9
284.95
285
285.05
0 5 10 15 20 25 30 35 40 45 50
Max wave amp (cm)
Max current speed (cm/s)

Figure 25

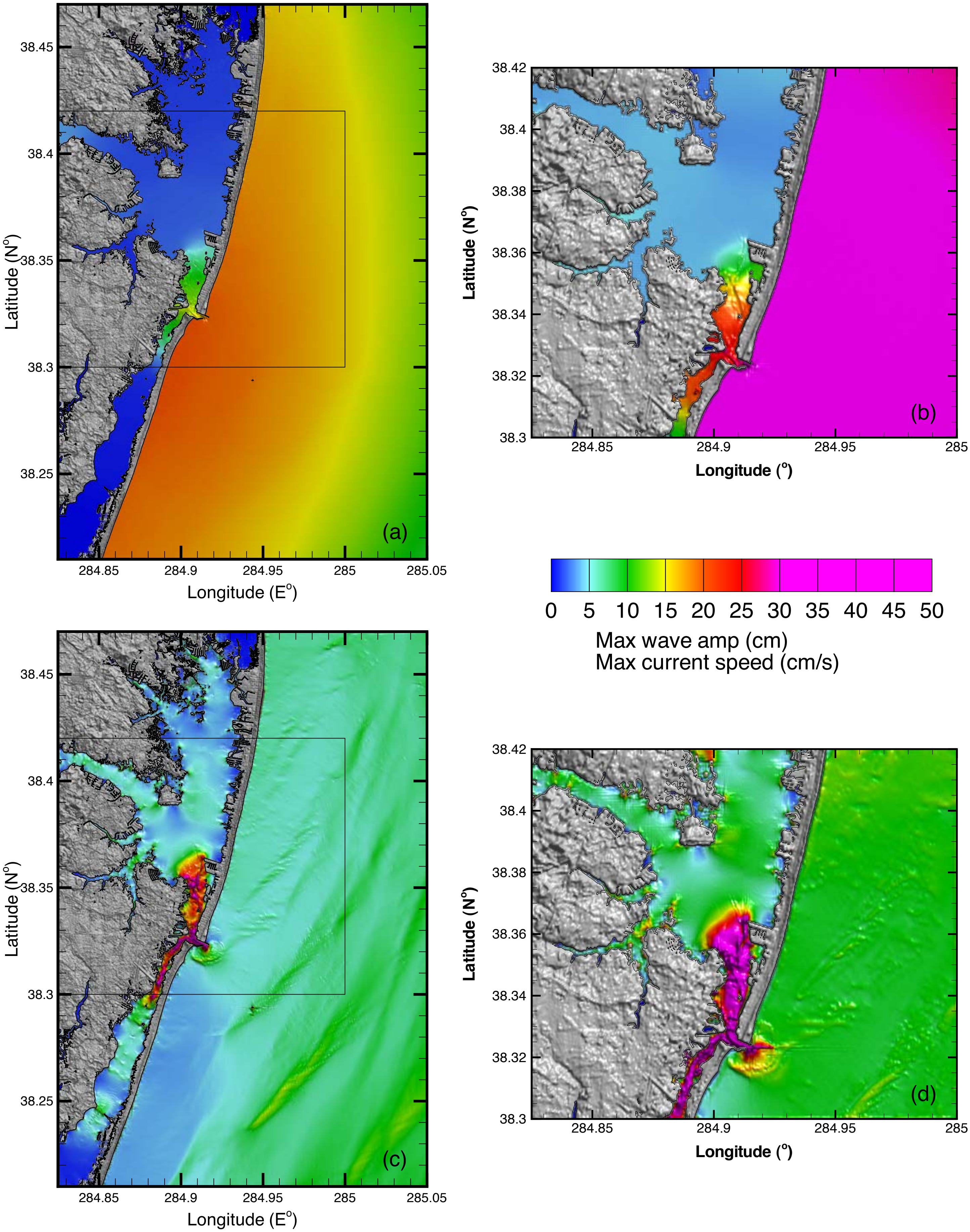

(a)
(b)
(c)
(d)
Latitude (N°)
Longitude (E°)
Latitude (N°)
Longitude (°)
38.45
38.4
38.35
38.3
38.25
284.85
284.9
284.95
285
285.05
38.42
38.4
38.38
38.36
38.34
38.32
38.3
0
5
10
15
20
25
30
35
40
45
50
Max wave amp (cm)
Max current speed (cm/s)

Figure 26

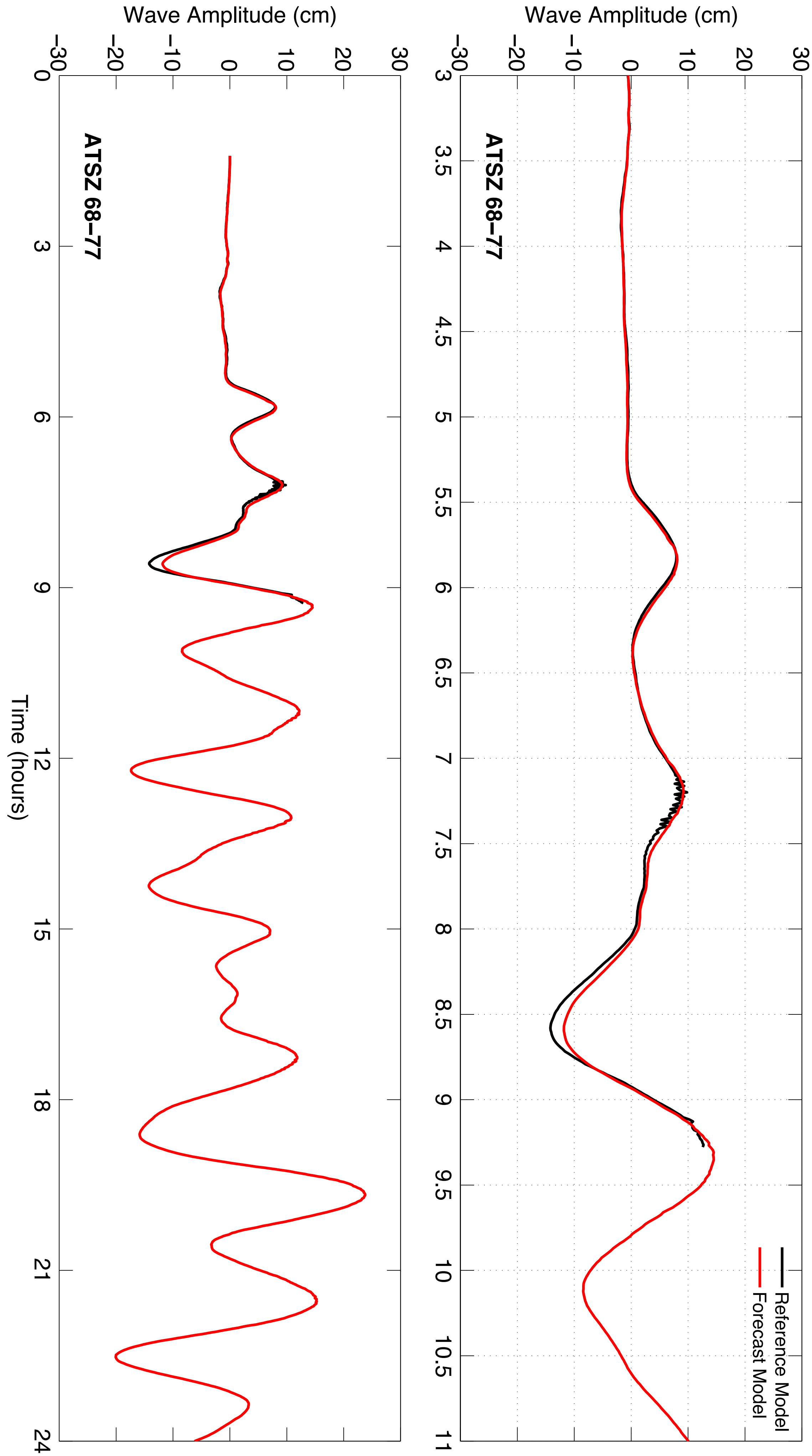

Wave Amplitude (cm)
ATSZ 68–77
Reference Model
Forecast Model
Time (hours)

Figure 27

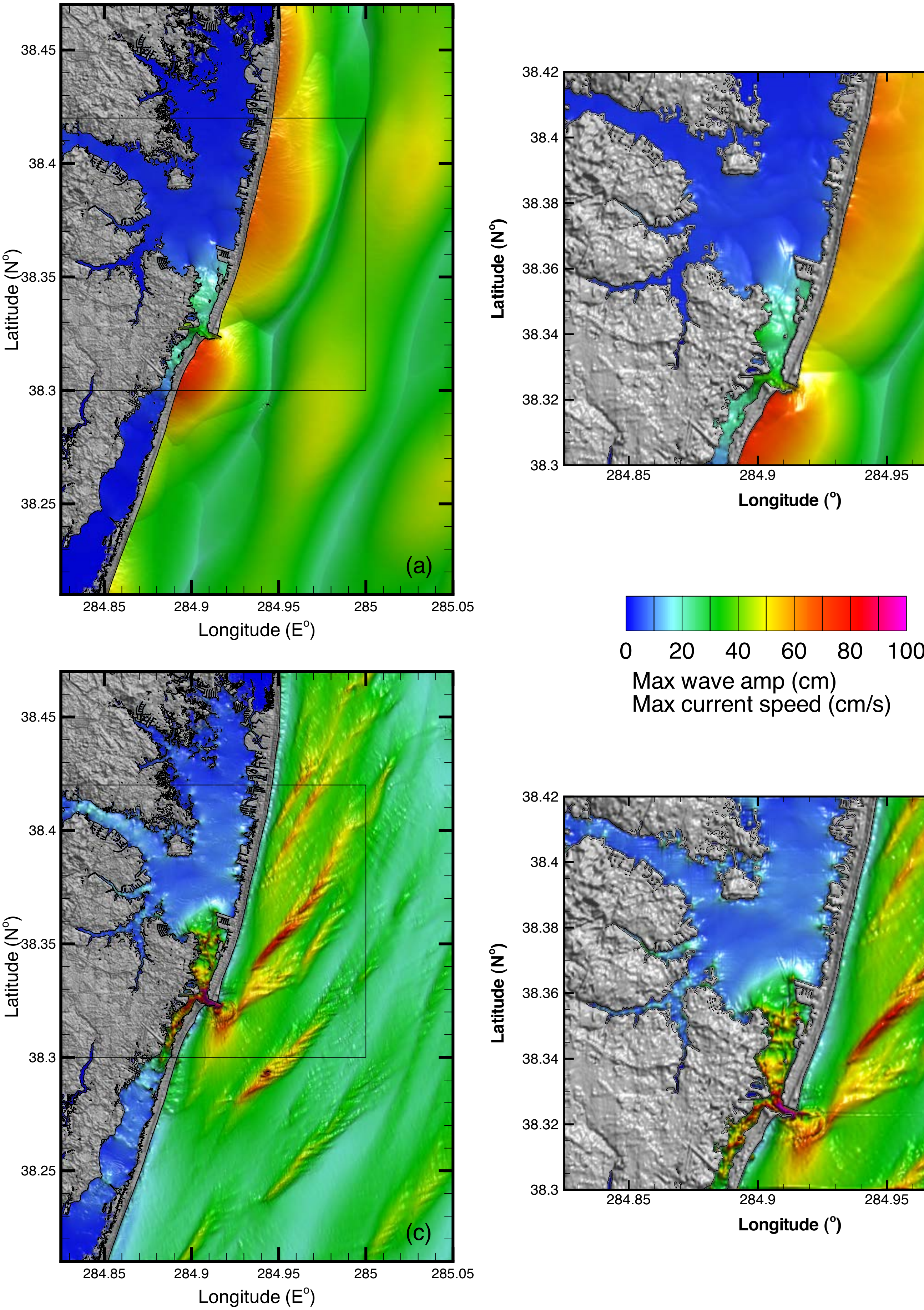
(a)
(b)
(c)
(d)
Latitude (N°)
Longitude (E°)
Longitude (°)
0
20
40
60
80
100
Max wave amp (cm)
Max current speed (cm/s)
38.45
38.4
38.35
38.3
38.25
38.42
38.38
38.36
38.34
38.32
284.85
284.9
284.95
285
285.05

Figure 28

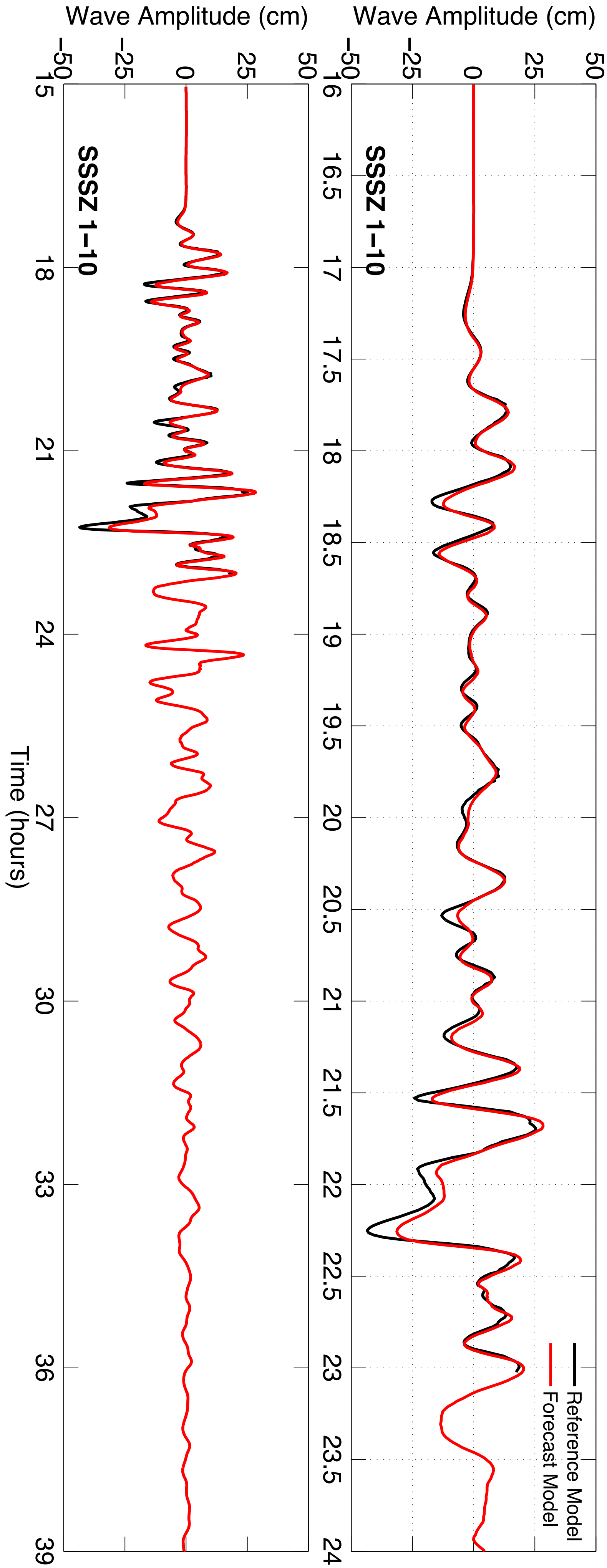

Wave Amplitude (cm)
Wave Amplitude (cm)
Reference Model
Forecast Model
SSSZ 1–10
SSSZ 1–10
Time (hours)

Figure 29

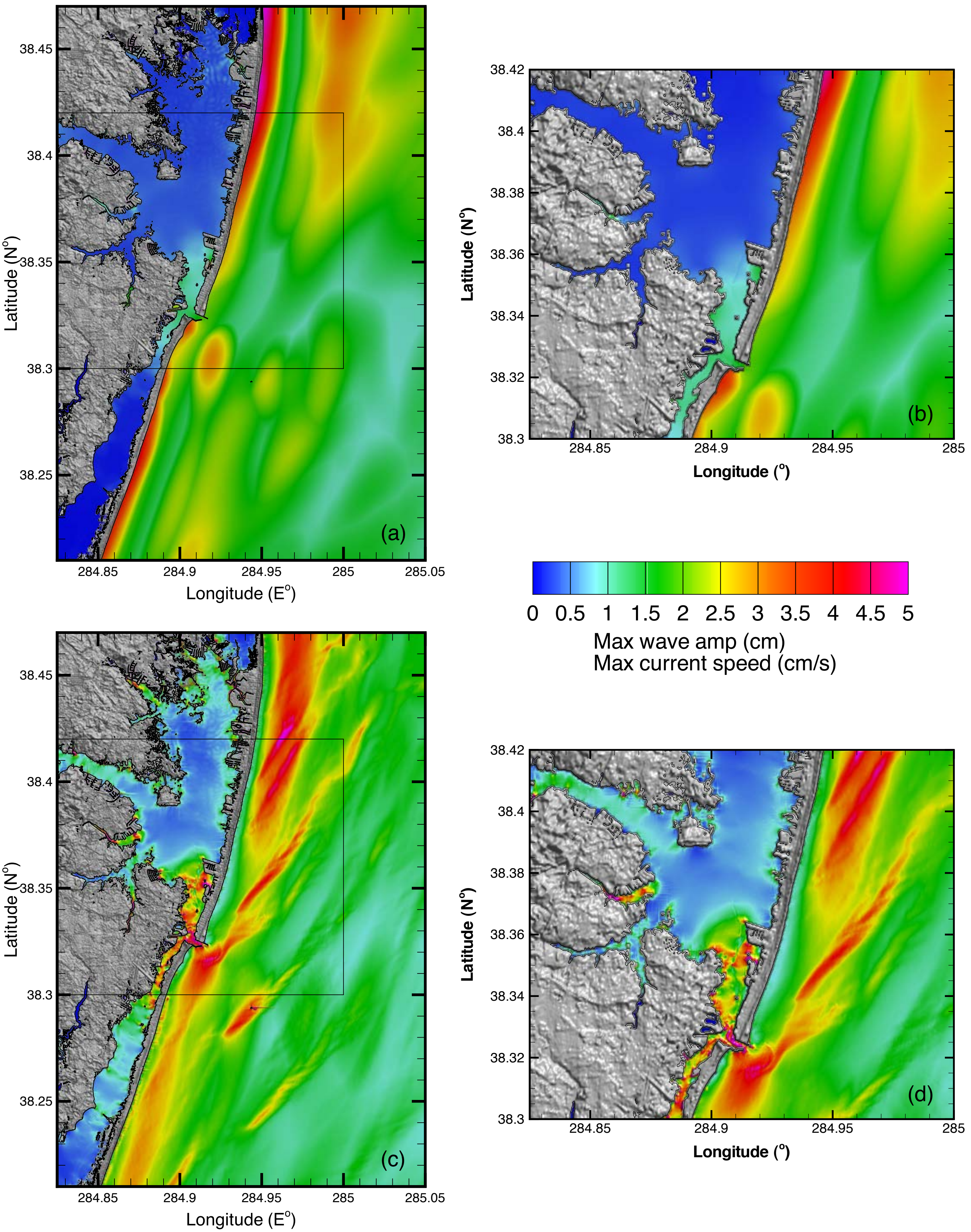

(a)
Latitude (N°)
Longitude (E°)
38.45
38.4
38.35
38.3
38.25
284.85
284.9
284.95
285
285.05
(b)
Latitude (N°)
Longitude (°)
38.42
38.4
38.38
38.36
38.34
38.32
38.3
(c)
(d)
0 0.5 1 1.5 2 2.5 3 3.5 4 4.5 5
Max wave amp (cm)
Max current speed (cm/s)

Figure 30

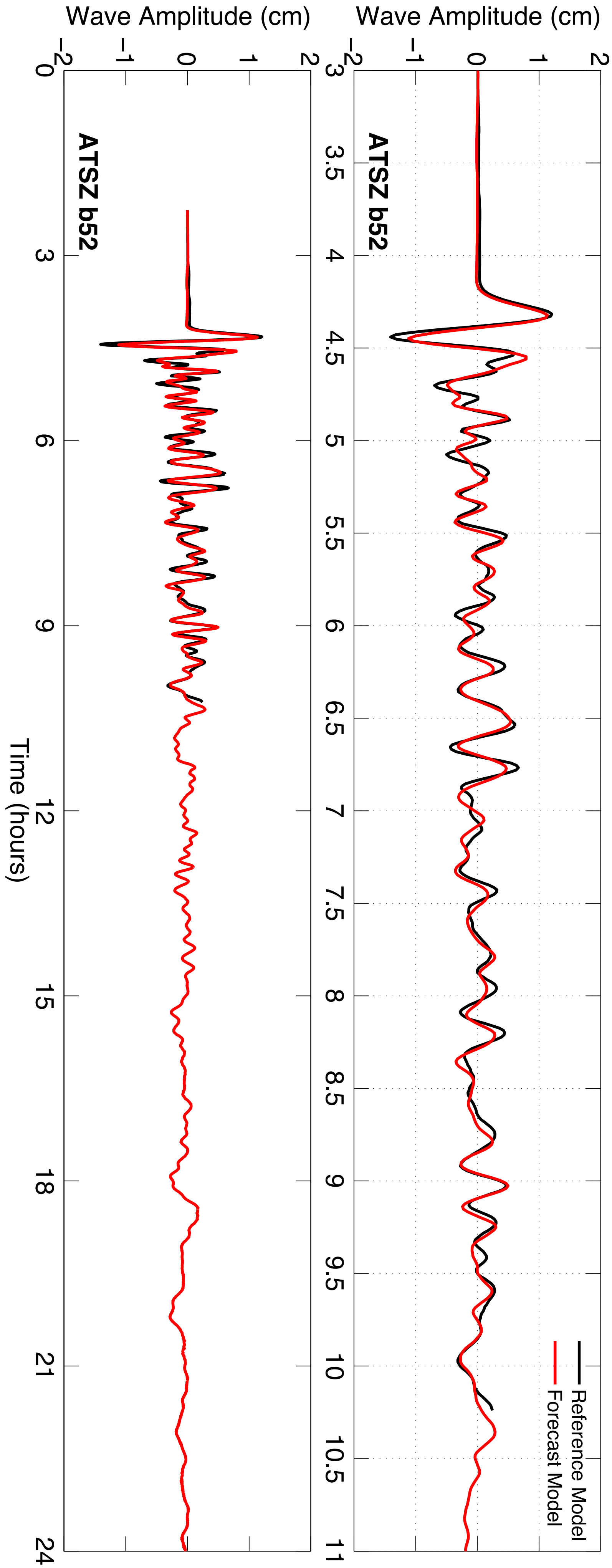

Wave Amplitude (cm)
Wave Amplitude (cm)
ATSZ b52
ATSZ b52
Reference Model
Forecast Model
Time (hours)

## Appendix A.

Development of the Ocean City, Maryland, tsunami forecast model occurred prior to parameters changes that were made to reflect modification to the MOST model code. As a result, the input file for running both the optimized tsunami forecast model and the high-resolution reference inundation model in MOST have been updated accordingly. Appendix A1 and A2 provide the updated files for Ocean City, Maryland.

### A1. Reference model *.in file for Ocean City, Maryland

```
1.0E-4 Minimum amplitude of input offshore wave (m)
1.0  Input minimum depth for offshore (m)
0.1   Input "dry land" depth for inundation (m)
0.0009 Input friction coefficient (n**2)
1     let a and b run up
90.0 blowup limit
1.8   input time step (sec)
16000 input amount of steps
2     Compute "A" arrays every n-th time step, n=
7     COmpute "B" arrays every n-th time step, n=
14   Input number of steps between snapshots
0   ...Starting from
1     ...saveing grid every n-th node, n=
```

### A2. Forecast model *.in file for Ocean City, Maryland

```
1.0E-4 Minimum amplitude of input offshore wave (m)
1.0  Input minimum depth for offshore (m)
0.1   Input "dry land" depth for inundation (m)
0.0009 Input friction coefficient (n**2)
1     let a and b run up
90.0 blowup limit
0.4   input time step (sec)
72000 input amount of steps
8     Compute "A" arrays every n-th time step, n=
7     Compute "B" arrays every n-th time step, n=
56   Input number of steps between snapshots
0    ...Starting from
1    ...saving grid every n-th node, n=
```

# Appendix B. Propagation database:

## Atlantic Ocean Unit Sources

These propagation source details reflect the database as of February 2013, and there may have been updates in the earthquake source parameters after this date.

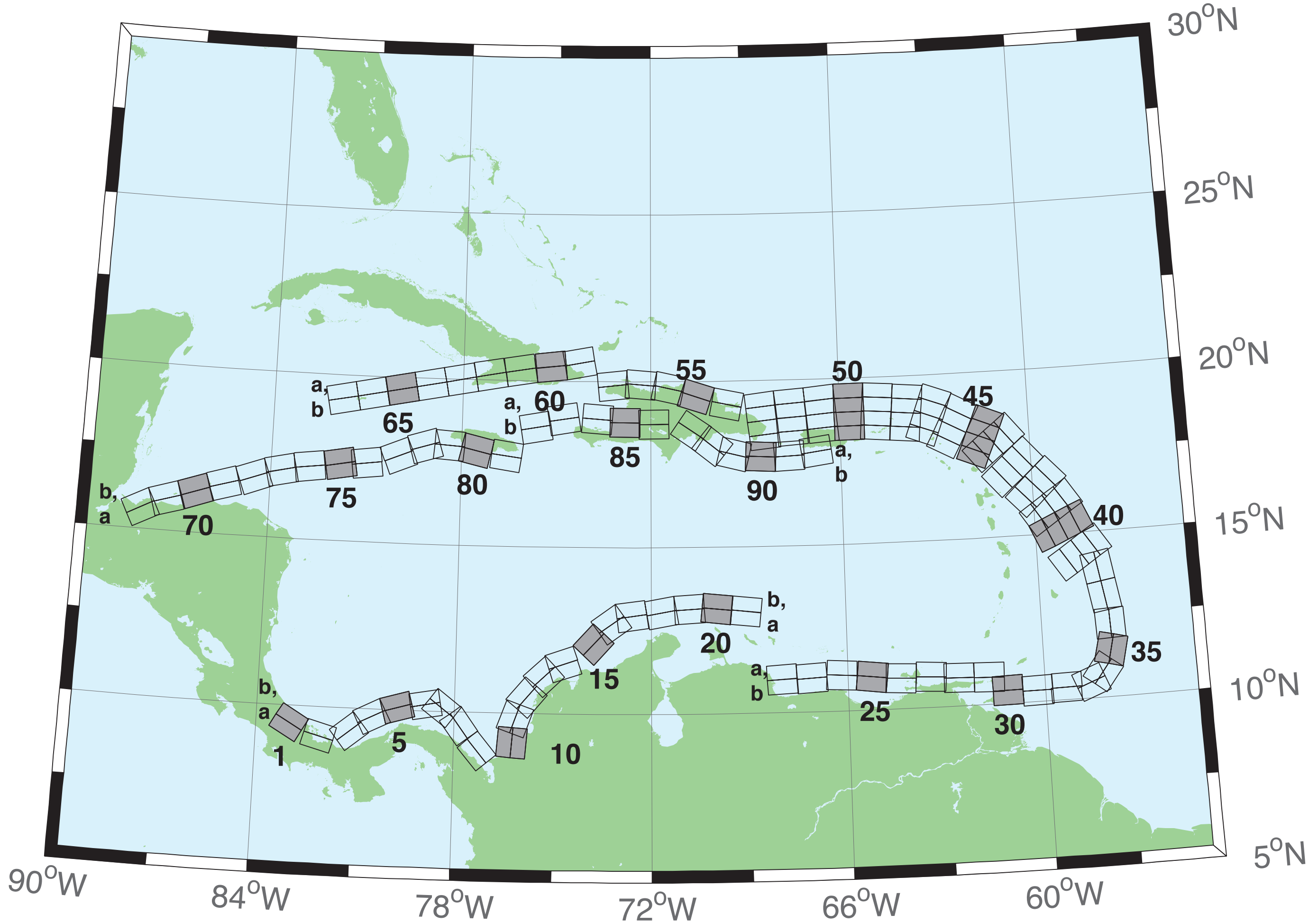


Figure B.1: Atlantic Source Zone unit sources.

Table B.1: Earthquake parameters for Atlantic Source Zone unit sources.

| Segment | Description | Longitude(°E) | Latitude(°N) | Strike(°) | Dip(°) | Depth (km) |
|---|---|---|---|---|---|---|
| atsz–1a | Atlantic Source Zone | -83.2020 | 9.1449 | 120 | 27.5 | 28.09 |
| atsz–1b | Atlantic Source Zone | -83.0000 | 9.4899 | 120 | 27.5 | 5 |
| atsz–2a | Atlantic Source Zone | -82.1932 | 8.7408 | 105.1 | 27.5 | 28.09 |
| atsz–2b | Atlantic Source Zone | -82.0880 | 9.1254 | 105.1 | 27.5 | 5 |
| atsz–3a | Atlantic Source Zone | -80.9172 | 9.0103 | 51.31 | 30 | 30 |
| atsz–3b | Atlantic Source Zone | -81.1636 | 9.3139 | 51.31 | 30 | 5 |
| atsz–4a | Atlantic Source Zone | -80.3265 | 9.4308 | 63.49 | 30 | 30 |
| atsz–4b | Atlantic Source Zone | -80.5027 | 9.7789 | 63.49 | 30 | 5 |
| atsz–5a | Atlantic Source Zone | -79.6247 | 9.6961 | 74.44 | 30 | 30 |
| atsz–5b | Atlantic Source Zone | -79.7307 | 10.0708 | 74.44 | 30 | 5 |
| atsz–6a | Atlantic Source Zone | -78.8069 | 9.8083 | 79.71 | 30 | 30 |
| atsz–6b | Atlantic Source Zone | -78.8775 | 10.1910 | 79.71 | 30 | 5 |
| atsz–7a | Atlantic Source Zone | -78.6237 | 9.7963 | 127.2 | 30 | 30 |
| atsz–7b | Atlantic Source Zone | -78.3845 | 10.1059 | 127.2 | 30 | 5 |
| atsz–8a | Atlantic Source Zone | -78.1693 | 9.3544 | 143.8 | 30 | 30 |
| atsz–8b | Atlantic Source Zone | -77.8511 | 9.5844 | 143.8 | 30 | 5 |
| atsz–9a | Atlantic Source Zone | -77.5913 | 8.5989 | 139.9 | 30 | 30 |
| atsz–9b | Atlantic Source Zone | -77.2900 | 8.8493 | 139.9 | 30 | 5 |
| atsz–10a | Atlantic Source Zone | -75.8109 | 9.0881 | 4.67 | 17 | 19.62 |
| atsz–10b | Atlantic Source Zone | -76.2445 | 9.1231 | 4.67 | 17 | 5 |
| atsz–11a | Atlantic Source Zone | -75.7406 | 9.6929 | 19.67 | 17 | 19.62 |
| atsz–11b | Atlantic Source Zone | -76.1511 | 9.8375 | 19.67 | 17 | 5 |
| atsz–12a | Atlantic Source Zone | -75.4763 | 10.2042 | 40.4 | 17 | 19.62 |
| atsz–12b | Atlantic Source Zone | -75.8089 | 10.4826 | 40.4 | 17 | 5 |
| atsz–13a | Atlantic Source Zone | -74.9914 | 10.7914 | 47.17 | 17 | 19.62 |
| atsz–13b | Atlantic Source Zone | -75.2890 | 11.1064 | 47.17 | 17 | 5 |
| atsz–14a | Atlantic Source Zone | -74.5666 | 11.0708 | 71.68 | 17 | 19.62 |
| atsz–14b | Atlantic Source Zone | -74.7043 | 11.4786 | 71.68 | 17 | 5 |
| atsz–15a | Atlantic Source Zone | -73.4576 | 11.8012 | 42.69 | 17 | 19.62 |
| atsz–15b | Atlantic Source Zone | -73.7805 | 12.0924 | 42.69 | 17 | 5 |
| atsz–16a | Atlantic Source Zone | -72.9788 | 12.3365 | 54.75 | 17 | 19.62 |
| atsz–16b | Atlantic Source Zone | -73.2329 | 12.6873 | 54.75 | 17 | 5 |
| atsz–17a | Atlantic Source Zone | -72.5454 | 12.5061 | 81.96 | 17 | 19.62 |
| atsz–17b | Atlantic Source Zone | -72.6071 | 12.9314 | 81.96 | 17 | 5 |
| atsz–18a | Atlantic Source Zone | -71.6045 | 12.6174 | 79.63 | 17 | 19.62 |
| atsz–18b | Atlantic Source Zone | -71.6839 | 13.0399 | 79.63 | 17 | 5 |
| atsz–19a | Atlantic Source Zone | -70.7970 | 12.7078 | 86.32 | 17 | 19.62 |
| atsz–19b | Atlantic Source Zone | -70.8253 | 13.1364 | 86.32 | 17 | 5 |
| atsz–20a | Atlantic Source Zone | -70.0246 | 12.7185 | 95.94 | 17 | 19.62 |
| atsz–20b | Atlantic Source Zone | -69.9789 | 13.1457 | 95.94 | 17 | 5 |
| atsz–21a | Atlantic Source Zone | -69.1244 | 12.6320 | 95.94 | 17 | 19.62 |
| atsz–21b | Atlantic Source Zone | -69.0788 | 13.0592 | 95.94 | 17 | 5 |
| atsz–22a | Atlantic Source Zone | -68.0338 | 11.4286 | 266.9 | 15 | 17.94 |
| atsz–22b | Atlantic Source Zone | -68.0102 | 10.9954 | 266.9 | 15 | 5 |
| atsz–23a | Atlantic Source Zone | -67.1246 | 11.4487 | 266.9 | 15 | 17.94 |
| atsz–23b | Atlantic Source Zone | -67.1010 | 11.0155 | 266.9 | 15 | 5 |
| atsz–24a | Atlantic Source Zone | -66.1656 | 11.5055 | 273.3 | 15 | 17.94 |
| atsz–24b | Atlantic Source Zone | -66.1911 | 11.0724 | 273.3 | 15 | 5 |
| atsz–25a | Atlantic Source Zone | -65.2126 | 11.4246 | 276.4 | 15 | 17.94 |
| atsz–25b | Atlantic Source Zone | -65.2616 | 10.9934 | 276.4 | 15 | 5 |
| atsz–26a | Atlantic Source Zone | -64.3641 | 11.3516 | 272.9 | 15 | 17.94 |
| atsz–26b | Atlantic Source Zone | -64.3862 | 10.9183 | 272.9 | 15 | 5 |
| atsz–27a | Atlantic Source Zone | -63.4472 | 11.3516 | 272.9 | 15 | 17.94 |

Continued on next page

**Table B.1 – continued from previous page**

| Segment | Description | Longitude(°E) | Latitude(°N) | Strike(°) | Dip(°) | Depth (km) |
|---|---|---|---|---|---|---|
| atsz–27b | Atlantic Source Zone | -63.4698 | 10.9183 | 272.9 | 15 | 5 |
| atsz–28a | Atlantic Source Zone | -62.6104 | 11.2831 | 271.1 | 15 | 17.94 |
| atsz–28b | Atlantic Source Zone | -62.6189 | 10.8493 | 271.1 | 15 | 5 |
| atsz–29a | Atlantic Source Zone | -61.6826 | 11.2518 | 271.6 | 15 | 17.94 |
| atsz–29b | Atlantic Source Zone | -61.6947 | 10.8181 | 271.6 | 15 | 5 |
| atsz–30a | Atlantic Source Zone | -61.1569 | 10.8303 | 269 | 15 | 17.94 |
| atsz–30b | Atlantic Source Zone | -61.1493 | 10.3965 | 269 | 15 | 5 |
| atsz–31a | Atlantic Source Zone | -60.2529 | 10.7739 | 269 | 15 | 17.94 |
| atsz–31b | Atlantic Source Zone | -60.2453 | 10.3401 | 269 | 15 | 5 |
| atsz–32a | Atlantic Source Zone | -59.3510 | 10.8123 | 269 | 15 | 17.94 |
| atsz–32b | Atlantic Source Zone | -59.3734 | 10.3785 | 269 | 15 | 5 |
| atsz–33a | Atlantic Source Zone | -58.7592 | 10.8785 | 248.6 | 15 | 17.94 |
| atsz–33b | Atlantic Source Zone | -58.5984 | 10.4745 | 248.6 | 15 | 5 |
| atsz–34a | Atlantic Source Zone | -58.5699 | 11.0330 | 217.2 | 15 | 17.94 |
| atsz–34b | Atlantic Source Zone | -58.2179 | 10.7710 | 217.2 | 15 | 5 |
| atsz–35a | Atlantic Source Zone | -58.3549 | 11.5300 | 193.7 | 15 | 17.94 |
| atsz–35b | Atlantic Source Zone | -57.9248 | 11.4274 | 193.7 | 15 | 5 |
| atsz–36a | Atlantic Source Zone | -58.3432 | 12.1858 | 177.7 | 15 | 17.94 |
| atsz–36b | Atlantic Source Zone | -57.8997 | 12.2036 | 177.7 | 15 | 5 |
| atsz–37a | Atlantic Source Zone | -58.4490 | 12.9725 | 170.7 | 15 | 17.94 |
| atsz–37b | Atlantic Source Zone | -58.0095 | 13.0424 | 170.7 | 15 | 5 |
| atsz–38a | Atlantic Source Zone | -58.6079 | 13.8503 | 170.2 | 15 | 17.94 |
| atsz–38b | Atlantic Source Zone | -58.1674 | 13.9240 | 170.2 | 15 | 5 |
| atsz–39a | Atlantic Source Zone | -58.6667 | 14.3915 | 146.8 | 15 | 17.94 |
| atsz–39b | Atlantic Source Zone | -58.2913 | 14.6287 | 146.8 | 15 | 5 |
| atsz–39y | Atlantic Source Zone | -59.4168 | 13.9171 | 146.8 | 15 | 43.82 |
| atsz–39z | Atlantic Source Zone | -59.0415 | 14.1543 | 146.8 | 15 | 30.88 |
| atsz–40a | Atlantic Source Zone | -59.1899 | 15.2143 | 156.2 | 15 | 17.94 |
| atsz–40b | Atlantic Source Zone | -58.7781 | 15.3892 | 156.2 | 15 | 5 |
| atsz–40y | Atlantic Source Zone | -60.0131 | 14.8646 | 156.2 | 15 | 43.82 |
| atsz–40z | Atlantic Source Zone | -59.6012 | 15.0395 | 156.2 | 15 | 30.88 |
| atsz–41a | Atlantic Source Zone | -59.4723 | 15.7987 | 146.3 | 15 | 17.94 |
| atsz–41b | Atlantic Source Zone | -59.0966 | 16.0392 | 146.3 | 15 | 5 |
| atsz–41y | Atlantic Source Zone | -60.2229 | 15.3177 | 146.3 | 15 | 43.82 |
| atsz–41z | Atlantic Source Zone | -59.8473 | 15.5582 | 146.3 | 15 | 30.88 |
| atsz–42a | Atlantic Source Zone | -59.9029 | 16.4535 | 137 | 15 | 17.94 |
| atsz–42b | Atlantic Source Zone | -59.5716 | 16.7494 | 137 | 15 | 5 |
| atsz–42y | Atlantic Source Zone | -60.5645 | 15.8616 | 137 | 15 | 43.82 |
| atsz–42z | Atlantic Source Zone | -60.2334 | 16.1575 | 137 | 15 | 30.88 |
| atsz–43a | Atlantic Source Zone | -60.5996 | 17.0903 | 138.7 | 15 | 17.94 |
| atsz–43b | Atlantic Source Zone | -60.2580 | 17.3766 | 138.7 | 15 | 5 |
| atsz–43y | Atlantic Source Zone | -61.2818 | 16.5177 | 138.7 | 15 | 43.82 |
| atsz–43z | Atlantic Source Zone | -60.9404 | 16.8040 | 138.7 | 15 | 30.88 |
| atsz–44a | Atlantic Source Zone | -61.1559 | 17.8560 | 141.1 | 15 | 17.94 |
| atsz–44b | Atlantic Source Zone | -60.8008 | 18.1286 | 141.1 | 15 | 5 |
| atsz–44y | Atlantic Source Zone | -61.8651 | 17.3108 | 141.1 | 15 | 43.82 |
| atsz–44z | Atlantic Source Zone | -61.5102 | 17.5834 | 141.1 | 15 | 30.88 |
| atsz–45a | Atlantic Source Zone | -61.5491 | 18.0566 | 112.8 | 15 | 17.94 |
| atsz–45b | Atlantic Source Zone | -61.3716 | 18.4564 | 112.8 | 15 | 5 |
| atsz–45y | Atlantic Source Zone | -61.9037 | 17.2569 | 112.8 | 15 | 43.82 |
| atsz–45z | Atlantic Source Zone | -61.7260 | 17.6567 | 112.8 | 15 | 30.88 |
| atsz–46a | Atlantic Source Zone | -62.4217 | 18.4149 | 117.9 | 15 | 17.94 |
| atsz–46b | Atlantic Source Zone | -62.2075 | 18.7985 | 117.9 | 15 | 5 |
| atsz–46y | Atlantic Source Zone | -62.8493 | 17.6477 | 117.9 | 15 | 43.82 |
| atsz–46z | Atlantic Source Zone | -62.6352 | 18.0313 | 117.9 | 15 | 30.88 |

Continued on next page

**Table B.1 – continued from previous page**

| Segment | Description | Longitude(°E) | Latitude(°N) | Strike(°) | Dip(°) | Depth (km) |
|---|---|---|---|---|---|---|
| atsz–47a | Atlantic Source Zone | -63.1649 | 18.7844 | 110.5 | 20 | 22.1 |
| atsz–47b | Atlantic Source Zone | -63.0087 | 19.1798 | 110.5 | 20 | 5 |
| atsz–47y | Atlantic Source Zone | -63.4770 | 17.9936 | 110.5 | 20 | 56.3 |
| atsz–47z | Atlantic Source Zone | -63.3205 | 18.3890 | 110.5 | 20 | 39.2 |
| atsz–48a | Atlantic Source Zone | -63.8800 | 18.8870 | 95.37 | 20 | 22.1 |
| atsz–48b | Atlantic Source Zone | -63.8382 | 19.3072 | 95.37 | 20 | 5 |
| atsz–48y | Atlantic Source Zone | -63.9643 | 18.0465 | 95.37 | 20 | 56.3 |
| atsz–48z | Atlantic Source Zone | -63.9216 | 18.4667 | 95.37 | 20 | 39.2 |
| atsz–49a | Atlantic Source Zone | -64.8153 | 18.9650 | 94.34 | 20 | 22.1 |
| atsz–49b | Atlantic Source Zone | -64.7814 | 19.3859 | 94.34 | 20 | 5 |
| atsz–49y | Atlantic Source Zone | -64.8840 | 18.1233 | 94.34 | 20 | 56.3 |
| atsz–49z | Atlantic Source Zone | -64.8492 | 18.5442 | 94.34 | 20 | 39.2 |
| atsz–50a | Atlantic Source Zone | -65.6921 | 18.9848 | 89.59 | 20 | 22.1 |
| atsz–50b | Atlantic Source Zone | -65.6953 | 19.4069 | 89.59 | 20 | 5 |
| atsz–50y | Atlantic Source Zone | -65.6874 | 18.1407 | 89.59 | 20 | 56.3 |
| atsz–50z | Atlantic Source Zone | -65.6887 | 18.5628 | 89.59 | 20 | 39.2 |
| atsz–51a | Atlantic Source Zone | -66.5742 | 18.9484 | 84.98 | 20 | 22.1 |
| atsz–51b | Atlantic Source Zone | -66.6133 | 19.3688 | 84.98 | 20 | 5 |
| atsz–51y | Atlantic Source Zone | -66.4977 | 18.1076 | 84.98 | 20 | 56.3 |
| atsz–51z | Atlantic Source Zone | -66.5353 | 18.5280 | 84.98 | 20 | 39.2 |
| atsz–52a | Atlantic Source Zone | -67.5412 | 18.8738 | 85.87 | 20 | 22.1 |
| atsz–52b | Atlantic Source Zone | -67.5734 | 19.2948 | 85.87 | 20 | 5 |
| atsz–52y | Atlantic Source Zone | -67.4781 | 18.0319 | 85.87 | 20 | 56.3 |
| atsz–52z | Atlantic Source Zone | -67.5090 | 18.4529 | 85.87 | 20 | 39.2 |
| atsz–53a | Atlantic Source Zone | -68.4547 | 18.7853 | 83.64 | 20 | 22.1 |
| atsz–53b | Atlantic Source Zone | -68.5042 | 19.2048 | 83.64 | 20 | 5 |
| atsz–53y | Atlantic Source Zone | -68.3575 | 17.9463 | 83.64 | 20 | 56.3 |
| atsz–53z | Atlantic Source Zone | -68.4055 | 18.3658 | 83.64 | 20 | 39.2 |
| atsz–54a | Atlantic Source Zone | -69.6740 | 18.8841 | 101.5 | 20 | 22.1 |
| atsz–54b | Atlantic Source Zone | -69.5846 | 19.2976 | 101.5 | 20 | 5 |
| atsz–55a | Atlantic Source Zone | -70.7045 | 19.1376 | 108.2 | 20 | 22.1 |
| atsz–55b | Atlantic Source Zone | -70.5647 | 19.5386 | 108.2 | 20 | 5 |
| atsz–56a | Atlantic Source Zone | -71.5368 | 19.3853 | 102.6 | 20 | 22.1 |
| atsz–56b | Atlantic Source Zone | -71.4386 | 19.7971 | 102.6 | 20 | 5 |
| atsz–57a | Atlantic Source Zone | -72.3535 | 19.4838 | 94.2 | 20 | 22.1 |
| atsz–57b | Atlantic Source Zone | -72.3206 | 19.9047 | 94.2 | 20 | 5 |
| atsz–58a | Atlantic Source Zone | -73.1580 | 19.4498 | 84.34 | 20 | 22.1 |
| atsz–58b | Atlantic Source Zone | -73.2022 | 19.8698 | 84.34 | 20 | 5 |
| atsz–59a | Atlantic Source Zone | -74.3567 | 20.9620 | 259.7 | 20 | 22.1 |
| atsz–59b | Atlantic Source Zone | -74.2764 | 20.5467 | 259.7 | 20 | 5 |
| atsz–60a | Atlantic Source Zone | -75.2386 | 20.8622 | 264.2 | 15 | 17.94 |
| atsz–60b | Atlantic Source Zone | -75.1917 | 20.4306 | 264.2 | 15 | 5 |
| atsz–61a | Atlantic Source Zone | -76.2383 | 20.7425 | 260.7 | 15 | 17.94 |
| atsz–61b | Atlantic Source Zone | -76.1635 | 20.3144 | 260.7 | 15 | 5 |
| atsz–62a | Atlantic Source Zone | -77.2021 | 20.5910 | 259.9 | 15 | 17.94 |
| atsz–62b | Atlantic Source Zone | -77.1214 | 20.1638 | 259.9 | 15 | 5 |
| atsz–63a | Atlantic Source Zone | -78.1540 | 20.4189 | 259 | 15 | 17.94 |
| atsz–63b | Atlantic Source Zone | -78.0661 | 19.9930 | 259 | 15 | 5 |
| atsz–64a | Atlantic Source Zone | -79.0959 | 20.2498 | 259.2 | 15 | 17.94 |
| atsz–64b | Atlantic Source Zone | -79.0098 | 19.8236 | 259.2 | 15 | 5 |
| atsz–65a | Atlantic Source Zone | -80.0393 | 20.0773 | 258.9 | 15 | 17.94 |
| atsz–65b | Atlantic Source Zone | -79.9502 | 19.6516 | 258.9 | 15 | 5 |
| atsz–66a | Atlantic Source Zone | -80.9675 | 19.8993 | 258.6 | 15 | 17.94 |
| atsz–66b | Atlantic Source Zone | -80.8766 | 19.4740 | 258.6 | 15 | 5 |
| atsz–67a | Atlantic Source Zone | -81.9065 | 19.7214 | 258.5 | 15 | 17.94 |

Continued on next page

**Table B.1 – continued from previous page**

| Segment | Description | Longitude(°E) | Latitude(°N) | Strike(°) | Dip(°) | Depth (km) |
|---|---|---|---|---|---|---|
| atsz–67b | Atlantic Source Zone | -81.8149 | 19.2962 | 258.5 | 15 | 5 |
| atsz–68a | Atlantic Source Zone | -87.8003 | 15.2509 | 62.69 | 15 | 17.94 |
| atsz–68b | Atlantic Source Zone | -88.0070 | 15.6364 | 62.69 | 15 | 5 |
| atsz–69a | Atlantic Source Zone | -87.0824 | 15.5331 | 72.73 | 15 | 17.94 |
| atsz–69b | Atlantic Source Zone | -87.2163 | 15.9474 | 72.73 | 15 | 5 |
| atsz–70a | Atlantic Source Zone | -86.1622 | 15.8274 | 70.64 | 15 | 17.94 |
| atsz–70b | Atlantic Source Zone | -86.3120 | 16.2367 | 70.64 | 15 | 5 |
| atsz–71a | Atlantic Source Zone | -85.3117 | 16.1052 | 73.7 | 15 | 17.94 |
| atsz–71b | Atlantic Source Zone | -85.4387 | 16.5216 | 73.7 | 15 | 5 |
| atsz–72a | Atlantic Source Zone | -84.3470 | 16.3820 | 69.66 | 15 | 17.94 |
| atsz–72b | Atlantic Source Zone | -84.5045 | 16.7888 | 69.66 | 15 | 5 |
| atsz–73a | Atlantic Source Zone | -83.5657 | 16.6196 | 77.36 | 15 | 17.94 |
| atsz–73b | Atlantic Source Zone | -83.6650 | 17.0429 | 77.36 | 15 | 5 |
| atsz–74a | Atlantic Source Zone | -82.7104 | 16.7695 | 82.35 | 15 | 17.94 |
| atsz–74b | Atlantic Source Zone | -82.7709 | 17.1995 | 82.35 | 15 | 5 |
| atsz–75a | Atlantic Source Zone | -81.7297 | 16.9003 | 79.86 | 15 | 17.94 |
| atsz–75b | Atlantic Source Zone | -81.8097 | 17.3274 | 79.86 | 15 | 5 |
| atsz–76a | Atlantic Source Zone | -80.9196 | 16.9495 | 82.95 | 15 | 17.94 |
| atsz–76b | Atlantic Source Zone | -80.9754 | 17.3801 | 82.95 | 15 | 5 |
| atsz–77a | Atlantic Source Zone | -79.8086 | 17.2357 | 67.95 | 15 | 17.94 |
| atsz–77b | Atlantic Source Zone | -79.9795 | 17.6378 | 67.95 | 15 | 5 |
| atsz–78a | Atlantic Source Zone | -79.0245 | 17.5415 | 73.61 | 15 | 17.94 |
| atsz–78b | Atlantic Source Zone | -79.1532 | 17.9577 | 73.61 | 15 | 5 |
| atsz–79a | Atlantic Source Zone | -78.4122 | 17.5689 | 94.07 | 15 | 17.94 |
| atsz–79b | Atlantic Source Zone | -78.3798 | 18.0017 | 94.07 | 15 | 5 |
| atsz–80a | Atlantic Source Zone | -77.6403 | 17.4391 | 103.3 | 15 | 17.94 |
| atsz–80b | Atlantic Source Zone | -77.5352 | 17.8613 | 103.3 | 15 | 5 |
| atsz–81a | Atlantic Source Zone | -76.6376 | 17.2984 | 98.21 | 15 | 17.94 |
| atsz–81b | Atlantic Source Zone | -76.5726 | 17.7278 | 98.21 | 15 | 5 |
| atsz–82a | Atlantic Source Zone | -75.7299 | 19.0217 | 260.1 | 15 | 17.94 |
| atsz–82b | Atlantic Source Zone | -75.6516 | 18.5942 | 260.1 | 15 | 5 |
| atsz–83a | Atlantic Source Zone | -74.8351 | 19.2911 | 260.8 | 15 | 17.94 |
| atsz–83b | Atlantic Source Zone | -74.7621 | 18.8628 | 260.8 | 15 | 5 |
| atsz–84a | Atlantic Source Zone | -73.6639 | 19.2991 | 274.8 | 15 | 17.94 |
| atsz–84b | Atlantic Source Zone | -73.7026 | 18.8668 | 274.8 | 15 | 5 |
| atsz–85a | Atlantic Source Zone | -72.8198 | 19.2019 | 270.6 | 15 | 17.94 |
| atsz–85b | Atlantic Source Zone | -72.8246 | 18.7681 | 270.6 | 15 | 5 |
| atsz–86a | Atlantic Source Zone | -71.9143 | 19.1477 | 269.1 | 15 | 17.94 |
| atsz–86b | Atlantic Source Zone | -71.9068 | 18.7139 | 269.1 | 15 | 5 |
| atsz–87a | Atlantic Source Zone | -70.4738 | 18.8821 | 304.5 | 15 | 17.94 |
| atsz–87b | Atlantic Source Zone | -70.7329 | 18.5245 | 304.5 | 15 | 5 |
| atsz–88a | Atlantic Source Zone | -69.7710 | 18.3902 | 308.9 | 15 | 17.94 |
| atsz–88b | Atlantic Source Zone | -70.0547 | 18.0504 | 308.4 | 15 | 5 |
| atsz–89a | Atlantic Source Zone | -69.2635 | 18.2099 | 283.9 | 15 | 17.94 |
| atsz–89b | Atlantic Source Zone | -69.3728 | 17.7887 | 283.9 | 15 | 5 |
| atsz–90a | Atlantic Source Zone | -68.5059 | 18.1443 | 272.9 | 15 | 17.94 |
| atsz–90b | Atlantic Source Zone | -68.5284 | 17.7110 | 272.9 | 15 | 5 |
| atsz–91a | Atlantic Source Zone | -67.6428 | 18.1438 | 267.8 | 15 | 17.94 |
| atsz–91b | Atlantic Source Zone | -67.6256 | 17.7103 | 267.8 | 15 | 5 |
| atsz–92a | Atlantic Source Zone | -66.8261 | 18.2536 | 262 | 15 | 17.94 |
| atsz–92b | Atlantic Source Zone | -66.7627 | 17.8240 | 262 | 15 | 5 |

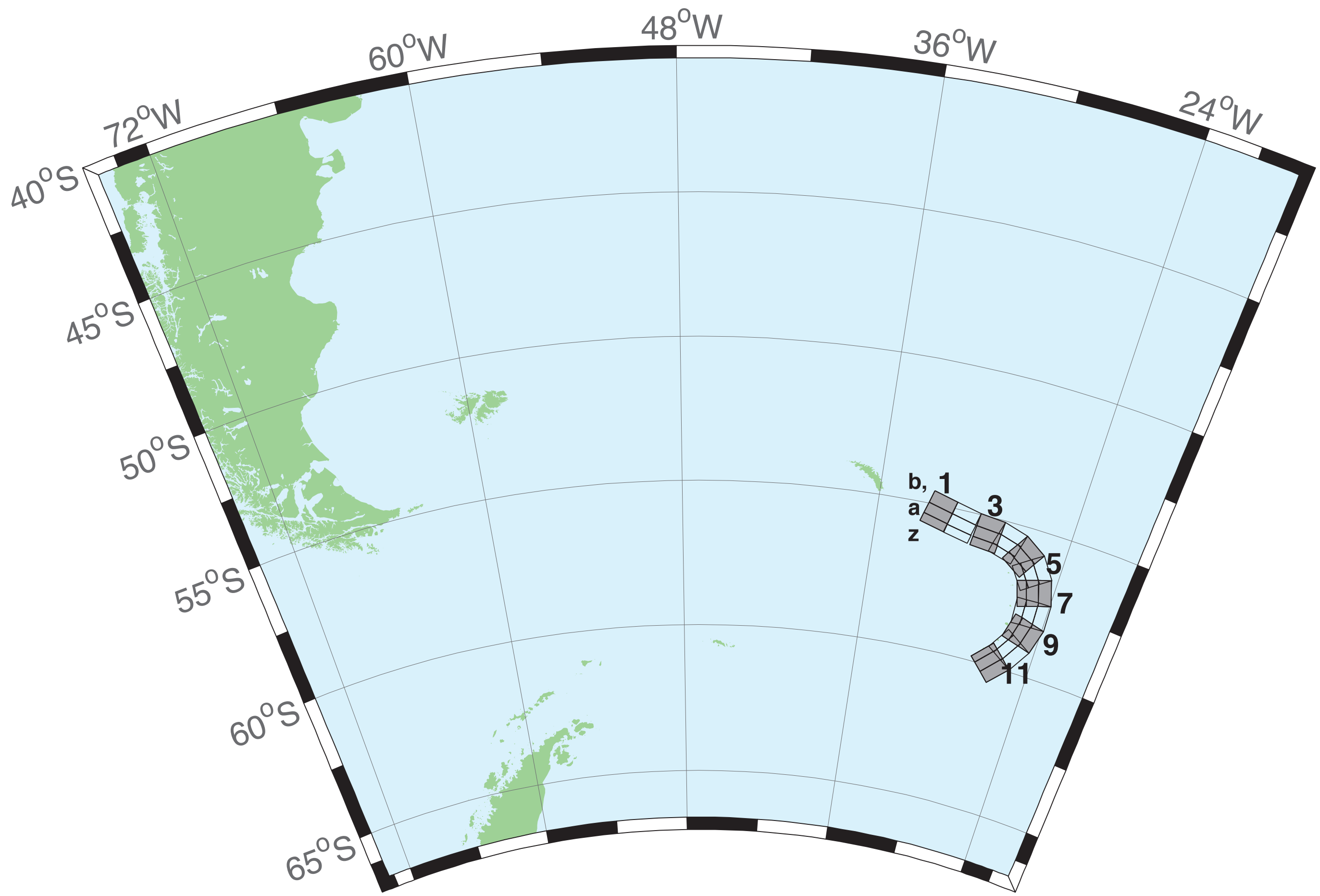


Figure B.2: South Sandwich Islands Subduction Zone.

Table B.2: Earthquake parameters for South Sandwich Islands Subduction Zone unit sources.

| Segment | Description | Longitude(°E) | Latitude(°N) | Strike(°) | Dip(°) | Depth (km) |
|---|---|---|---|---|---|---|
| sssz–1a | South Sandwich Islands Subduction Zone | -32.3713 | -55.4655 | 104.7 | 28.53 | 17.51 |
| sssz–1b | South Sandwich Islands Subduction Zone | -32.1953 | -55.0832 | 104.7 | 9.957 | 8.866 |
| sssz–1z | South Sandwich Islands Subduction Zone | -32.5091 | -55.7624 | 104.7 | 46.99 | 41.39 |
| sssz–2a | South Sandwich Islands Subduction Zone | -30.8028 | -55.6842 | 102.4 | 28.53 | 17.51 |
| sssz–2b | South Sandwich Islands Subduction Zone | -30.6524 | -55.2982 | 102.4 | 9.957 | 8.866 |
| sssz–2z | South Sandwich Islands Subduction Zone | -30.9206 | -55.9839 | 102.4 | 46.99 | 41.39 |
| sssz–3a | South Sandwich Islands Subduction Zone | -29.0824 | -55.8403 | 95.53 | 28.53 | 17.51 |
| sssz–3b | South Sandwich Islands Subduction Zone | -29.0149 | -55.4468 | 95.53 | 9.957 | 8.866 |
| sssz–3z | South Sandwich Islands Subduction Zone | -29.1353 | -56.1458 | 95.53 | 46.99 | 41.39 |
| sssz–4a | South Sandwich Islands Subduction Zone | -27.8128 | -55.9796 | 106.1 | 28.53 | 17.51 |
| sssz–4b | South Sandwich Islands Subduction Zone | -27.6174 | -55.5999 | 106.1 | 9.957 | 8.866 |
| sssz–4z | South Sandwich Islands Subduction Zone | -27.9659 | -56.2744 | 106.1 | 46.99 | 41.39 |
| sssz–5a | South Sandwich Islands Subduction Zone | -26.7928 | -56.2481 | 123.1 | 28.53 | 17.51 |
| sssz–5b | South Sandwich Islands Subduction Zone | -26.4059 | -55.9170 | 123.1 | 9.957 | 8.866 |
| sssz–5z | South Sandwich Islands Subduction Zone | -27.0955 | -56.5052 | 123.1 | 46.99 | 41.39 |
| sssz–6a | South Sandwich Islands Subduction Zone | -26.1317 | -56.6466 | 145.6 | 23.28 | 16.11 |
| sssz–6b | South Sandwich Islands Subduction Zone | -25.5131 | -56.4133 | 145.6 | 9.09 | 8.228 |
| sssz–6z | South Sandwich Islands Subduction Zone | -26.5920 | -56.8194 | 145.6 | 47.15 | 35.87 |
| sssz–7a | South Sandwich Islands Subduction Zone | -25.6787 | -57.2162 | 162.9 | 21.21 | 14.23 |
| sssz–7b | South Sandwich Islands Subduction Zone | -24.9394 | -57.0932 | 162.9 | 7.596 | 7.626 |
| sssz–7z | South Sandwich Islands Subduction Zone | -26.2493 | -57.3109 | 162.9 | 44.16 | 32.32 |
| sssz–8a | South Sandwich Islands Subduction Zone | -25.5161 | -57.8712 | 178.2 | 20.33 | 15.91 |
| sssz–8b | South Sandwich Islands Subduction Zone | -24.7233 | -57.8580 | 178.2 | 8.449 | 8.562 |
| sssz–8z | South Sandwich Islands Subduction Zone | -26.1280 | -57.8813 | 178.2 | 43.65 | 33.28 |
| sssz–9a | South Sandwich Islands Subduction Zone | -25.6657 | -58.5053 | 195.4 | 25.76 | 15.71 |
| sssz–9b | South Sandwich Islands Subduction Zone | -24.9168 | -58.6127 | 195.4 | 8.254 | 8.537 |
| sssz–9z | South Sandwich Islands Subduction Zone | -26.1799 | -58.4313 | 195.4 | 51.69 | 37.44 |
| sssz–10a | South Sandwich Islands Subduction Zone | -26.1563 | -59.1048 | 212.5 | 32.82 | 15.65 |
| sssz–10b | South Sandwich Islands Subduction Zone | -25.5335 | -59.3080 | 212.5 | 10.45 | 6.581 |
| sssz–10z | South Sandwich Islands Subduction Zone | -26.5817 | -58.9653 | 212.5 | 54.77 | 42.75 |
| sssz–11a | South Sandwich Islands Subduction Zone | -27.0794 | -59.6799 | 224.2 | 33.67 | 15.75 |
| sssz–11b | South Sandwich Islands Subduction Zone | -26.5460 | -59.9412 | 224.2 | 11.32 | 5.927 |
| sssz–11z | South Sandwich Islands Subduction Zone | -27.4245 | -59.5098 | 224.2 | 57.19 | 43.46 |

# Appendix C. SIFT testing results

Authors: Jean Newman, Yong Wei

## 1.0 PURPOSE

Forecast models are tested with synthetic tsunami events covering a range of tsunami source locations. Testing is also done with selected historical tsunami events when available.

The purpose of forecast model testing is three-fold. The first objective is to assure that the results obtained with NOAA's tsunami forecast system, which has been released to the Tsunami Warning Centers for operational use, are identical to those obtained by the researcher during the development of the forecast model. The second objective is to test the forecast model for consistency, accuracy, time efficiency, and quality of results over a range of possible tsunami locations and magnitudes. The third objective is to identify bugs and issues in need of resolution by the researcher who developed the Forecast Model or by the forecast software development team before the next version release to NOAA's two Tsunami Warning Centers.

Local hardware and software applications, and tools familiar to the researcher(s), are used to run the Method of Splitting Tsunamis (MOST) model during the forecast model development. The test results presented in this report lend confidence that the model performs as developed and produces the same results when initiated within the forecast application in an operational setting as those produced by the researcher during the forecast model development. The test results assure those who rely on the Ocean City tsunami forecast model that consistent results are produced irrespective of system.

## 2.0 TESTING PROCEDURE

The general procedure for forecast model testing is to run a set of synthetic tsunami scenarios through the forecast system application and compare the results with those obtained by the researcher during the forecast model development and presented in the Tsunami Forecast Model Report. Specific steps taken to test the model include:

1. Identification of testing scenarios, including the standard set of synthetic events and customized synthetic scenarios that may have been used by the researcher(s) in developing the forecast model.
2. Creation of new events to represent customized synthetic scenarios used by the researcher(s) in developing the forecast model, if any.
3. Submission of test model runs with the forecast system, and export of the results from A, B, and C grids, along with time series.
4. Recording applicable metadata, including the specific version of the forecast system used for testing.
5. Examination of forecast model results from the forecast system for instabilities in both time series and plot results.
6. Comparison of forecast model results obtained through the forecast system with those obtained during the forecast model development.
7. Summarization of results with specific mention of quality, consistency, and time efficiency.
8. Reporting of issues identified to modeler and forecast software development team.

9. Retesting the forecast models in the forecast system when reported issues have been addressed or explained.

Synthetic model runs were tested on a DELL PowerEdge R510 computer equipped with two Xeon E5670 processors at 2.93 Ghz, each with 12 MBytes of cache and 32GB memory. The processors are hex core and support hyperthreading, resulting in the computer performing as a 24 processor core machine. Additionally, the testing computer supports 10 Gigabit Ethernet for fast network connections. This computer configuration is similar or the same as the configurations of the computers installed at the Tsunami Warning Centers so the compute times should only vary slightly.

## Results

The Ocean City forecast model was tested with NOAA's tsunami forecast system version 3.2.

The Ocean City, Maryland forecast model was tested with three synthetic scenarios. Test results from the forecast system and comparisons with the results obtained during the forecast model development are shown numerically in Table 2 and graphically in Figures 1 to 3. The results show that the forecast model is stable and robust, with consistent and high quality results across geographically distributed tsunami sources and mega-event tsunami magnitudes. The model run time (wall clock time) was under 30 minutes for 8 hours of simulation time, and under 15 minutes for 4 hours. This run time is over the 10 minute run time for 4 hours of simulation time that satisfies time efficiency requirements. This is because coverage of the A grid needs to be extended further offshore of the continental shelf to better adapt the model boundary conditions from the propagation database. As the shallow continental shelf slows down the tsunami propagation and allows more time for warning and forecast, it is understandable that forecast models in the east coast, such as Ocean City, take more time to finish.

Three synthetic events were run on the Ocean City forecast model. The modeled scenarios were stable for all cases tested, with no instabilities or ringing. Results show that the largest modeled height was 126.87 cm and originated in the Caribbean (ATSZ 48-57) source. Amplitudes greater than 100 cm were recorded for the one of three test sources. The smallest signal of 25.58 cm was recorded for the far field South Sandwich Islands (SSSZ 1-10) source. Direct comparisons, of output from the forecast tool with results from available development synthetic events, demonstrated that the wave pattern is similar in shape, pattern and amplitude but does not match by eye. These discrepancies are mainly caused by different propagation databases used to provide the boundary conditions for model runs. Developed in 2010, the forecast model report shows the Ocean City model results based on an old tsunami propagation database, while the SIFT testing results in Appendix C reflect the tsunami propagation database that was updated in December of 2011. Table 1 shows the computed maximum and minimum wave amplitude by SIFT and by model based on old tsunami propagation database. It is known that the new propagation database will lead to improvement of the model results.

| Source Zone | Tsunami Source | $\alpha$ [m] | SIFT Max (cm) | Development Max (cm) | SIFT Min (cm) | Development Min (cm) |
|---|---|---|---|---|---|---|
| ATSZ | A38-A47, B38-B47 | 25 | 58.945 | 56.4 | -34.556 | -45.58 |
| ATSZ | A48-A57, B48-B57 | 25 | 126.869 | 139.2 | -58.821 | -62.44 |
| SSSZ | A1-A10, B1-B10 | 25 | 25.581 | 28.36 | -13.811 | -31.41 |

**Table 1.** Table of maximum and minimum amplitudes (cm) at the Ocean City, Maryland warning point for synthetic and historical events tested using SIFT 3.2 and obtained during development.

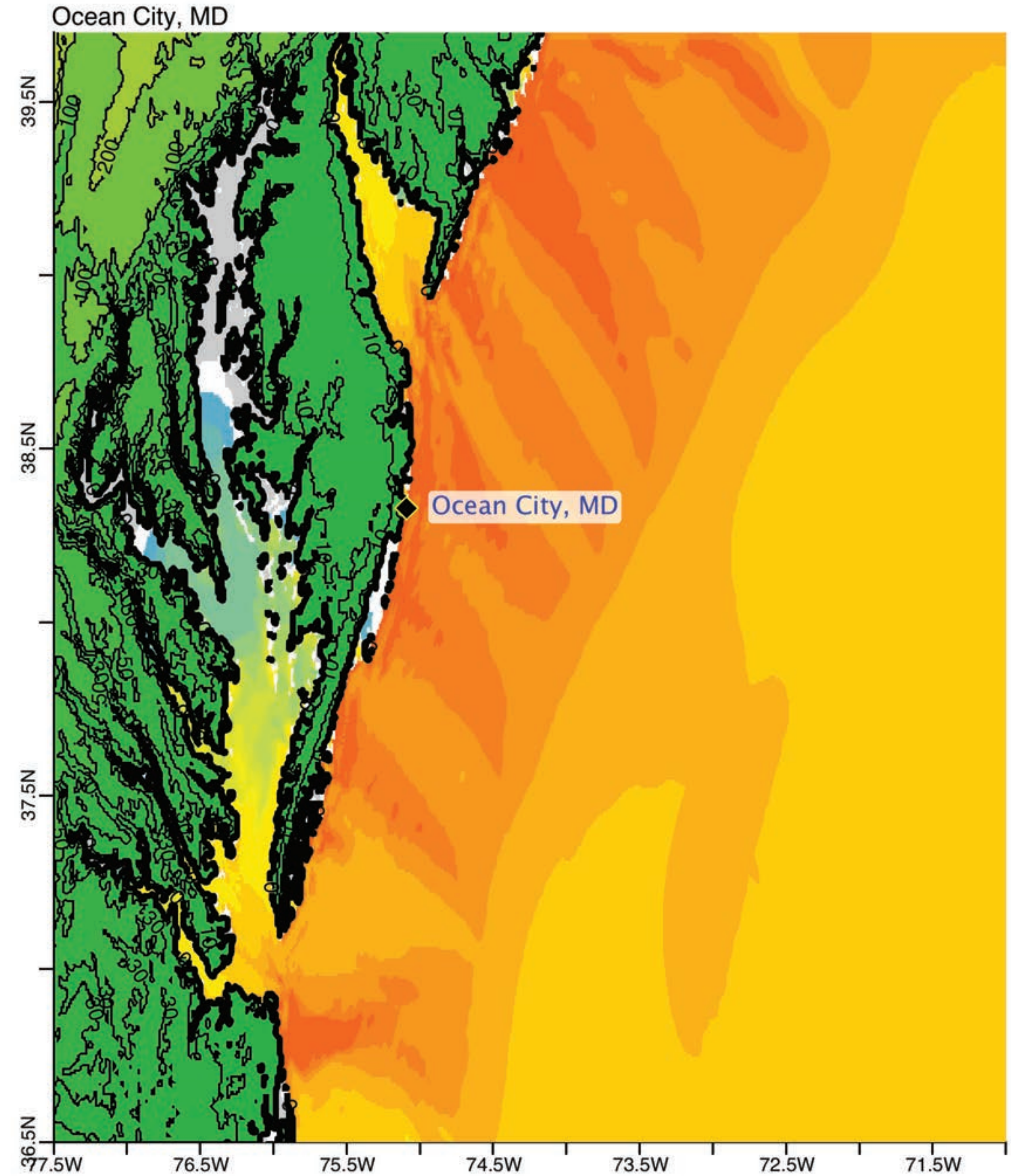


Figure 1. Max computed wave amplitude of A grid, Ocean City, Maryland, for synthetic event ATSZ 38-47.

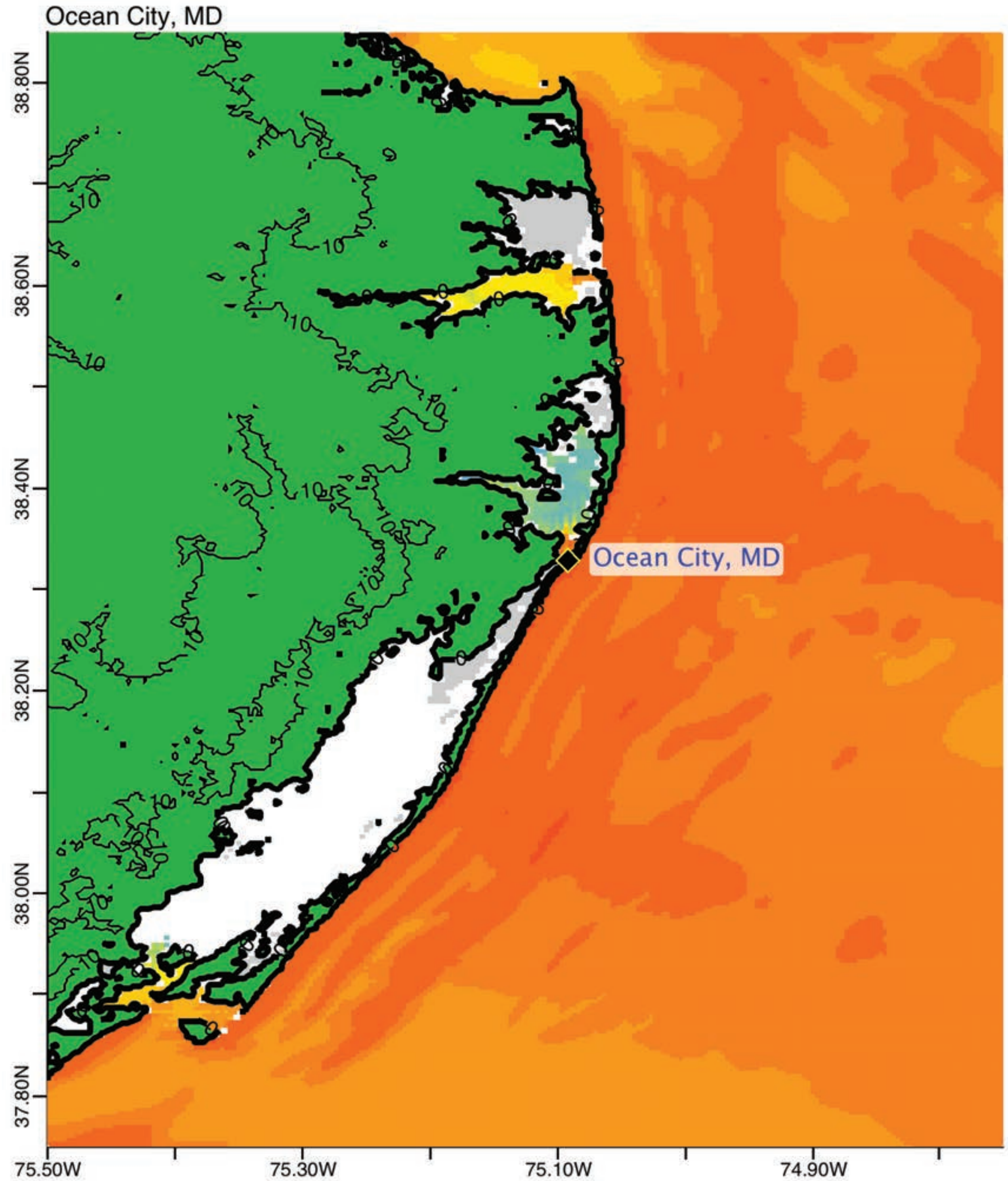


Figure 2. Max computed wave amplitude of B grid, Ocean City, Maryland, for synthetic event ATSZ 38-47.

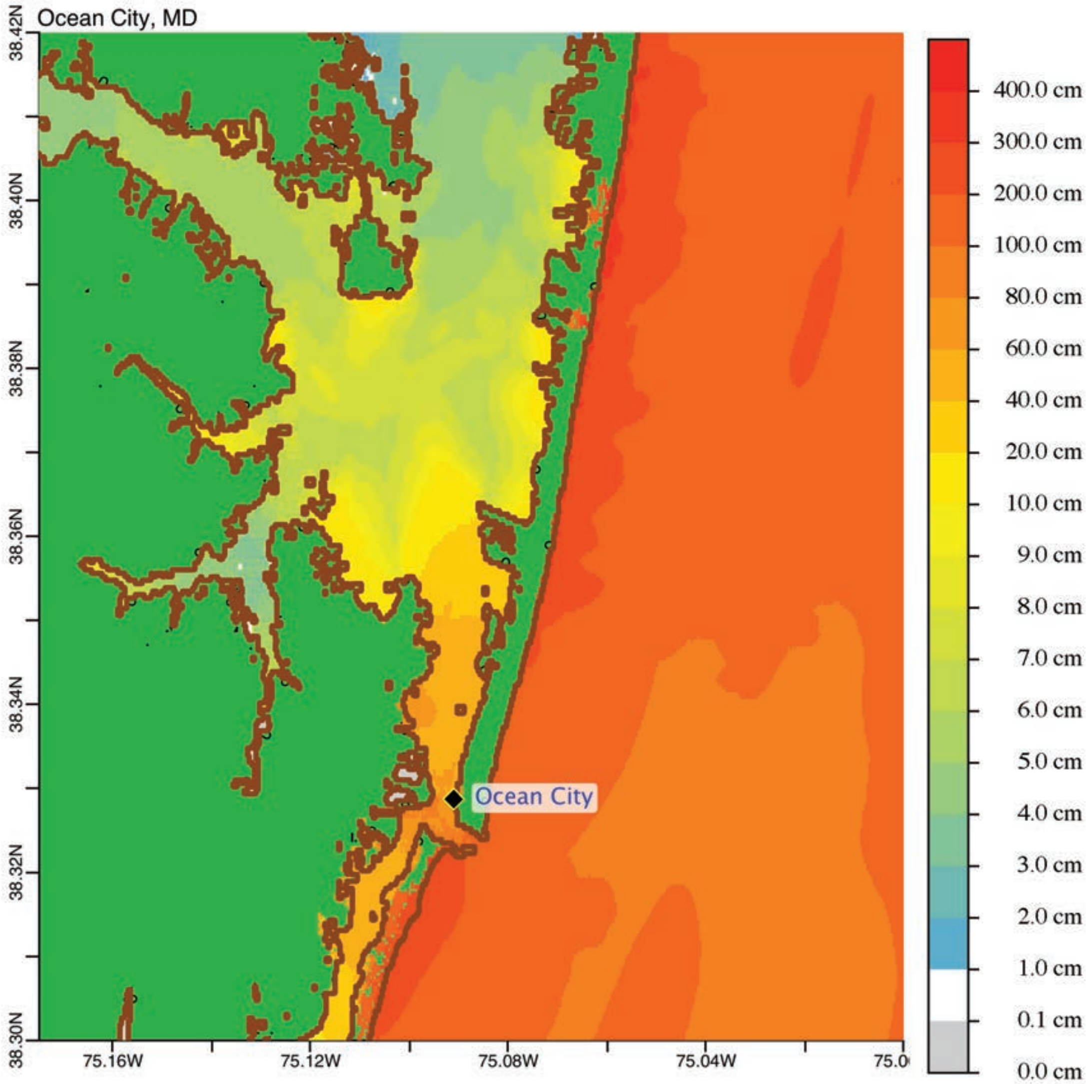


Figure 3. Max computed wave amplitude of C grid, Ocean City, Maryland, for synthetic event ATSZ 38-47.

(a)

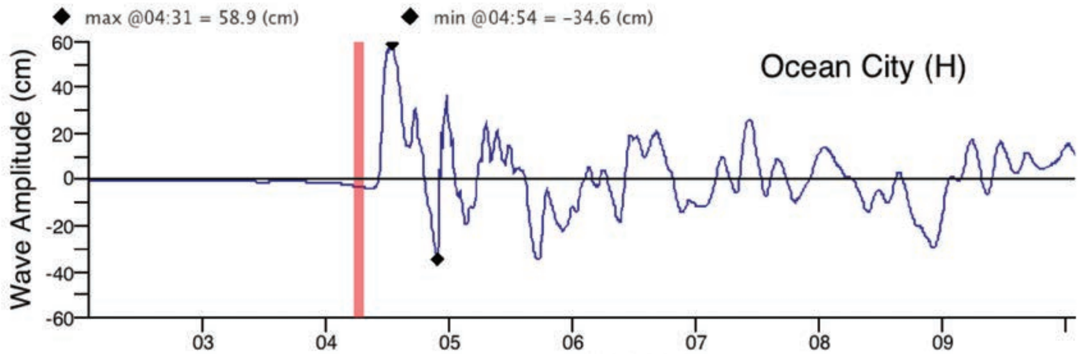


(b)

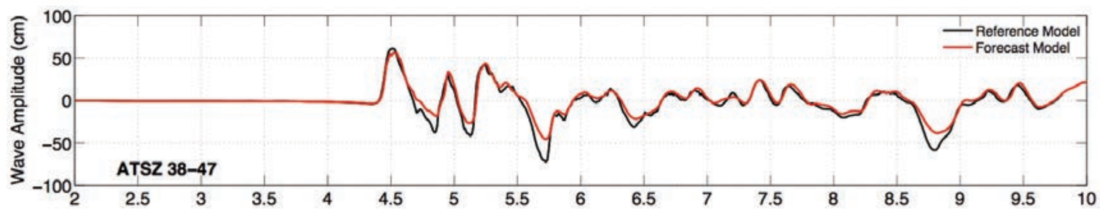


Figure 4. Computed time series at Ocean City tide gage, for synthetic event ATSZ 38-47: (a) time series computed in the forecast system; (b) time series shown in the forecast model report.

Figure 5. Max computed wave amplitude of A grid, Ocean City, Maryland, for synthetic event ATSZ 48-57.

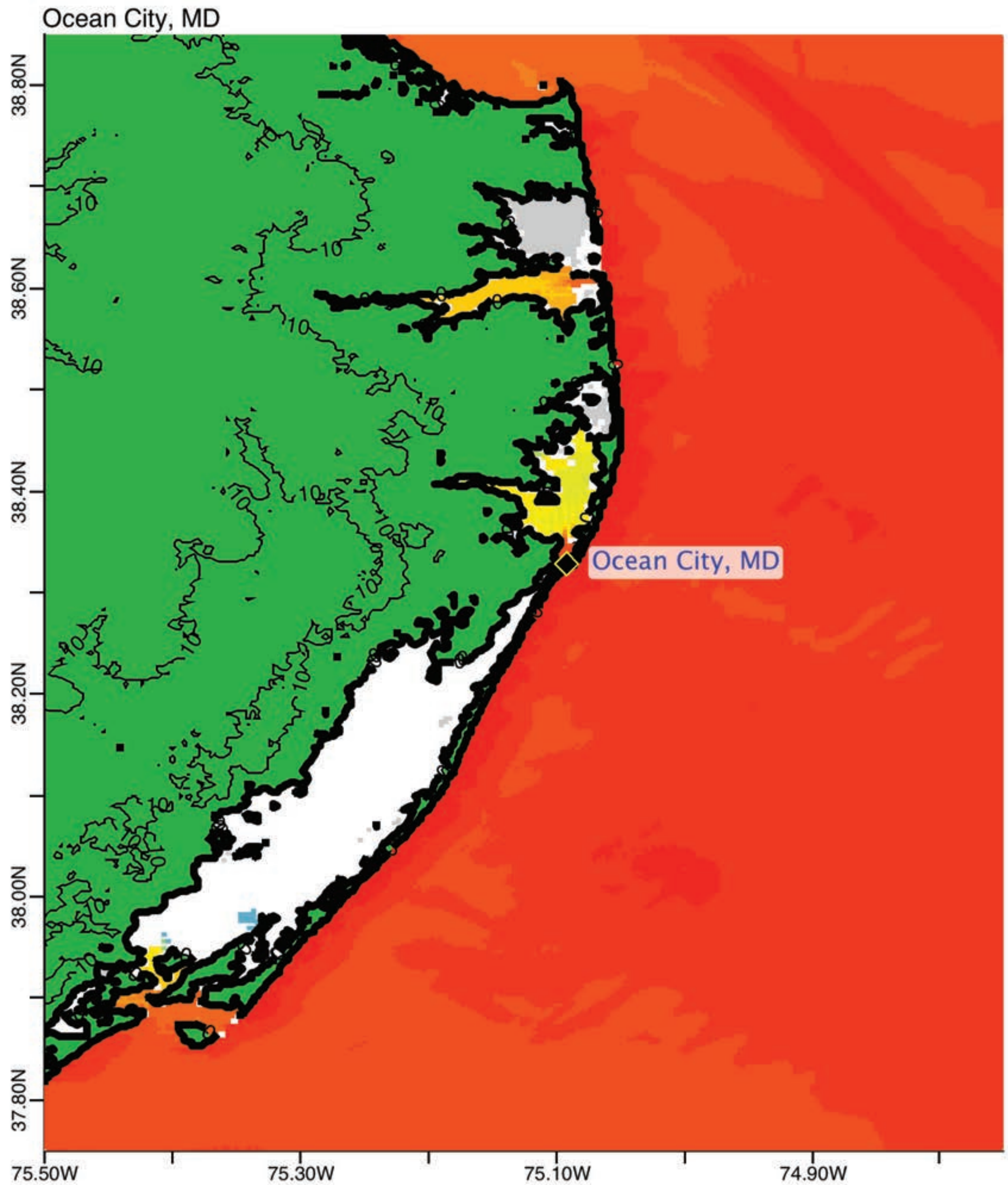

Figure 6. Max computed wave amplitude of B grid, Ocean City, Maryland, for synthetic event ATSZ 48-57.

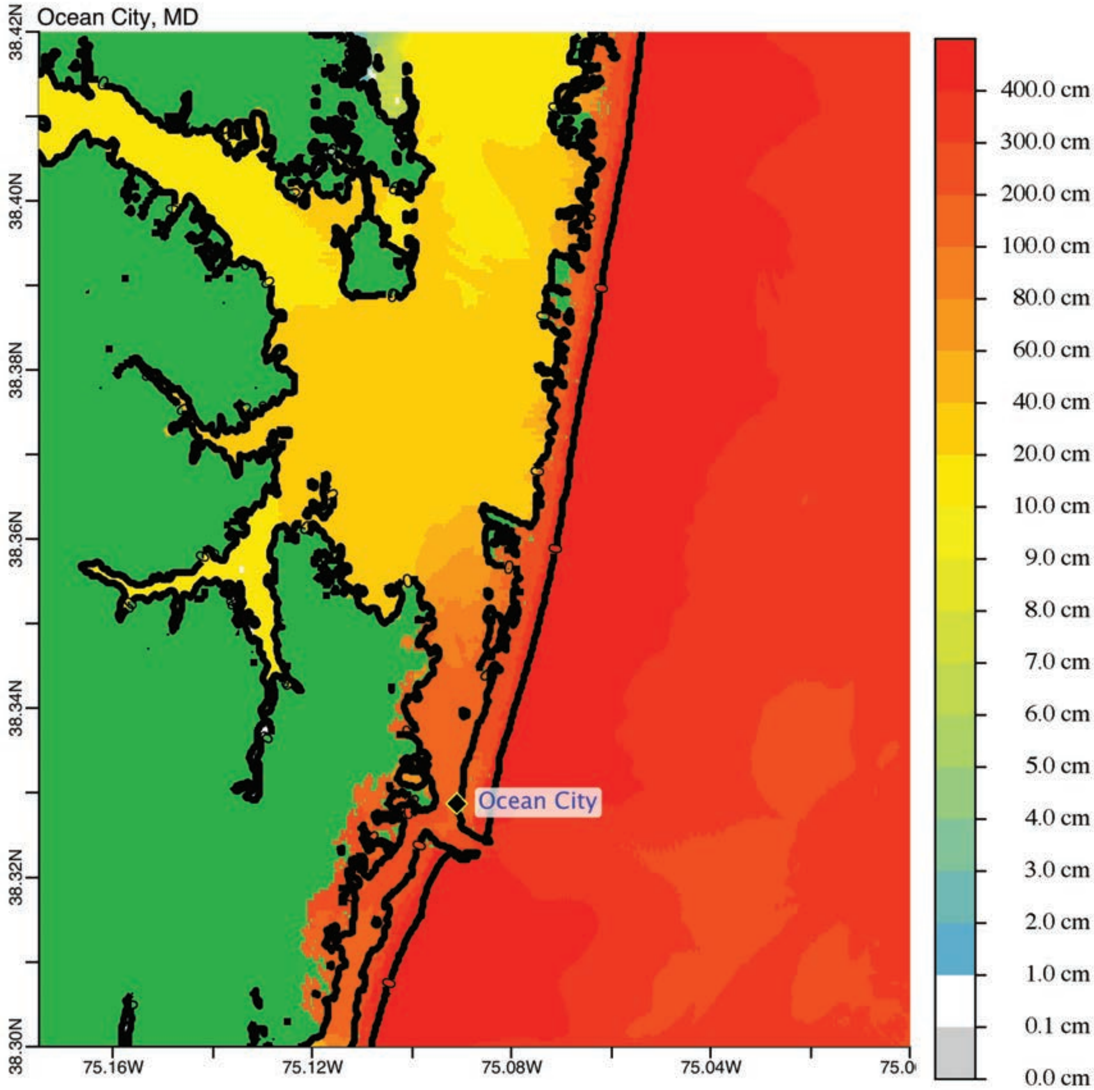


Figure 7. Max computed wave amplitude of C grid, Ocean City, Maryland, for synthetic event ATSZ 48-57.

(a)

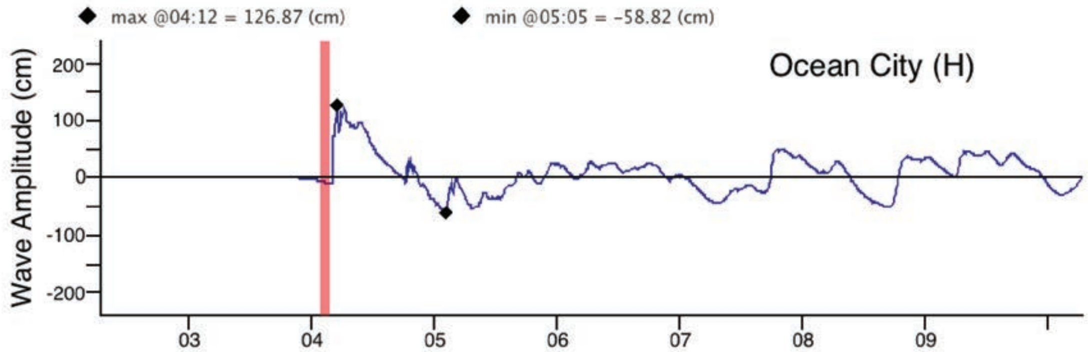


(b)

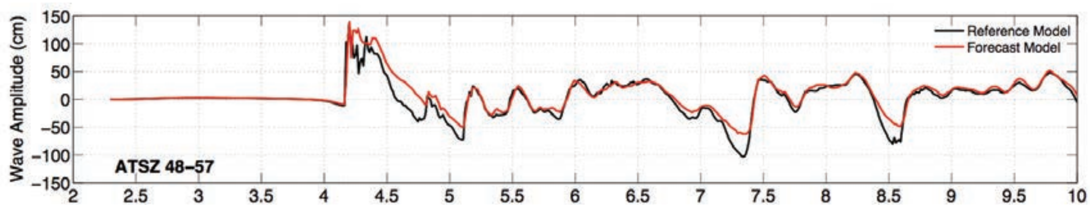


Figure 8. Computed time series at Ocean City tide gage, for synthetic event ATSZ 48-57: (a) time series computed in the forecast system; (b) time series shown in the forecast model report.

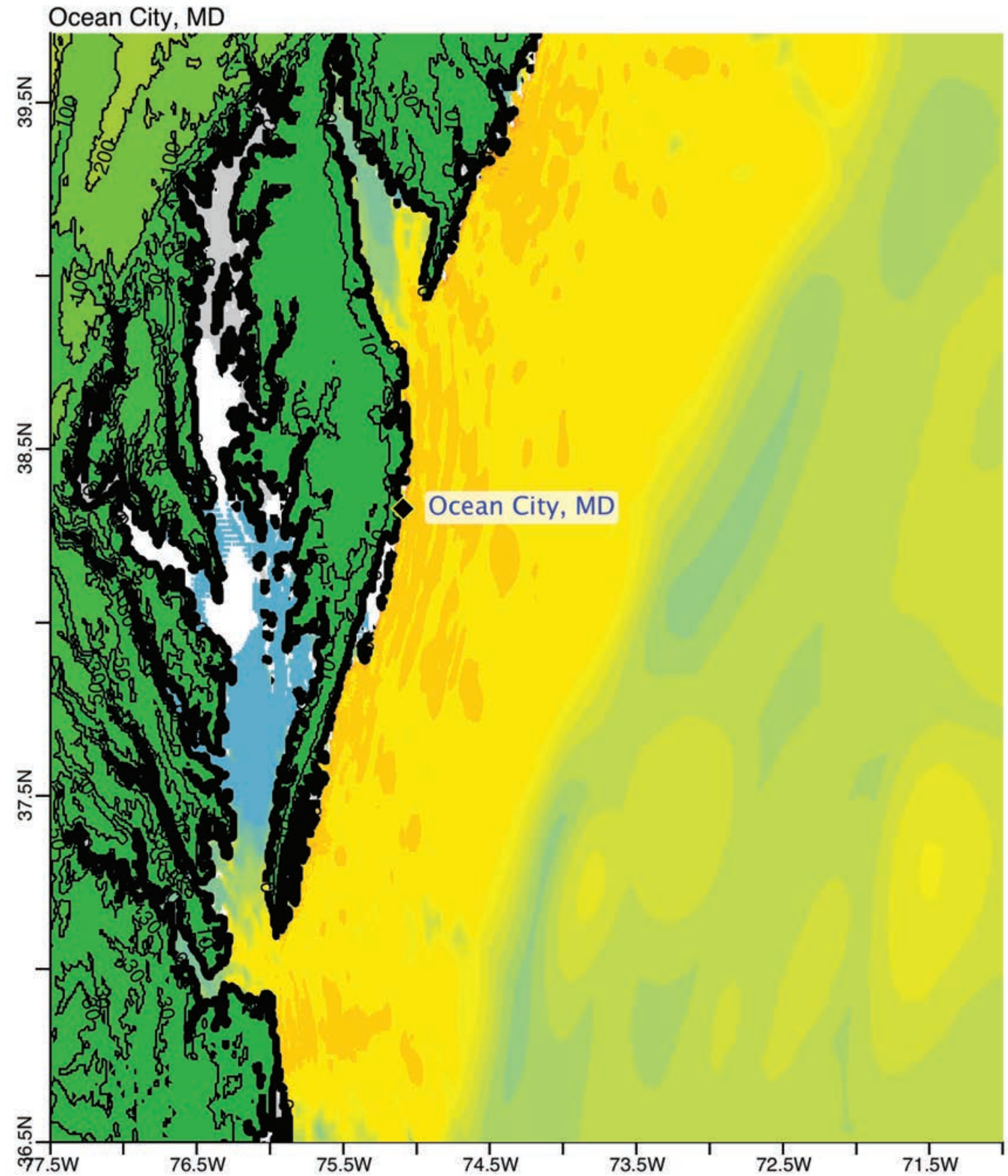


Figure 9. Max computed wave amplitude of A grid, Ocean City, Maryland, for synthetic event SSSZ 1-10.

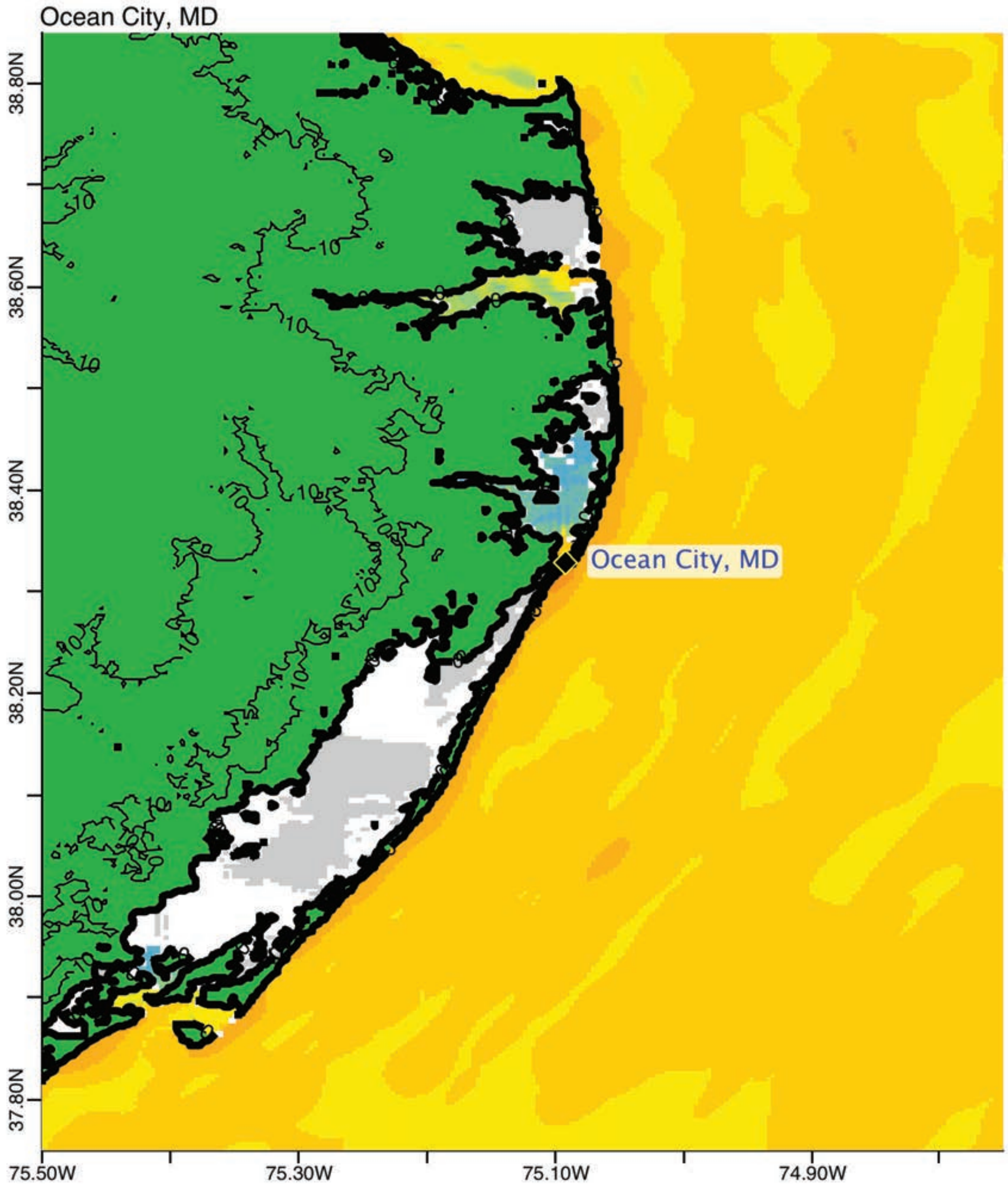


Figure 10. Max computed wave amplitude of B grid, Ocean City, Maryland, for synthetic event SSSZ 1-10.

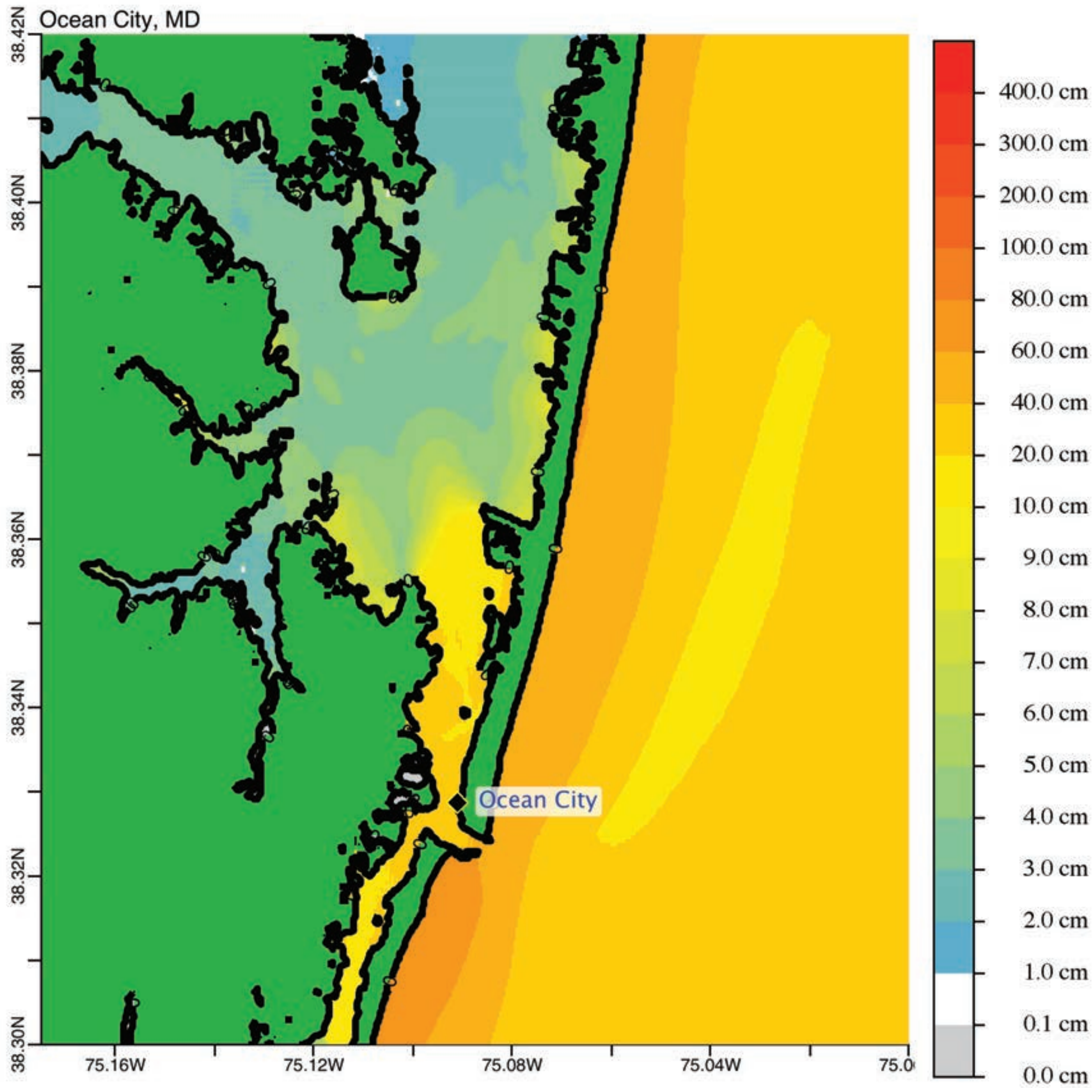


Figure 11. Max computed wave amplitude of C grid, Ocean City, Maryland, for synthetic event SSSZ 1-10.

(a)

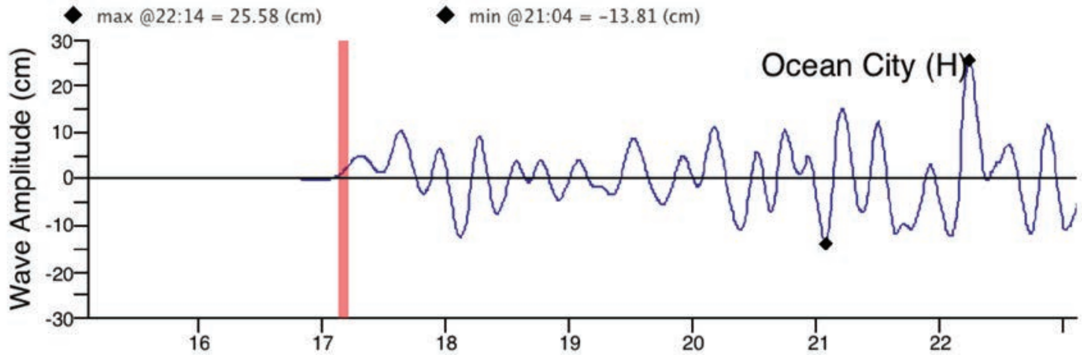


(b)

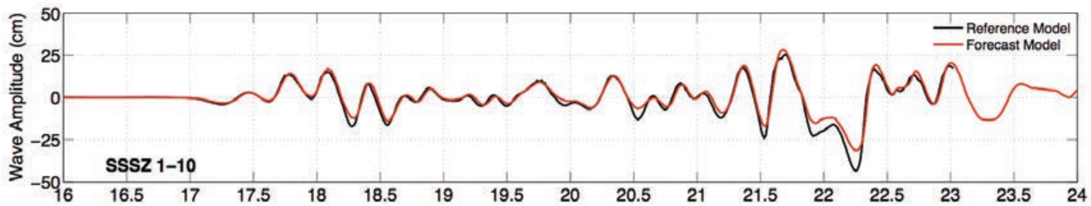


Figure 12. Computed time series at Ocean City tide gage, for synthetic event SSSZ 1-10: (a) time series computed in the forecast system; (b) time series shown in the forecast model report.